

Version from July 3, 2015

On Infrared Excesses Associated With Li-Rich K Giants

Luisa M. Rebull¹, Joleen K. Carlberg^{2,3}, John C. Gibbs⁴, J. Elin Deeb⁵, Estefania Larsen⁶, David V. Black⁷, Shailyn Altepeter⁶, Ethan Bucksbee⁶, Sarah Cashen⁴, Matthew Clarke⁶, Ashwin Datta⁴, Emily Hodgson⁴, Megan Lince⁴

ABSTRACT

Infrared (IR) excesses around K-type red giants (RGs) have previously been discovered using Infrared Astronomy Satellite (IRAS) data, and past studies have suggested a link between RGs with overabundant Li and IR excesses, implying the ejection of circumstellar shells or disks. We revisit the question of IR excesses around RGs using higher spatial resolution IR data, primarily from the Wide-field Infrared Survey Explorer (WISE). Our goal was to elucidate the link between three unusual RG properties: fast rotation, enriched Li, and IR excess. Our sample of RGs includes those with previous IR detections, a sample with well-defined rotation and Li abundance measurements with no previous IR measurements, and a large sample of RGs asserted to be Li-rich in the literature; we have 316 targets thought to be K giants, about 40% of which we take to be Li-rich. In 24 cases with previous detections of IR excess at low spatial resolution, we believe that source confusion is playing a role, in that either (a) the source that is bright in the optical is not responsible for the IR flux, or (b) there is more than one source responsible for the IR flux as measured in IRAS. We looked for IR excesses in the remaining sources, identifying 28 that have significant IR excesses by $\sim 20 \mu\text{m}$ (with possible excesses for 2 additional sources). There appears to be an intriguing correlation in that the largest IR excesses are all in Li-rich K giants, though very few Li-rich K giants have IR excesses (large or small). These largest IR excesses also tend to be found in the fastest rotators. There is no correlation of IR excess with the carbon isotopic ratio, $^{12}\text{C}/^{13}\text{C}$. IR excesses by $20 \mu\text{m}$, though relatively rare, are at least twice as common among our sample of Li-rich K giants. If dust shell production is a common by-product of Li enrichment mechanisms, these observations suggest that the IR excess stage is very short-lived, which is supported by theoretical calculations. Conversely, the Li-enrichment mechanism may only occasionally produce dust, and an additional parameter (e.g., rotation) may control whether or not a shell is ejected.

Subject headings: stars: late-type; stars: evolution; infrared: stars

¹Spitzer Science Center (SSC) and Infrared Science Archive (IRSA), Infrared Processing and Analysis Center (IPAC), 1200 E. California Blvd., California Institute of Technology, Pasadena, CA 91125 USA; rebull@ipac.caltech.edu

²NASA Goddard Space Flight Center, Code 667, Greenbelt MD 20771 USA

³NASA Postdoctoral Program Fellow

⁴Glencoe High School, 2700 NW Glencoe Rd., Hillsboro, OR 97124 USA

⁵Bear Creek High School, 9800 W. Dartmouth Pl., Lakewood, CO 80227 USA

⁶Millard South High School, 14905 Q St., Omaha, NE 68137 USA

⁷Walden School of Liberal Arts, 4230 N. University Ave., Provo, UT 84604 USA

1. Introduction

As stars evolve from the main-sequence (MS) to the red giant branch (RGB), they exhibit several characteristic changes. As the outer layers expand and cool, the star’s rotation rate slows, the convection zone deepens and a series of shell-burning and core-burning phases begin to take place. A number of RGB K-type giants, however, exhibit uncharacteristically rapid rotation rates that also seem to be correlated with high lithium abundances, $A(\text{Li})$ (e.g., Carlberg et al. 2012, hereafter C12). These higher rotation rates and $A(\text{Li})$ are inconsistent with those predicted by standard stellar evolutionary models. It has also been suggested that many of these high-Li RGB stars have infrared (IR) excesses suggestive of a circumstellar shell or disk (de la Reza et al. 1996, 1997, Drake et al. 2002, and references therein). Various hypotheses have been proposed to explain the combination of high Li, rapid rotation rates and IR excesses, including the accretion of nearby giant planets equivalent to a few Jupiter masses (e.g., Siess & Livio 1999) or a newly triggered nuclear fusion stage that could eject a dusty shell (e.g., de la Reza et al. 2015 and references therein).

The de la Reza et al. (1997; dIR97) study (and related studies) used data from the Infrared Astronomy Satellite (IRAS; Neugebauer et al. 1984), which surveyed at 12, 25, 60, and 100 μm . The spatial resolution, however, was relatively low, up to a few arcminutes. Despite the relatively low spatial resolution, many stars with IR excesses were identified (e.g., Gillett 1986, Paresce & Burrows 1987). In some regions with high source density, identifying the optical counterpart to the infrared source can be difficult, but in many cases, the counterparts are easily identifiable. dIR97, as well as other studies, used these IRAS data to look for K giants with IR excesses.

Data are now available from the much higher spatial resolution (6-12'') and much more sensitive Wide-field Infrared Survey Explorer (WISE; Wright et al. 2010). WISE surveyed the whole sky at 3.4, 4.6, 12, and 22 μm . While WISE does not detect wavelengths longer than IRAS channel 2 (25 μm), it is much higher spatial resolution, and can provide insight into how to interpret the IRAS data at 60 and 100 μm .

Some investigations subsequent to dIR97 have begun to question the connection between IR excesses and lithium abundance in RGs. Fekel & Watson (1998) found 6 giants with larger than typical lithium abundances out of 39 giants with IR excess (as determined from IRAS), which they point out is a similar fraction of stars with enhanced Li as found in normal field giants. Jasniewicz et al. (1999) finds 8 Li-rich stars out of 29 stars with IR excesses (also as determined via IRAS), finding no correlation between Li abundance and IR excess. Lebzelter et al. (2012) report on 3 Li-rich giants (out of more than 400 studied), none of which have IR excesses suggestive of mass loss. The IR excesses in their paper were identified based on WISE data, but were limited to 12 μm and shorter because few of their targets were detected at 22 μm . However, they also looked for evidence of gas mass loss in their spectra, and found none. Kumar et al. (2015) report on a search for IR excesses in 2000 K giants. None of their far-IR excess sources are lithium-rich, and of their 40 Li-rich sources, they identify 7 as having IR excess of any sort. These authors combined IRAS and WISE data to look for IR excesses.

In the present paper, we have also combined IRAS and WISE data, as well as data from several other IR surveys as discussed below. Large IR excesses are easily identified in the SEDs, and we used tools developed in the context of the study of young stars to look for small but significant excesses. We started with the dIR97 IRAS-selected targets; these IRAS-selected targets are all quite bright in the IR. We added to this the sample from C12, who assembled a set of K giants consisting of rapid and slow rotators in which the relationship between $v \sin i$, lithium abundances, and carbon isotope ratios ($^{12}\text{C}/^{13}\text{C}$) could be explored with an intention of exploring evidence for planetary accretion. The C12 sample was assembled without regard

to IR excess, so these objects are on average much fainter in the IR than the dLR97 sample. Finally, many Li-rich K giants (and candidates) have been reported in the literature, many of which are not in the dLR97 or C12 samples. We have included such Li-rich K giants in our sample. We looked for IR excesses among all of these targets, performing visual inspection of multi-wavelength images and assembling broadband spectral energy distributions (SEDs) for our targets.

We now assemble the list of targets (Sec. 2), and search various archives for images and photometry for these targets (Sec. 3). Then we drop some stars from our sample, some by necessity due to missing data, and some because they are likely subject to source confusion (Sec. 4). From the remaining sample, we can identify sources likely to have an IR excess (Sec. 5). Then we discuss some properties of the sample as a whole (Sec. 6). We find few stars with IR excesses, so our ability to find correlations with abundances is somewhat limited, but we discuss this in Sec. 7 before summarizing in Sec. 8.

2. Assembling the Target List

There are 82 targets published in dLR97. They obtained spectra of the targets on their list, and reported the targets as Li-rich if the Li line at $\lambda 6708$ had an intensity comparable to or higher than the Ca I line at $\lambda 6718$. If the Li abundance was actually known, they took those with abundances larger than $\log \epsilon(\text{Li})=1.2$ dex as Li-rich. Many of the targets have HD numbers, and thus finding coordinates for an optical counterpart is straightforward. However, many of their targets have only IRAS names, and so they took spectra of objects they believed to be counterparts of the sources listed; see discussion below. The target position we used for these sources is that reported in the IRAS catalogs.

There are 86 K giants reported in C12. Comparing this to the targets from dLR97, there is only one source in common between them, HD 31993. C12 reports lithium abundances, $v \sin i$, and $^{12}\text{C}/^{13}\text{C}$ ratios, among other things, for their targets. Not all of these targets are Li-rich.

There is wide-ranging literature reporting on Li-rich K giants (and candidates). We compiled 149 additional targets that have been identified either consistently or at one time as confirmed or possible Li-rich K giants, but not included in either the dLR97 or the C12 samples. They include targets from Adamów et al. (2014), Anthony-Twarog et al. (2013), Carney et al. (1998), Carlberg et al. (in prep), Castilho et al. (2000), Drake et al. (2002), Fekel & Watson (1998), Hill & Pasquini (1999), Jasniewicz et al. (1999), Kirby et al. (2012), Kraft et al. (1999), Kumar et al. (2011) and references therein, Liu et al. (2014), Luck & Heiter (2007), Martell et al. (2013), Monaco et al. (2014), Pilachowski et al. (2003), Ruchti et al. (2011), Silva Aguirre et al. (2014), Smith et al. (1999), and Torres et al. (2000). Kumar et al. (2015) appeared as we were finishing our analysis, and it has similar goals as the present paper. It uses as a starting point the list of 2000 low-mass K giants from Kumar et al. (2011), so all of the Li-rich sources from that sample are already in our sample. All of the literature sources are identified simply as ‘literature sources’ in Table 1; the Appendix identifies the paper of origin for any given target.

Our complete list of 316 targets appears in Table 1. We obtained RA, Dec positions for these targets, most of which are quite bright in the optical, primarily from SIMBAD, though literature was consulted for fainter sources as required. The positions we used are in Table 1, which also includes all the bandmerged brightness measurements discussed below. In the Appendix, Table 6 collects a few special notes about any special circumstances attached to that star, e.g., information about typos in previously published tables, or necessary tweaks to the positions. There are copious notes in the main text about targets called out as special (e.g., those with IR excesses).

Table 1. Contents of Online Catalog^a

Format	Units	Label	Explanations
A26	—	name	name of source
F11.6	dec	RA	right ascension of source (J2000)
F11.6	dec	Dec	declination of source (J2000)
A6	—	dIR97	flag to indicate source is part of the dIR97 sample
A4	—	C12	flag to indicate star is part of the C12 sample
A5	—	lit	flag to indicate star is selected from the literature as a Li-rich giant (but not C12 or dIR97)
A4	—	LirichLit	value of ‘yes’ means source is identified in the literature as a Li-rich giant
A4	—	LirichHere	value of ‘yes’ means source is selected here as a Li-rich giant
F7.2	—	ALiNLTE	A(Li) under the assumption of NLTE from the literature
A2	—	ALiLTE	limit flag for A(Li) under the assumption of LTE from the literature
F7.2	—	ALiLTE	A(Li) under the assumption of LTE from the literature
A2	—	Cratiol	limit flag on $^{12}\text{C}/^{13}\text{C}$ ratio
F5.1	—	Cratio	$^{12}\text{C}/^{13}\text{C}$ ratio
F5.1	km s ⁻¹	vsini	projected rotational velocity $v \sin i$ in km s ⁻¹ from the literature
I5	K	Teff	Effective temperature from the literature
F5.1	—	logg	log g from the literature
F6.2	mag	Umag	Vega-based magnitude in U band
F6.2	mag	Umerr	Vega-based magnitude error in U band; taken to be 20% unless specified
F6.2	mag	Bmag	Vega-based magnitude in B band
F6.2	mag	Bmerr	Vega-based magnitude error in B band; taken to be 20% unless specified
F6.2	mag	Vmag	Vega-based magnitude in V band
F6.2	mag	Vmerr	Vega-based magnitude error in V band; taken to be 20% unless specified
F6.2	mag	Rmag	Vega-based magnitude in R band
F6.2	mag	Rmerr	Vega-based magnitude error in R band; taken to be 20% unless specified
F6.2	mag	umag	AB SDSS magnitude in u band
F6.2	mag	umerr	AB SDSS magnitude error in u band
F6.2	mag	gmag	AB SDSS magnitude in g band
F6.2	mag	gmerr	AB SDSS magnitude error in g band
F6.2	mag	rmag	AB SDSS magnitude in r band
F6.2	mag	rmerr	AB SDSS magnitude error in r band
F6.2	mag	imag	AB SDSS magnitude in i band
F6.2	mag	imerr	AB SDSS magnitude error in i band
F6.2	mag	zmag	AB SDSS magnitude in z band
F6.2	mag	zmerr	AB SDSS magnitude error in z band
A22	—	2Mname	Name from 2MASS or 2MASX catalog
A2	—	Jlim	limit flag for 2MASS J band
F6.2	mag	Jmag	Vega-based magnitude in 2MASS J band
F6.2	mag	Jmerr	Vega-based magnitude error in 2MASS J band
A2	—	Jqual	2MASS data quality flag for J (A=best)
A2	—	Hlim	limit flag for 2MASS H band
F6.2	mag	Hmag	Vega-based magnitude in 2MASS H band
F6.2	mag	Hmerr	Vega-based magnitude error in 2MASS H band
A2	—	Hqual	2MASS data quality flag for H (A=best)
A2	—	Klim	limit flag for 2MASS K_s band
F6.2	mag	Kmag	Vega-based magnitude in 2MASS K_s band
F6.2	mag	Kmerr	Vega-based magnitude error in 2MASS K_s band
A2	—	Kqual	2MASS data quality flag for K_s (A=best)
A18	—	DENISname	Name from DENIS catalog
F6.2	mag	Imag	Vega-based DENIS magnitude in I band
F6.2	mag	Imerr	Vega-based DENIS magnitude error in I band
F6.2	mag	Jmag	Vega-based DENIS magnitude in J band
F6.2	mag	Jmerr	Vega-based DENIS magnitude error in J band
F6.2	mag	Kmag	Vega-based DENIS magnitude in K band
F6.2	mag	Kmerr	Vega-based DENIS magnitude error in K band
A26	—	WISEname	Name from WISE (AllWISE) catalog or reject catalog

Table 1—Continued

Format	Units	Label	Explanations
A2	—	W1lim	limit flag for WISE-1 ([3.4])
F6.2	mag	W1mag	Vega-based magnitude in WISE-1 ([3.4])
F6.2	mag	W1merr	Vega-based magnitude error in WISE-1 ([3.4]); value of -9 for those measures that are limits
A2	mag	W1qual	WISE-1 ([3.4]) data quality flag (A=best)
A2	—	W2lim	limit flag for WISE-2 ([4.6])
F6.2	mag	W2mag	Vega-based magnitude in WISE-2 ([4.6])
F6.2	mag	W2merr	Vega-based magnitude error in WISE-2 ([4.6]); value of -9 for those measures that are limits
A2	mag	W2qual	WISE-2 ([4.6]) data quality flag (A=best)
A2	—	W3lim	limit flag for WISE-3 ([12])
F6.2	mag	W3mag	Vega-based magnitude in WISE-3 ([12])
F6.2	mag	W3merr	Vega-based magnitude error in WISE-3 ([12]); value of -9 for those measures that are limits
A2	mag	W3qual	WISE-3 ([12]) data quality flag (A=best)
A2	—	W4lim	limit flag for WISE-4 ([22])
F6.2	mag	W4mag	Vega-based magnitude in WISE-4 ([22])
F6.2	mag	W4merr	Vega-based magnitude error in WISE-4 ([22]); value of -9 for those measures that are limits
A2	mag	W4qual	WISE-4 ([22]) data quality flag (A=best)
A27	—	SEIPname	Name from SEIP source list
F6.2	mag	I1mag	Vega-based magnitude in IRAC-1 ([3.6])
F6.2	mag	I1merr	Vega-based magnitude error in IRAC-1 ([3.6])
F6.2	mag	I2mag	Vega-based magnitude in IRAC-2 ([4.5])
F6.2	mag	I2merr	Vega-based magnitude error in IRAC-2 ([4.5])
F6.2	mag	I3mag	Vega-based magnitude in IRAC-3 ([5.8])
F6.2	mag	I3merr	Vega-based magnitude error in IRAC-3 ([5.8])
F6.2	mag	I4mag	Vega-based magnitude in IRAC-4 ([8])
F6.2	mag	I4merr	Vega-based magnitude error in IRAC-4 ([8])
F6.2	mag	M1mag	Vega-based magnitude in MIPS-1 ([24])
F6.2	mag	M1merr	Vega-based magnitude error in MIPS-1 ([24])
A14	—	IRASPCname	Name from IRAS Point Source Catalog (PSC)
F6.2	mag	IRAS1PSCmag	Vega-based magnitude in IRAS-1 ([12]) from PSC; errors taken to be 0.22 mags
F9.2	Jy	IRAS1PSCfd	flux density in Jy in IRAS-1 from PSC
A2	mag	IRAS1PSCqual	Data quality flag for IRAS-1 from PSC (3=best, 1=limit)
F6.2	mag	IRAS2PSCmag	Vega-based magnitude in IRAS-2 ([25]) from PSC; errors taken to be 0.22 mags
F9.2	Jy	IRAS2PSCfd	flux density in Jy in IRAS-2 from PSC
A2	mag	IRAS2PSCqual	Data quality flag for IRAS-2 from PSC (3=best, 1=limit)
F6.2	mag	IRAS3PSCmag	Vega-based magnitude in IRAS-3 ([60]) from PSC; errors taken to be 0.22 mags
F9.2	Jy	IRAS3PSCfd	flux density in Jy in IRAS-3 from PSC
A2	mag	IRAS3PSCqual	Data quality flag for IRAS-3 from PSC (3=best, 1=limit)
F6.2	mag	IRAS4PSCmag	Vega-based magnitude in IRAS-4 ([100]) from PSC; errors taken to be 0.22 mags
F9.2	Jy	IRAS4PSCfd	flux density in Jy in IRAS-4 from PSC
A2	mag	IRAS4PSCqual	Data quality flag for IRAS-4 from PSC (3=best, 1=limit)
A14	—	IRASFSCname	Name from IRAS Faint Source Catalog (FSC)
F6.2	mag	IRAS1FSCmag	Vega-based magnitude in IRAS-1 ([12]) from FSC; errors taken to be 0.22 mags
F9.2	Jy	IRAS1FSCfd	flux density in Jy in IRAS-1 from FSC
A2	mag	IRAS1FSCqual	Data quality flag for IRAS-1 from FSC (3=best, 1=limit)
F6.2	mag	IRAS2FSCmag	Vega-based magnitude in IRAS-2 ([25]) from FSC; errors taken to be 0.22 mags
F9.2	Jy	IRAS2FSCfd	flux density in Jy in IRAS-2 from FSC
A2	mag	IRAS2FSCqual	Data quality flag for IRAS-2 from FSC (3=best, 1=limit)
F6.2	mag	IRAS3FSCmag	Vega-based magnitude in IRAS-3 ([60]) from FSC; errors taken to be 0.22 mags
F9.2	Jy	IRAS3FSCfd	flux density in Jy in IRAS-3 from FSC
A2	mag	IRAS3FSCqual	Data quality flag for IRAS-3 from FSC (3=best, 1=limit)
F6.2	mag	IRAS4FSCmag	Vega-based magnitude in IRAS-4 ([100]) from FSC; errors taken to be 0.22 mags
F9.2	Jy	IRAS4FSCfd	flux density in Jy in IRAS-4 from FSC
A2	mag	IRAS4FSCqual	Data quality flag for IRAS-4 from FSC (3=best, 1=limit)
A28	—	AKARIIRCname	Name from AKARI IRC catalog, v1
F9.2	Jy	AKARI9fd	flux density in Jy in 9 microns from AKARI IRC

Table 1—Continued

Format	Units	Label	Explanations
F9.2	Jy	AKARI9fderr	error in flux density in Jy in 9 microns from AKARI IRC
F9.2	Jy	AKARI18fd	flux density in Jy in 18 microns from AKARI IRC
F9.2	Jy	AKARI18fderr	error in flux density in Jy in 18 microns from AKARI IRC
A28	—	AKARIFISname	Name from AKARI FIS catalog, v1
F9.2	Jy	AKARI65fd	flux density in Jy in 65 microns from AKARI FIS
F9.2	Jy	AKARI65fderr	error in flux density in Jy in 65 microns from AKARI FIS
F9.2	Jy	AKARI90fd	flux density in Jy in 90 microns from AKARI FIS
F9.2	Jy	AKARI90fderr	error in flux density in Jy in 90 microns from AKARI FIS
F9.2	Jy	AKARI140fd	flux density in Jy in 140 microns from AKARI FIS
F9.2	Jy	AKARI140fderr	error in flux density in Jy in 140 microns from AKARI FIS
F9.2	Jy	AKARI160fd	flux density in Jy in 160 microns from AKARI FIS
F9.2	Jy	AKARI160fderr	error in flux density in Jy in 160 microns from AKARI FIS
A18	—	MSXname	Name from MSX catalog
F9.2	Jy	MsxAfd	flux density in Jy in MSX Band A (7.76 μm)
F9.2	Jy	MsxAfderr	error in flux density in Jy in MSX Band A (7.76 μm) – as reported, may be very large
F9.2	Jy	MsxB1fd	flux density in Jy in MSX Band B1 (4.29 μm)
F9.2	Jy	MsxB1fderr	error in flux density in Jy in MSX Band B1 (4.29 μm) – as reported, may be very large
F9.2	Jy	MsxB2fd	flux density in Jy in MSX Band B2 (4.35 μm)
F9.2	Jy	MsxB2fderr	error in flux density in Jy in MSX Band B2 (4.35 μm) – as reported, may be very large
F9.2	Jy	MsxCfd	flux density in Jy in MSX Band C (11.99 μm)
F9.2	Jy	MsxCfderr	error in flux density in Jy in MSX Band C (11.99 μm) – as reported, may be very large
F9.2	Jy	MsxDfd	flux density in Jy in MSX Band D (14.55 μm)
F9.2	Jy	MsxDfderr	error in flux density in Jy in MSX Band D (14.55 μm) – as reported, may be very large
F9.2	Jy	MsxEfd	flux density in Jy in MSX Band E (20.68 μm)
F9.2	Jy	MsxEfderr	error in flux density in Jy in MSX Band E (20.68 μm) – as reported, may be very large

^aThis catalog is available in its entirety in the online version of Table 1.

Table 2. Overview of Photometric Studies and Data Included

Dataset	Band(s) used	Search radius ^a (")	Fraction with match	notes
2MASS	JHK_s (1.2-2.2 μm)	1 ^b	304/316=96%	primary catalog; many saturated
WISE	3.4, 4.5, 12, 22 μm	1	311/316=98%	primary catalog; many saturated in part. (~20% of sample required >1" counterpart match)
IRAS	12, 25, 60, 100 μm	<20	PSC: 159/316=50%; FSC: 121/316=38%	data used for original de la Reza studies
AKARI	9, 18, 65, 90, 140, 160 μm	1	IRC: 221/316=70%; FIS: 36/316=11%	supplementary data (~20% of IRC sources that had matches required >1" counterpart match, most of the FIS required >1".)
MSX	4.3, 4.4, 7.8, 12.0, 14.6, 20.6 μm	20	54/316=17%	supplementary data
SEIP	3.6, 4.5, 5.8, 8, 24 μm	1	39/316=12%	very low fractional coverage
DENIS	0.82, 1.25, 2.15 μm	1	83/316=26%	provides deeper K_s than 2MASS; only 58 have K_s , and none of those are lacking in 2MASS K_s
SDSS	$ugriz$ (0.29-0.91 μm)	2	94/316=30%	supplementary data
NOMAD,C12	$UBVR$ (0.36-0.7 μm)	1	277/316=88%	literature data from NOMAD or C12

^aCharacteristic distance to source match; some sources with poor positions required a much larger search radius.

^bMost sources found a match within 1" (histogram of distances peaks strongly below 0.2"), but ~10% required larger (by-eye) matches.

3. Archival Data

In this section, we discuss the catalogs we searched for detections of our sources; they are summarized in Table 2, along with the fraction of the sample having matches in each of these catalogs. Table 1 includes all the crossmatched sources (names and reported brightnesses) discussed below.

3.1. Overall Approach to Archival Data

All of the large-area catalogs described here were merged by position with a catalog-dependent search radius to the position we obtained for our targets as described above. Typically, the closest source by position was taken to be the match, and often the best match was within $1''$. However, each source was investigated in the images from the Palomar Observatory Digital Sky Survey, the Sloan Digital Sky Survey, the Two-Micron All Sky Survey, and WISE. Nebulosity, source confusion, or extended sources were all noted. Spectral energy distributions (SEDs) were constructed (using zero points if necessary as provided in the corresponding survey documentation) as an additional check on the source matching – obvious discontinuities in the SED suggested problems with source matching, and a better match was sought (but not always found). If a source other than the closest source by position was determined to be a better match, then the match was forced to be the better match, even if it was $> 1''$ away. We primarily used the Infrared Science Archive (IRSA) tool FinderChart¹ for this process, along with the one-to-one catalog matching feature in the IRSA catalog search tool. Significant issues with images and SEDs will be discussed in the next section (§4).

3.2. Primary Catalogs

The Two-Micron All Sky Survey (2MASS; Skrutskie et al. 2006) obtained data over the whole sky at JHK_s bands. We found matches to most of our sources well within $1''$ – a histogram of distances peaks strongly below $0.2''$. However, $\sim 10\%$ of the targets (largely those still having original coordinates from IRAS) required larger (by-eye) matches, up to $15''$ away. Many of our targets are quite bright and are therefore saturated in the 2MASS catalog. For most of these, we can obtain at least estimates of K_s from the Naval Observatory Merged Astrometric Dataset (NOMAD; Zacharias et al. 2005), though empirically we have found that the errors as reported there are likely significantly underestimated, perhaps representing statistical errors only (not including systematics). For one source, the JHK_s brightnesses had to be retrieved from the extended source catalog (rather than the point source catalog). For many of our bright targets, the formal photometric quality as reported in 2MASS may be poor, but the points are in good agreement with the rest of the SED assembled here. We thus retained 2MASS measurements even if the photometric quality was deemed poor by the 2MASS pipeline. (About 60% of the sources with 2MASS counterparts have K_s photometric quality ‘A’; $\sim 35\%$ have nominal photometric quality ‘D’ or worse.) Limits reported in the catalog were retained as limits here.

2MASS provides the coordinate system to which other catalogs including WISE are anchored, so, given the very close positional matches for 2MASS, we expected (and found) comparable high-quality matches with those other catalogs.

IRAS surveyed the sky in 1983 in four bands, 12, 25, 60, and $100 \mu\text{m}$. As the first all-sky infrared survey,

¹<http://irsa.ipac.caltech.edu/applications/finderchart/>

it is relatively low spatial resolution and relatively shallow. The Point Source Catalog (PSC; Beichman et al. 1988) reports on sources smaller than $0.5\text{-}2'$ in the in-scan direction (where the native survey pixels are rectangular). The typical full width at half max (FWHM) of sources in the IRAS Sky Survey Atlas (ISSA) data products (which is what appears in FinderChart) is $3.4'\text{-}4.7'^2$. The IRAS Faint Source Catalog (FSC; Moshir et al. 1992) is a reprocessing of the IRAS data that obtains, among other things, better positional accuracy and reaches fainter flux densities. We searched both the IRAS PSC and FSC for counterparts to our sources. Since the dIR97 sources were selected based on IRAS properties, all of them have detections in the PSC, and 36 are also detected in the FSC. Nearly half (103/235) of our remaining sources have IRAS detections in either the PSC or FSC in any band, though only about a third of the C12 sources have an IRAS detection (in any band). Overall, 181 have sources in either the PSC or FSC, and 99 have counterparts in both the PSC and FSC.

The IRAS data (where available) for our targets appear in Table 1. We used the non-color corrected flux density at the various bands as reported in the catalogs, and used the Vega zero points as reported in the online IRAS documentation³ to convert the flux densities to magnitudes, namely 28.3, 6.73, 1.19, and 0.43 Jy for the four bands, respectively. No errors are reported, so we took a flat 20% flux density uncertainty, which is 0.22 mag. We merged catalogs without regard to flux quality, though the quality is noted in our catalog. Nearly all of the detected sources are the highest quality (qual=3) in both the PSC and FSC at $12\ \mu\text{m}$, but $>80\%$ of these sources are the *lowest* quality in the PSC and FSC at $100\ \mu\text{m}$ (qual=1). The lowest quality measurements are, according to the documentation, meant to be limits. In some cases, even the nominal limits are in good agreement with detections from other instruments. We retained the measurements and the flux quality flags in our database.

WISE surveyed the whole sky at 3.4, 4.6, 12, and $22\ \mu\text{m}$; all of the available WISE data taken between 2010 Jan and 2011 Feb were incorporated into the AllWISE catalog (Cutri et al. 2014), which we used for this work. In three cases, brightnesses for a target had to be retrieved from the AllWISE catalog of rejects. Since the dIR97 sources were selected based on the relatively shallow IRAS data, many were saturated in at least one WISE band; many fewer of the C12 sources were saturated. Of the WISE detections, only those with data quality flags ‘A’, ‘B’, or ‘C’ were retained, but most detections were ‘A’ or ‘B’; the fraction of detections with data quality flag ‘C’ is 10%, 5%, 1%, and 3% for the four WISE channels, respectively. For many of our very bright targets, the formal photometric quality as reported in WISE may be poor, but the points are in good agreement with the rest of the SED; limits from the catalog were retained in our database.

Given the relatively low spatial resolution of IRAS compared to 2MASS or WISE, we did not necessarily expect to find very close positional matches to sources with solely IRAS positions. However, many sources whose coordinates were the original IRAS positions found very close matches in 2MASS and/or WISE, demonstrating the high quality of those original IRAS positions. The places where IRAS did not match well were largely those where source confusion pulled the photocenter position off from the brightest source in WISE; see additional discussion on source confusion issues below.

All of the abundances and associated information (T_{eff} , $\log g$) were most often taken from the papers reporting the star as Li-rich – see the Appendix table for the specific literature reference. We allowed $A(\text{Li})$ from the non-local-thermodynamic-equilibrium (NLTE) estimates to take precedence over LTE estimates, but in some cases, only LTE abundances were available. In a few cases, only Li equivalent widths were

²<http://irsa.ipac.caltech.edu/IRASdocs/issa.exp.sup/ch1/C.html>

³<http://irsa.ipac.caltech.edu/IRASdocs/exp.sup/ch6/C2a.html>

available in the literature, in which case we did not even attempt to estimate an $A(\text{Li})$, and thus the sources are effectively dropped from analysis requiring $A(\text{Li})$. In ~ 20 cases, McDonald et al. (2012) provided a T_{eff} estimate when no other was available from the literature. For the 14 stars with super-solar metallicities in C12, we provide corrected NLTE abundances here.

3.3. Secondary Catalogs

The AKARI mission (Murakami et al. 2007) surveyed the sky in 2006-2007, in wavelengths between 1.8 and 180 μm using two instruments, the Infrared Camera (IRC) and the Far-Infrared Surveyor (FIS). We searched the IRC catalog for counterparts at 9 and 18 μm , and the FIS catalog for counterparts at 65, 90, 140, and 160 μm . A large fraction ($\sim 70\%$) of our sources have a counterpart in at least one IRC band; relatively few ($\sim 11\%$) of our sources have a counterpart in at least one FIS band. The AKARI data cover the whole sky, and can provide valuable data to help populate the SEDs of our targets. For the majority of targets where we have AKARI counterparts, the AKARI data are consistent with WISE and/or IRAS measurements. We did not sort the AKARI matches by photometric quality; because our sources are bright, even those with low photometric quality flags matched the existing SED quite well. For the FIS sources where the photometric quality is the lowest, no errors are given, so we adopted a conservative uncertainty of 50% for those sources.

The Midcourse Space Experiment (MSX; Egan et al. 2003) surveyed the Galactic Plane in 1996-1997 at several bands between 8 and 21 μm – Band A=7.76 μm , B1=4.29 μm , B2=4.35 μm , C=11.99 μm , D=14.55 μm , and E=20.68 μm . The spatial resolution of these images range from 20'' to 72''. Relatively few (just 54) of our targets have MSX counterparts, in no small part because of sky coverage, but the lower sensitivity of the MSX instruments also plays a role. The errors we report in Table 1 are the errors reported in the MSX catalog, and as such may be very large.

The Deep Near Infrared Survey of the Southern Sky (DENIS) conducted a survey of the southern sky at I , J , and K bands. It is deeper than 2MASS. In several cases, because the search radius for a counterpart had to be large, it was clear upon construction of the SEDs that the nearest source by position was not the best match (often because a fainter source was closer to the given position than the real target), and so the match was rejected. In the end, only 58 of our targets have a K_s magnitude from DENIS, and none of those are lacking a 2MASS K_s . Therefore, the DENIS measurements do not play a role in identification of IR excesses, but were retained in those few cases to better define the SED.

The entire archive of photometric 3-24 μm cryogenic-era Spitzer Space Telescope (Werner et al. 2004) data has been reprocessed and images and source lists released as part of the Enhanced Imaging Products (SEIP). Spitzer is generally more sensitive (and has higher spatial resolution) than WISE or AKARI. However, the SEIP source list is limited to those with signal-to-noise ratios greater than 10. Because Spitzer is a pointed mission, the entire sky is not covered, and only 12% of our sources have counterparts in the SEIP source list. These measurements were retained in those few cases specifically because they are higher spatial resolution, and can provide valuable insight into the reliability of the flux densities provided by IRAS, AKARI, and WISE. We have found that the errors as reported in the SEIP are likely statistical and probably do not include a calibration uncertainty floor. We have added 4% errors in quadrature to the reported errors.

The Sloan Digital Sky Survey (SDSS; see, e.g., Ahn et al. 2014 and references therein) has surveyed a significant fraction of the sky at $ugriz$ (optical) bands. These data, where available, help define the Wien side of our objects' SEDs; they do not aid in calculation of IR excesses, but they 'guide the eye' to identify

the photosphere. About 30% of our targets have SDSS counterparts in at least one band. Several more of our targets appear in SDSS images, but are far too bright for reliable photometry. We used images and photometry as retrieved via IRSA’s FinderChart.

The Digitized Sky Survey (DSS) is a digitization of the photographic sky survey plates from the Palomar (the Palomar Observatory Sky Survey, POSS) and UK Schmidt telescopes. We used images from the DSS retrieved via IRSA’s FinderChart to check on source confusion and multiplicity.

NOMAD reports broadband optical photometry for most of our targets; C12 reports optical photometry for their targets. Those values were included in our database, as for the SDSS optical data above, to define the short-wavelength side of the SED.

4. Dropped Sources

In this section, we describe the set of targets that we have to drop from our dataset because they are not detected at sufficient bands (Sec. 4.1, Sec. 4.2), or that are likely subject to source confusion where the IRAS detection is likely composed of more than one source, or where the bright source in POSS is not responsible for the IR flux (Sec. 4.3). The 24 sources we identify as subject to source confusion come from studies with sources first identified in the low spatial resolution IRAS data and followed up in the optical.

4.1. Sources with Very Sparse SEDs

There are 10 sources that do not appear in many of the catalogs we used here, such that they have very sparsely populated SEDs. These SEDs are sparse enough that they cannot be handled in the same way as the other sources in the set – they have no K_s or [22] measures, and sometimes no WISE data at all. These sources are listed in Table 3. All of these very sparse SED stars are from Kirby et al. (2012), and are in dwarf spheroidal galaxies. They are just too far away to be detected in enough bands in the surveys we used. Comments on these objects appear in Table 3. For each source, we inspected the SED and the photometry, looking for any evidence of IR excess at the available bands, and found none.

These 10 sparse SED sources are, of necessity, frequently dropped from subsequent figures and discussion here. We reiterate, however, that they are all from the ‘additional literature’ sample; none are from C12 or dIR97.

4.2. Sources with Relatively Sparse SEDs beyond 10 μm

There are 36 sources that have relatively well-populated SEDs, but are missing detections past 10 or 20 μm . We cannot treat those sources in exactly the same way as the rest of the stars in the set, but at least we can constrain whether or not there is an IR excess, more so than for the stars in the previous section. These sources are listed in Table 3. There are two sources for which an IR excess cannot be ruled out given the available detections. The star known as “For 90067” could be consistent with an IR excess at 8 μm , given the available IRAC data, but the error on the [8] point is large. (Following the approach below in Sec. 5.4, but customized to this star, $\chi_{K,[8]}$ is 3.1.) SDSS J0632+2604 has a much more convincing excess, with a [3.4]–[12]=1.45.

These sources do not often appear in the subsequent figures and discussion, because they are, for example, missing [22], and thus cannot appear in a figure plotting [3.4]–[22]. However, the two possible excess sources here are sometimes included in the counts of sources with IR excesses, and where we do so, we note it explicitly. Nearly all of these sources (26/36) are objects we take to be Li-rich. Of these, SDSS J0632+2604 has the largest IR excess and also the largest Li abundance, with $A(\text{Li})_{\text{LTE}} = 4.2$ dex.

None of these relatively sparse sources are from the dIR97 sample. Seven of them are from C12, and the remainder are from the ‘additional literature’ sample.

Table 3. Objects with Sparse SEDs

name	very sparse SED? ^a	IR excess? ^b	notes
Scl 1004838	x	...	Distant object; not well-populated SED. No evidence for IR excess.
Scl 1004861	x	...	Distant object; not well-populated SED. No evidence for IR excess.
For 55609	No W3W4 but 3 IRAC bands; no evidence for excess.
For 60521	No W3W4 but 3 IRAC bands; no evidence for excess.
For 90067	...	x	No W3W4, but all 4 IRAC bands. Excess possible at 8 μm despite large error. Following the approach in Sec. 5.4 below, but customized to this star, $\chi_{K,[8]}$ is 3.1.
For 100650	x	...	Distant object; not well-populated SED. No evidence for IR excess.
G0300+00.29	No W4; no evidence for excess
SDSS J0304+3823	No W3W4; no evidence for excess
RAVEJ043154.1-063210	No W4; no evidence for excess
G0453+00.90	No W4; no evidence for excess
SDSS J0535+0514	No W4; no evidence for excess
Be 21 T50	No W4; no evidence for excess
SDSS J0632+2604	...	x	No W4; W3 suggests most likely has excess ($[3.4]-[12]=1.45$).
Tr5 3416	No W4; colors suggest could have small excess at $[12]$ ($[3.4]-[12]=0.41$); following the approach in Sec. 5.4 below, but customized to this star, $\chi_{[3.4],[12]}=1.97$, not significant.
SDSS J0654+4200	No W4; no evidence for excess
G0653+16.552	No W4; no evidence for excess
G0654+16.235	No W4; no evidence for excess
SDSS J0720+3036	No W3W4; no evidence for excess
SDSS J0808-0815	No W4; no evidence for excess
SDSS J0831+5402	No W3W4; no evidence for excess
SDSS J0936+2935	No W3W4; no evidence for excess
G0935-05.152	No W4; no evidence for excess
G0946+00.48	No W4; no evidence for excess
LeoI 71032	x	...	Distant object; not well-populated SED. No evidence for IR excess.
LeoI 60727	x	...	Distant object; not well-populated SED. No evidence for IR excess.
LeoI 32266	x	...	Distant object; not well-populated SED. No evidence for IR excess.
LeoI 21617	x	...	Distant object; not well-populated SED. No evidence for IR excess.
C1012254-203007	No W4; no evidence for excess
SDSS J1105+2850	No W3W4; no evidence for excess
LeoII C-7-174	x	...	Distant object; not well-populated SED. No evidence for IR excess.
LeoII C-3-146	x	...	Distant object; not well-populated SED. No evidence for IR excess.
G1127-11.60	No W4; no evidence for excess
M68-A96=C1* NGC 4590 HAR 1257	No W4, but all 4 IRAC bands. No evidence for excess.
SDSS J1310-0012	No W3W4; no evidence for excess
CVnI 195.195	No W3W4, but 3 IRAC bands. No evidence for excess.
CVnI 196.129	x	...	Distant object; not well-populated SED. No evidence for IR excess.
M3-IV101=C1* NGC 5272 SK 557	No W4, but all 4 IRAC bands. No evidence for excess.
SDSS J1432+0814	No W3W4; no evidence for excess
SDSS J1522+0655	No W3W4; no evidence for excess
SDSS J1607+0447	No W3W4; no evidence for excess
SDSS J1901+3808	No W4; no evidence for excess
SDSS J1909+3837	No W4; no evidence for excess

Table 3—Continued

name	very sparse SED? ^a	IR excess? ^b	notes
KIC 4937011	No W4, but all 4 IRAC bands. No evidence for excess.
SDSS J2019+6012	No W4; no evidence for excess
SDSS J2200+4559	No W4; no evidence for excess
SDSS J2206+4531	No W4; no evidence for excess

^aThis column is populated if the SED is very sparse (Sec. 4.1).

^bThis column is populated if the object could have an IR excess by 8 to 12 μm (Sec. 4.2).

4.3. Source Confusion

As mentioned above, it is often the case that a bright source in IRAS is also a bright source in the optical, but sometimes this is not a good assumption. Now that 2MASS and WISE images are available, it is far easier than it was in the 1990s to identify sources over 3 orders of magnitude in wavelength (0.5 to 100 μm). In 24 of our targets, we believe that there are likely issues of source confusion. In these cases, at least one of the following things can be seen in the images: (a) the IR excess seen in the IRAS images is due to more than one WISE (or 2MASS) source, likely unresolved in the IRAS catalog; or (b) the nearest bright source in POSS, which is most likely the source for which an optical spectrum to measure lithium was obtained, is not responsible for most of the IR flux density detected via IRAS.

For the first kind of source confusion, where the IR excess seen in IRAS is due to more than one WISE source, understanding the original IRAS resolution is important, because these issues of IRAS spatial resolution can be subtle. Figure 1 shows a WISE 12 μm image of one of our targets, IRAS06365+0223, with circles overlaid to represent the various possible IRAS resolutions. The image is $300''=5'$ on a side. The original IRAS PSC was derived from images that had pixels that were substantially rectangular, but included sources believed to be point sources with sizes less than $\sim 0.5\text{--}2.0'$ in the *in-scan direction*⁴. The small green circle in Fig. 1 is representative of this 12 μm 0.5' resolution, and the large blue circle is representative of this 100 μm 2' resolution. Note that these are shown in the figure as circles, whereas in reality, this resolution is only obtained in the in-scan direction, which is roughly along lines of ecliptic longitude; the resolution is considerably worse in the cross-scan direction. (For this target, lines of ecliptic longitude are locally about 5° east of North, but this angle varies over the sky.) The typical FWHM of sources in the ISSA data products (ISSA images are shown in FinderChart) is $3.4'\text{--}4.7'$ ⁵, which is represented by the large red circle in Fig. 1 at 3.4' (diameter). The multiple sources seen in this WISE image, for example, are likely convolved together for at least some of the IRAS measurements. This is an important factor in several of the IRAS sources we discuss in this section, meaning that the IR flux attributed to a single optical source may not be correct, and the IR excess previously measured for a given optical source may be significantly overestimated.

The second kind of source confusion, where the bright source in POSS is not responsible for the IR flux, is source confusion of a different nature. In many cases, it is a good assumption that the bright source in IRAS is also the bright source in POSS. However, in a significant number of cases, all the sources in the region are of comparable brightness in POSS, or the optically bright source is not the source of most of the IR light. Now that 2MASS and WISE are available, we can trace the source across wavelengths to securely identify the optical counterpart in the POSS images. In these cases, however, the spectrum obtained to assess lithium may very well have been of the bright POSS source, and not of the origin of the IR flux at all, especially in those cases where no optical counterpart can be found in the POSS images.

To demonstrate these issues of source confusion, we provide POSS, 2MASS, and WISE images for each of the 24 targets in Figures 2–7, specifically to allow readers to follow the same sources across wavelengths. (The FITS images can be interactively explored via IRSA's FinderChart.) For each of these figures, either a multi-color or single band image appears for each of POSS, 2MASS, and WISE, and the images are $300''$ on a side unless specified. For POSS, it is either DSS2 Blue/Red/IR for the blue, green, and red bands, respectively, or it is a single-band DSS2 Red. For 2MASS, JHK_s corresponds to blue/green/red, respectively, and for WISE, [3.4], [4.5], and [12] correspond to blue/green/red unless specified. The source position is

⁴<http://irsa.ipac.caltech.edu/IRASdocs/exp.sup/ch5/A2.html>

⁵<http://irsa.ipac.caltech.edu/IRASdocs/issa.exp.sup/ch1/C.html>

indicated with a small blue circle; white or black hash marks above and to the left help guide the eye to this position. A brief discussion of each of these sources appears in Table 4; a briefer still summary appears in the Figure itself and the caption.

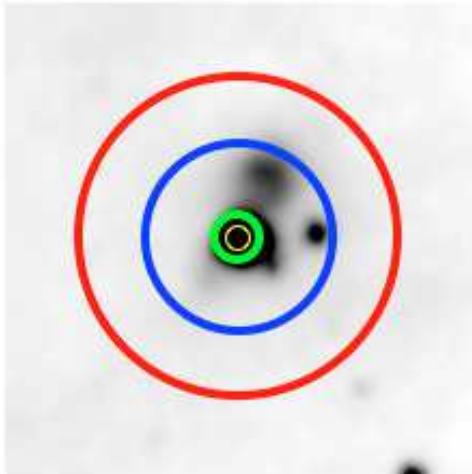


Fig. 1.— Image of IRAS06365+0223 in [12], reverse greyscale, $300''$ on a side as most of the subsequent image postage stamps are. The circles represent the range of IRAS spatial resolutions; see text for more discussion. The red circle is $3.4'$ in diameter, representative of the typical FWHM of shorter-wavelengths sources in the ISSA images. The blue circle and the green circle are 2 and $0.5'$ in diameter, and represent the in-scan direction resolution of the IRAS PSC. The small yellow circle here is $15''$ in diameter, representative of the ‘target’ blue circle in subsequent $300''$ images. (It is yellow instead of blue just for enhanced visibility in this reverse greyscale image.)

SEDs for these 24 sources appear in Figures 8 and 9. These SEDs correspond in most cases to the source position measured in IRAS, but may or may not be the origin of all of the IRAS flux density, or correspond to the optically bright source. Because we are matching sources largely by position to the sources in the catalogs, in several of the cases illustrated in Figure 2-7 where the true counterpart is impossible to match, the counterparts across catalogs are not the same source, and the SED clearly betrays this conglomeration of sources (see notes in Table 4). IRAS18334-0631(PDS524) (Fig. 9, 3rd row center) is the clearest example of this, where AKARI and MSX are seeing the same source, but it is a different source than the source that 2MASS, DENIS, and WISE identify, both of which are inconsistent with the flux densities measured in IRAS.

Eight of these sources have SEDs that do not resemble isolated stars. They rise steadily from 1 to 20 or even $100 \mu\text{m}$ and beyond. These would be SEDs consistent with extragalactic sources, or very heavily obscured stars of any age. These sources are noted in Table 4; IRAS16128-5109 is one of the best examples (Fig. 8, 3rd row center). This source has measurements from 2MASS, WISE, MSX, AKARI, and IRAS, with the energy density at $\sim 20 \mu\text{m}$ being ~ 5 orders of magnitude larger than the energy density at $\sim 1 \mu\text{m}$. The IRAS data suggest a rollover in this SED near $60 \mu\text{m}$. Most of these steep SEDs turn over at long wavelengths, but two of these eight sources have a peak in the SED at $\sim 22\text{-}25 \mu\text{m}$, shorter than the others. These two sources, IRAS17582-2619 and IRAS19083+0119(PDS562), could be of a different nature than the others.

One of these sources, IRAS17211-3458, is worthy of a few additional comments here because it is the most borderline of these source confusion cases. The images shown in Fig. 5 (second row) show a small concave arc of sources in the optical near the target location; by H (middle panel), it is a convex arc of sources, where only two sources (including our target) are bright in the POSS+2MASS images – they appear white in the 2MASS image in Fig. 5. We identified source confusion here in part because these two sources are of comparable brightness at POSS, but also because WISE has trouble resolving the three close, IR-bright sources. WISE identifies some faint nebulosity here; in the WISE image in Fig. 5, the surface brightness is barely visible. However, there are Spitzer data here too, which resolves complex striated nebulosity; see Figure 10. The IRAS target position is $\sim 2''$ from the nearest 2MASS source, which is larger than typical uncertainties over the whole catalog. The Spitzer source corresponding to this object does not appear in the SEIP, perhaps because it either is or appears to be slightly resolved because of the high surface brightness nebulosity surrounding it. The SED (Fig. 9, top center) is the source closest to the target position, where available. On the face of it, its shape would be consistent with a photosphere with large excess. That, plus the fact that there is a POSS source exactly at the location of the IRAS source (and is presumably the object for which an optical spectrum to assess lithium was obtained), could conceivably place it in the set of objects with large excesses identified and discussed below. However, based on the images, bands longer than $12\ \mu\text{m}$ (WISE, MSX, AKARI, IRAS) certainly are measuring net flux density from more than one point source, plus nebulosity near (in projection) to the source. This is also the point at which the SED starts to significantly diverge from the apparent photosphere. Because of this ambiguity, we have left it in the set of confused sources. It is not tagged as a Li-rich source in dLR97, so even if we were able to add it to the analysis we perform below, it is unlikely to have contributed significantly.

Because of the ambiguity about the sources and their counterparts, these 24 sources have to be dropped from our sample. IRAS07419-2514 was identified as a possible K giant in Torres et al. (2000), and PDS97 (IRAS17554-3822) is from de la Reza, Drake, & da Silva (1996). The remaining 22 sources compose $\sim 30\%$ of the original dLR97 sample. We drop these sources from the bulk of our analysis, but show them in certain plots where relevant below.

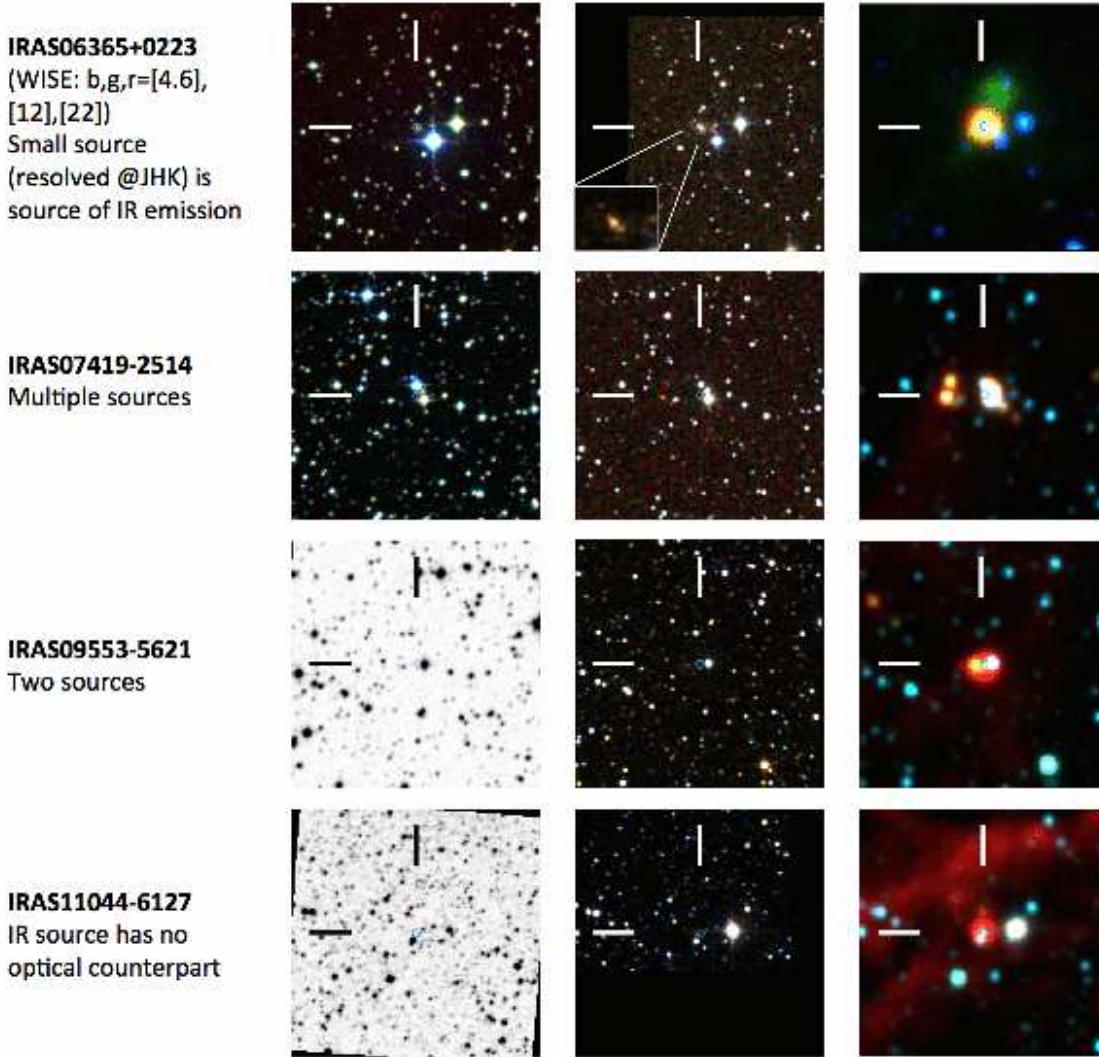


Fig. 2.— First image column: POSS 3-color (DSS2 Blue/Red/IR for b/g/r planes), or it is a single-band reverse greyscale DSS2 Red. Second image column: 2MASS JHK_s color image. Third image column: WISE [3.4], [4.6], [12] for b/g/r, respectively, unless specified. Images are all $300''$ on a side unless specified. North-up. Small blue circle centered on position used for the target, and white/black hash marks above and to the left help guide the eye to this position. Four rows are: (1) IRAS06365+0223, where the 2MASS image has an additional inset with an enlargement of the source of the IR flux, and WISE has b,g,r=[4.6],[12],[22]. The target position is correctly the source of most of the long-wavelength flux, but is not a match to either of the optically bright sources. (2) IRAS07419-2514. The target position is in amongst a small cluster of sources, and corresponds to the photocenter of the aggregate source seen by IRAS. (3) IRAS09553-5621. The target position is in between two sources bright at WISE bands, but only one source appears at K_s . That source that appears at K_s also appears in POSS images. The sources are not separable at [22], and are likely both contributing to the measured IRAS flux density. (4) IRAS11044-6127. There is no easily visible source at the target position in POSS; the bright source seen as white immediately to the West of the target is the brightest source in the field in the DSS-IR and 2MASS, but it is comparably bright to the other stars in DSS.

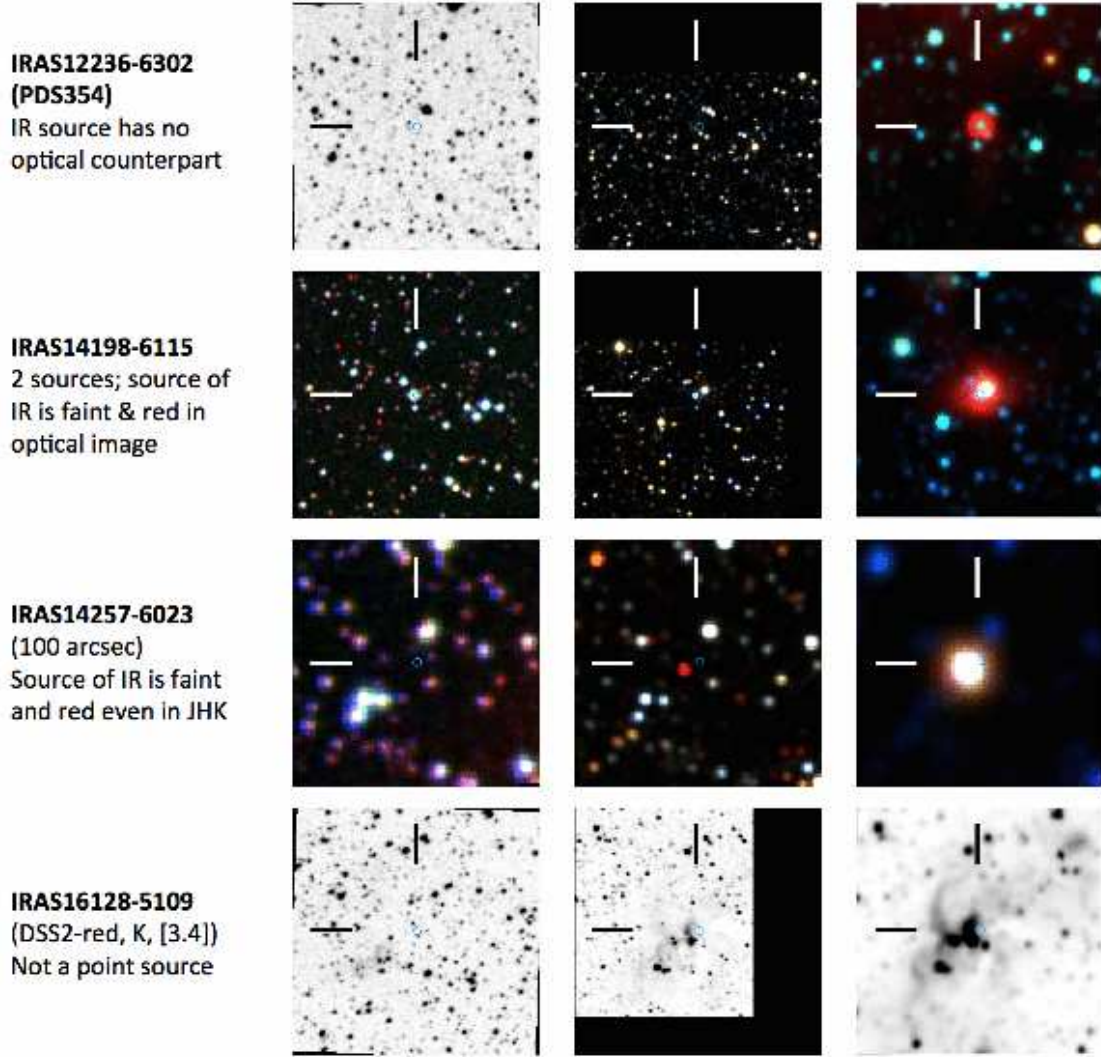


Fig. 3.— (Notation is as in Fig. 2.) Four rows are: (1) IRAS12236-6302 (PDS354). The blue arc immediately above the target in WISE can be seen to be 3 distinct sources in 2MASS and, combined, are the brightest thing in the POSS 300'' images. These sources are not responsible for most of the IR flux measured at the target position. (2) IRAS14198-6115. There are two sources here that are distinct in 2MASS and marginally resolved in [3.4], but are indistinguishable by [22]. (3) IRAS14257-6023. Images are 100'' on a side to better show the source that is very red in 2MASS and is dominating the measured flux by WISE bands. The brightest source in POSS is the source appearing as white in 2MASS to the North and slightly West of the target position, but it is not responsible for the IR flux. (4) IRAS16128-5109. This is not a point source in the IR, and is very bright (saturated in WISE) by [22]. Single bands are shown in the optical, NIR, and MIR to better show the nebulosity.

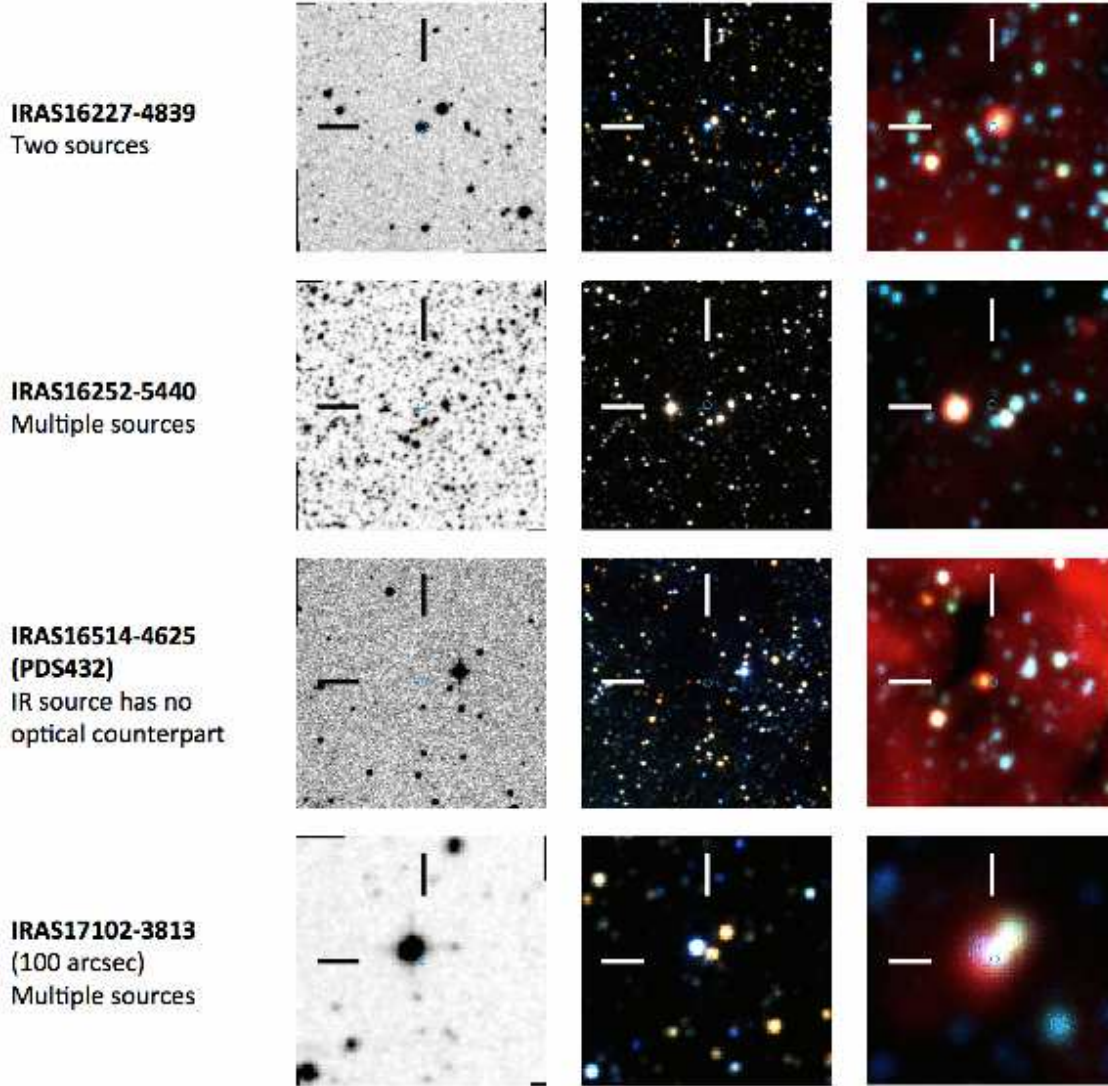


Fig. 4.— (Notation is as in Fig. 2.) Four rows are: (1) IRAS16227-4839. There are two sources here that are resolved in 2MASS and marginally resolved at [3.4], but merged by [22], with the more northerly source dominating the IR flux. The more southerly source is brighter in POSS. (2) IRAS16252-5440. There is a cluster of sources that is responsible for the IR flux, with the target position at the photocenter. The field has no clearly dominant source in POSS. (3) IRAS16514-4625(PDS432). A dark cloud is apparent in 2MASS and WISE. The brightest source in the optical is the center of the source seen in WISE as blue but not a point source because it aggregates 3 sources seen in 2MASS. The source that dominates by [22] is faint at [3.4]. (4) IRAS17102-3813. Images are 100'' on a side to better show the trio of sources seen at JHK_s that become a smear dominated by the two sources to the southeast by [22]. The optically brightest source may contribute some but not all of the 22 μm flux density.

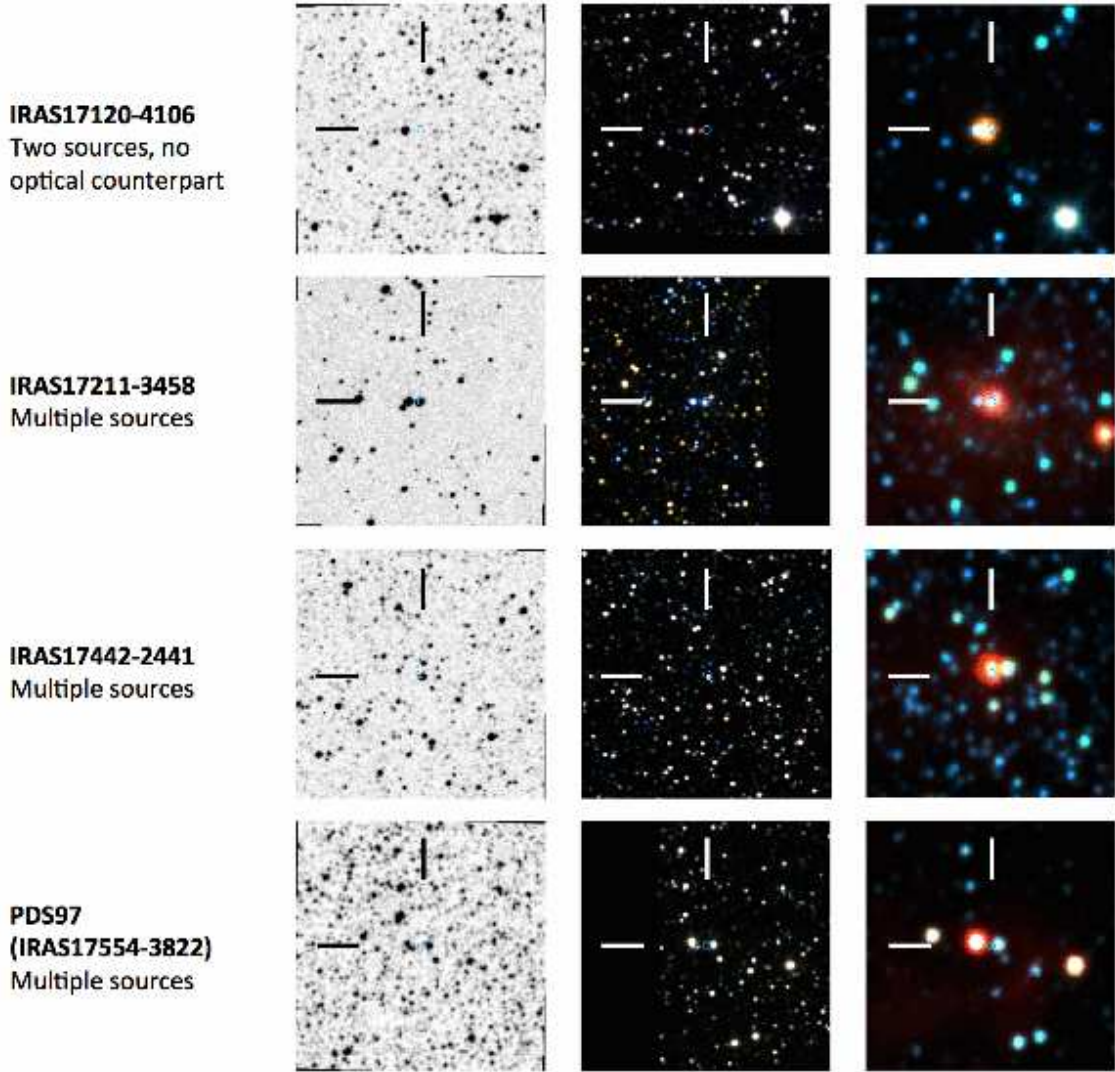


Fig. 5.— (Notation is as in Fig. 2.) Four rows are: (1) IRAS17120-4106. Two sources are barely resolved at [3.4] that merge by [12] and [22]. There is no optical counterpart at the source position. (2) IRAS17211-3458. There are multiple sources that are barely resolved at [3.4], which merge at longer wavelengths. This is a complicated source; see the text. (3) IRAS17442-2441. Two sources at the source position are barely resolved at [3.4] that merge by [12] and [22] with each other and with other sources in the region. (4) PDS97(IRAS17554-3822). Source position is in between two sources that are of comparable brightness at [3.4] (and, for that matter, POSS and 2MASS), with the easterly source dominating by [22].

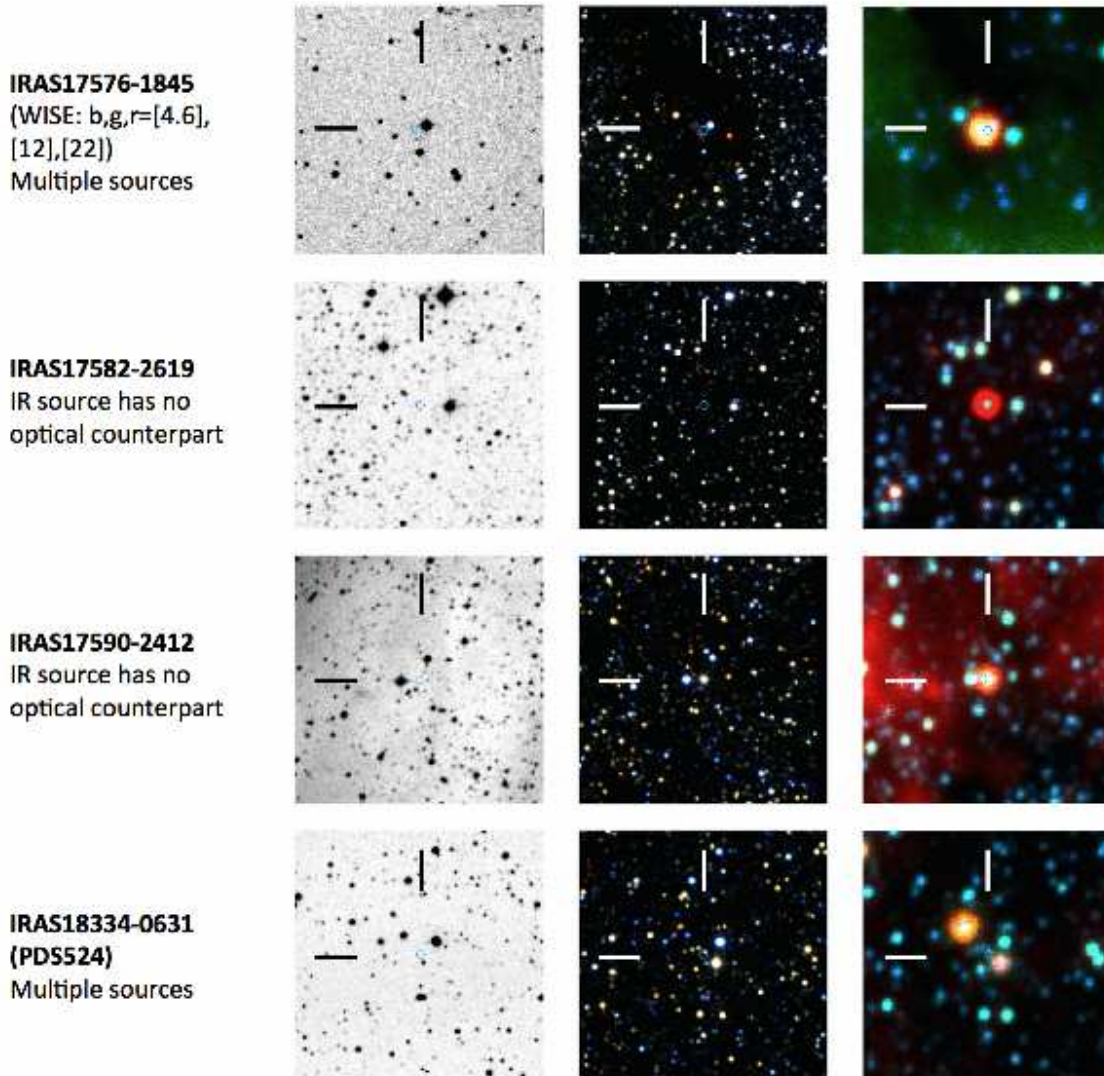


Fig. 6.— (Notation is as in Fig. 2.) Four rows are: (1) IRAS17576-1845. The source dominating at [22] (and presumably IRAS bands) is smeary at [3.4]. The brightest source at POSS bands is not the source of the IR. (2) IRAS17582-2619. The brightest source in the IR has no optical counterpart, and is strongly dominated by the longest wavelengths. (3) IRAS17590-2412. The brightest source in the IR has no optical counterpart, and is strongly dominated by the longest wavelengths. Diffuse emission can also be seen. (4) IRAS18334-0631(PDS524). There is no optical source at the target position; the target’s IRAS flux has contributions from several sources in this vicinity, including the arc of blue in WISE precisely at the target position. The brightest POSS source is blue in WISE.

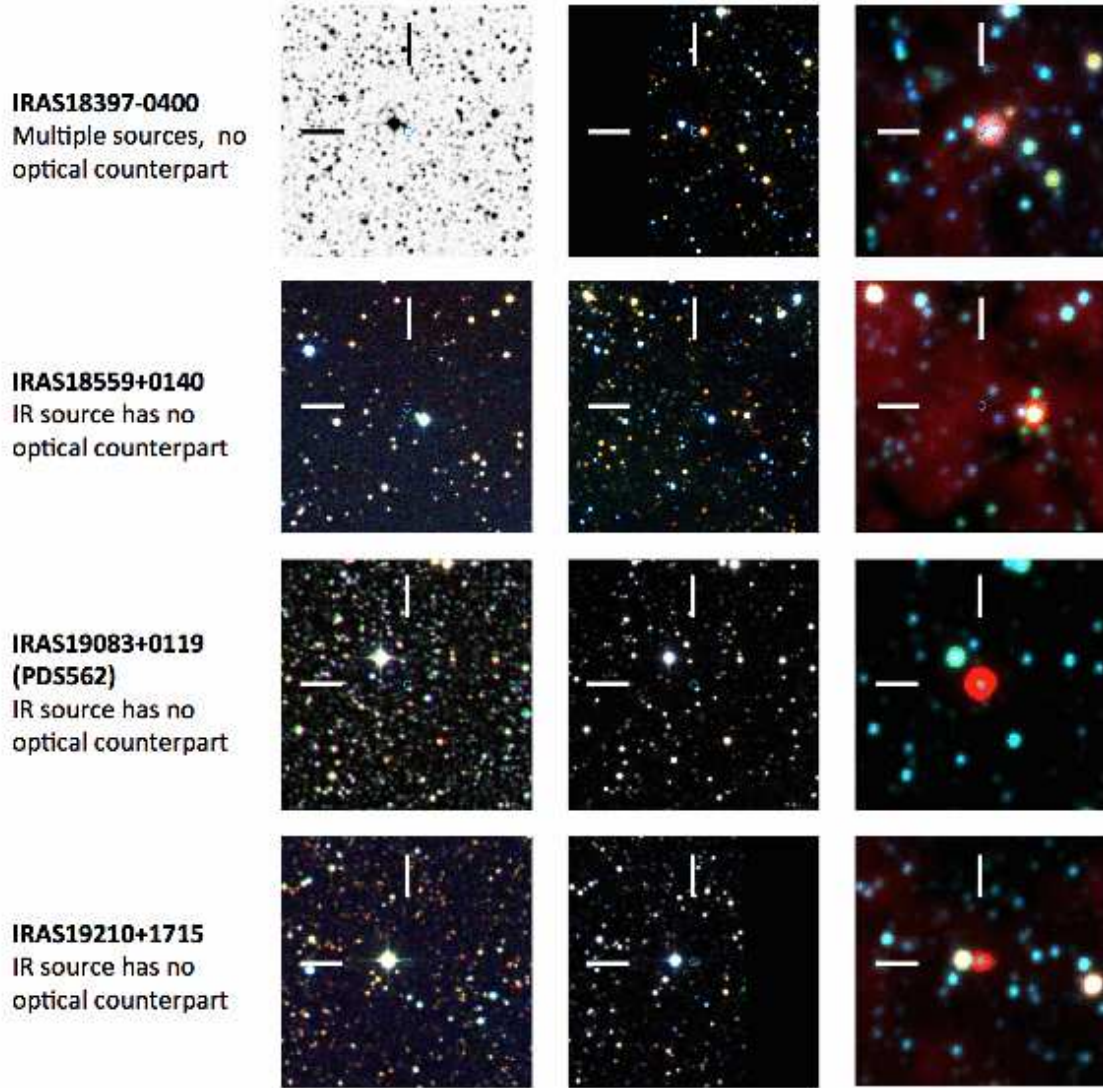


Fig. 7.— (Notation is as in Fig. 2.) Four rows are: (1) IRAS18397-0400. The brightest source in the IR has no optical counterpart, and is dominated by the longest wavelengths. The brightest POSS source is blue in WISE. (2) IRAS18559+0140. There is no optical source at the target position; the bright POSS source to the southwest is not bright at all in the IR and is blue in the WISE data; the target’s IRAS flux has contributions from several sources, most likely including the flux from the bright source to the upper left, pulling the photocenter off of the bright clump of sources to the right. (3) IRAS19083+0119(PDS562). The brightest source in the IR has no optical counterpart, and is strongly dominated by the longest wavelengths. The brightest POSS source is blue in WISE. (4) IRAS19210+1715. There is no optical source at the target position; the bright POSS source to the east can be seen in the IR, but the target position matches the very red source to the west, which most likely dominates the IRAS flux.

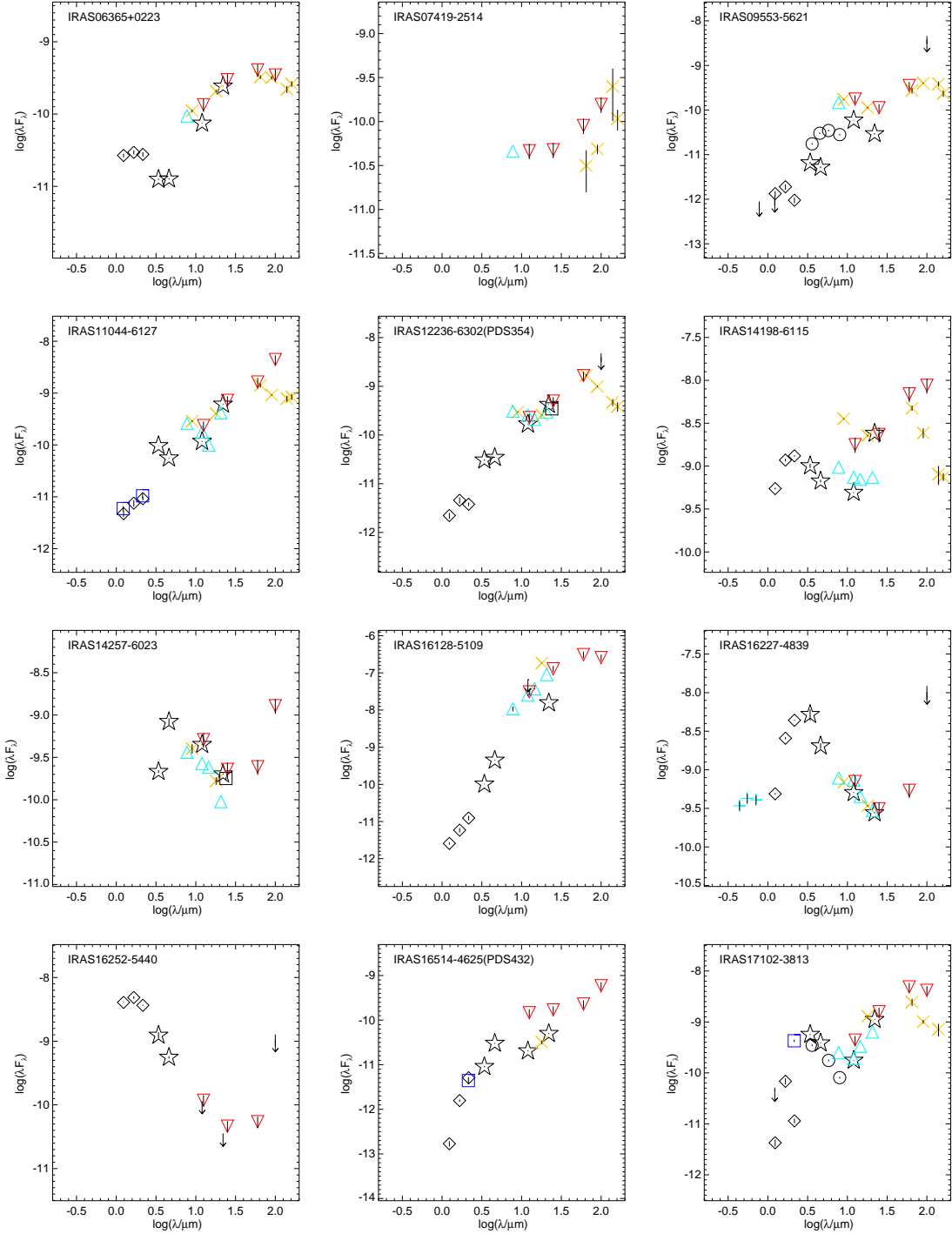


Fig. 8.— SEDs for things that are likely subject to source confusion, part 1. Notation for all SEDs in this paper is as follows. The axes are $\log \lambda F_\lambda$ in cgs units ($\text{ergs s}^{-1} \text{cm}^{-2}$) and $\log \lambda$ in microns. Symbols: cyan + are literature $UBRI_c$; black + are SDSS $ugriz$; black diamonds are 2MASS JHK_s ; blue squares are Denis IJK ; black circles are from Spitzer/IRAC; black stars are WISE; yellow \times are AKARI; cyan triangles are MSX; black squares are Spitzer/MIPS ($24 \mu\text{m}$); red downward pointing triangles are IRAS PSC and FSC. Any arrows are limits at the corresponding wavelength. Error bars are indicated as vertical black bars at the center of each point. See text and Table 4 for discussion of individual objects.

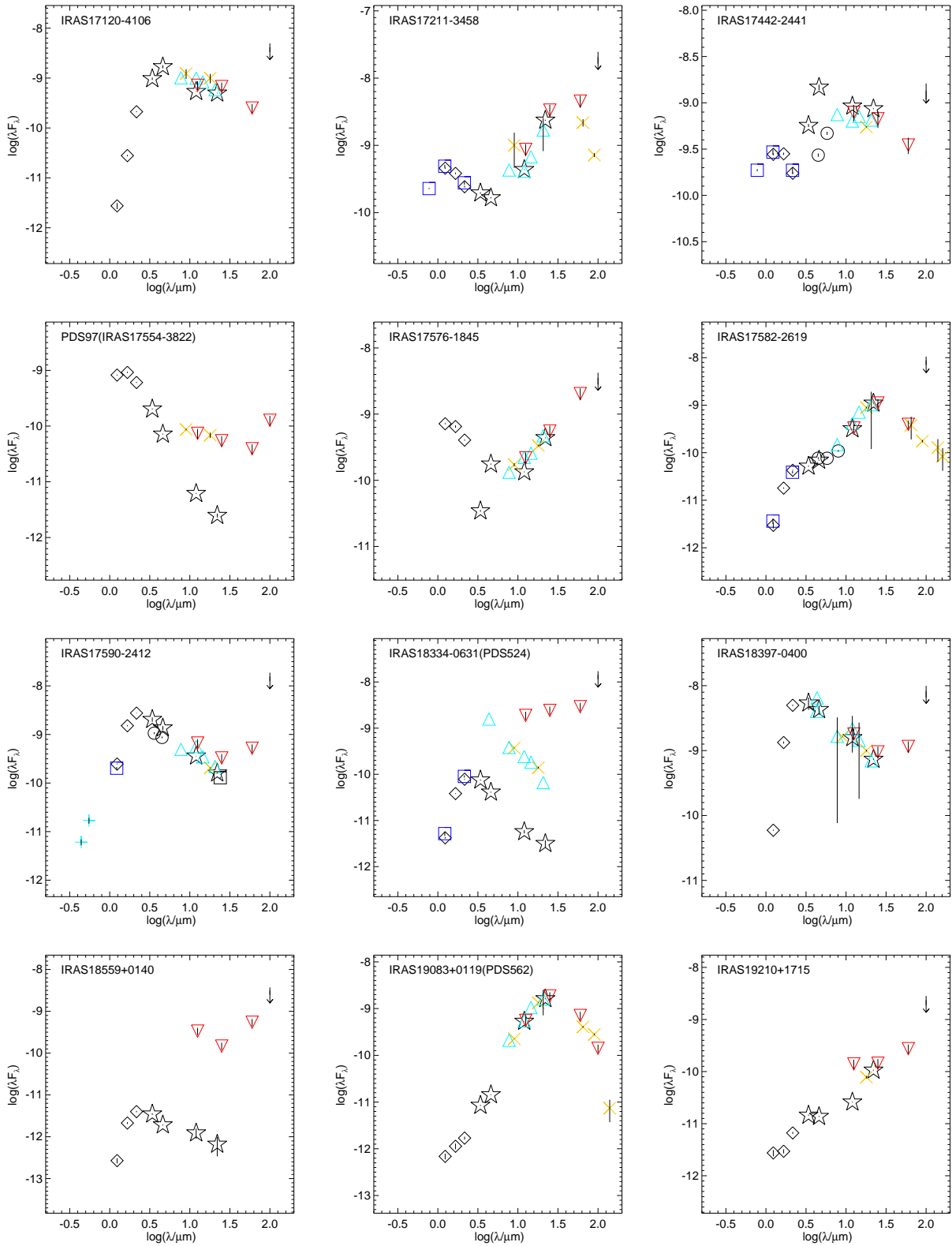


Fig. 9.— SEDs for things that are likely subject to source confusion, part 2; notation is as described in Fig. 8. See text and Table 4 for discussion of individual objects.

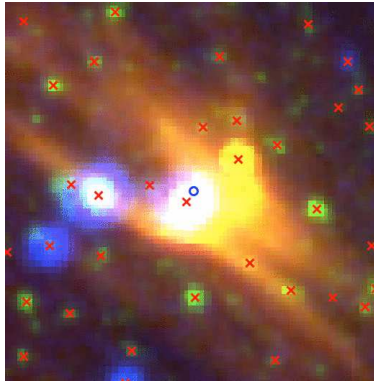


Fig. 10.— 3-color image of IRAS17211-3458, about an arcminute on a side, North-up. Blue plane is DSS 2 red plates, green plane is IRAC-2 ($4.5 \mu\text{m}$), and red plane is IRAC-4 ($8 \mu\text{m}$). Blue circle is target position, and red \times are sources from the 2MASS (point source) catalog. The target position is $\sim 2''$ from the source taken as the 2MASS match. There is complex long-wavelength emission here. Photometric measurements $>10 \mu\text{m}$ combine flux densities from more than one source, plus nebulosity, and so we have left this source in the set of sources likely subject to source confusion.

Table 4. Objects that are dropped from the main sample

name	src conf? ^a	steep SED? ^b	notes
IRAS06365+0223	x	...	Target position on an optically faint source within a grouping of optically bright sources, and corresponds to a very red, resolved source seen as resolved in K_s (fluxes retrieved from 2MASS extended source catalog). This extended source is the origin of most of the long-wavelength flux. dIR97 source.
IRAS07419-2514	x	...	Target position in amongst a grouping of optically bright sources, with somewhat different sources bright in the IR. Position corresponds to the photocenter of the aggregate source seen by IRAS. Because target center does not correspond to an optically detected source, there are no short-wavelength measurements in the SED (so it appears to have a sparse SED). Source identified in Torres et al. (2000), and notes there say that IRAS flux may come from CO cloud WB 1046. IRAS flux probably attributable to ≤ 5 IR-bright sources seen in WISE.
IRAS09553-5621	x (m?)	x	Target position in between two sources that are comparably bright at 4.6 μm . Only one source is apparent at optical through K_s , and by 22 μm , the sources have merged into one apparent source, likely responsible for the measured IRAS flux. SED assembled from closest source by position and thus may represent fluxes from different sources. Steep SED. AKARI consistent with IRAS at longest bands. dIR97 source.
IRAS11044-6127	x	x	High surface density of comparably bright sources in the optical; no easily visible source exactly at the target position in the optical. There is a faint source that starts to appear in 2MASS images, and a source to the West that becomes bright. The source exactly at the target position is still faint and blended with a source to the south at 3.4 μm . The target source is rising fast and dominates by 12 μm , dominating all the sources in the field by 22 μm (and therefore probably dominates the measured IRAS flux). Steep SED. dIR97 source.
IRAS12236-6302(PDS354)	x	x	Another crowded field with comparably bright sources in POSS; there is an optically brighter source above and to the West of the target position that can be seen to be three distinct sources in 2MASS. In WISE, these sources are not resolved and form a blue arc immediately above the target. A source at the target location strongly dominates the field at 12 and 22 μm , and is presumably responsible for most of the IRAS flux (and, for that matter, that from MSX and AKARI). Steep SED. dIR97 source. Torres et al. (2000) mention that their optical spectrum of the source they took to be the counterpart of the IR emission has strong H α emission and could be an H II region.
IRAS14198-6115	x (m?)	...	There are two sources here that are distinct in 2MASS and marginally resolved in [3.4] (though AllWISE catalog identifies only one), but are indistinguishable by [22]. There are several sources in this vicinity in the optical. SED assembled from closest source by position and thus likely represents fluxes from different sources. dIR97 source.
IRAS14257-6023	x (m?)	...	The brightest source in POSS is to the North and slightly West of the target position, but it is not responsible for the IR flux. There is a source to the southeast that is very red in 2MASS and is dominating the measured flux by WISE bands, and is likely responsible for the IRAS flux. SED assembled from closest source by position and thus may represent fluxes from different sources. dIR97 source.
IRAS16128-5109	x	x	This is not a point source in the IR, and is very bright (saturated) by [22]. It appears in SIMBAD as an H II region; the morphology of the image suggests a dense clump of sources from which emanate long streamers of extended emission. Steep SED. dIR97 source.
IRAS16227-4839	x		There are two sources that are resolved in 2MASS and marginally resolved at [3.4], but merged by [22], with the more northerly source dominating the IR flux. The more southerly source is brighter in POSS. Some extended emission visible in WISE. dIR97 source.
IRAS16252-5440	x		This is also PDS 146. In POSS, there is a high surface density of comparably bright sources. By 2MASS, an aggregate of at least 4 IR-bright sources is apparent. In WISE, it can be seen that the target position corresponds roughly to the photocenter of the aggregate of sources seen at [12]. The brightest source by [22] is to the East of the target position and is probably responsible for most of the IRAS flux. The SED we have assembled for this source corresponds to the source closest by position to the target position, and as such does not represent correctly the source of the longest wavelength flux. dIR97 source. Torres et al. (1995) lists this as “other” and “probably not young”, and later implies it may be a normal MS star.

Table 4—Continued

name	src conf? ^a	steep SED? ^b	notes
IRAS16514-4625(PDS432)	x	x	A dark cloud is apparent near this source in WISE images. The brightest source in the optical is to the northwest of the target position, which is resolved into at least 3 sources in 2MASS. The source that dominates the IR by [22] (and probably also IRAS) is faint at [3.4]. Steep SED. d1R97 source. Torres et al. (2000) list it as a confirmed giant but the source that was measured may not be responsible for the IR flux.
IRAS17102-3813	x (m?)	...	A trio of sources seen at 2MASS become a smear dominated by the two sources to the southeast by [22]. The optically brightest source may contribute some but not all of the [22] (and IRAS) flux. SED assembled from closest source by position and thus may represent fluxes from different sources. d1R97 source.
IRAS17120-4106	x		Nothing is at the target position in POSS, though there is a source straight East of the target position. That easterly source persists through [3.4]. There is a faint source closer to the target position appearing by K_s . The two sources are barely resolved at [3.4], and merge by [12] and [22]. Given the [22] photocenter, some flux is likely attributable to each source, even in WISE. d1R97 source.
IRAS17211-3458	x (m?)	...	Two comparably bright sources are resolved in POSS, and in 2MASS. The two sources are barely resolved at [3.4] and merge by [12] and [22]. SED assembled from closest source by position, so may represent fluxes from different sources. d1R97 source. See text for additional discussion.
IRAS17442-2441	x (m?)	...	The DSS images are dense with sources of comparable brightness, though there is a source close to the target position. Similarly, in 2MASS, no source dominates, though there is a source close to the target location. There is a source at the target position and another comparably bright one to the West just resolved at [3.4]; they merge by [12] and [22]. SED assembled from closest source by position and thus may represent fluxes from different sources. d1R97 source.
PDS97(IRAS17554-3822)	x (m?)	...	Target position in between two sources of comparable brightness at POSS and 2MASS. It is also between two comparably bright sources at [3.4] and [4.6]; by [12] the easterly source dominates, and by [22], all the flux is likely from the easterly source. Source from la Reza, Drake, & da Silva (1996). Gregorio-Hetem et al. (1992) list it as a high velocity giant with strong Li, and “incorrect identification in PSC” because KL Cra is $78''$ to east, outside error ellipse. SIMBAD lists it as a T Tauri.
IRAS17576-1845	x		The multi-wavelength images suggest extinction in this field. The source position is reasonably close to a bright POSS source, but the target position can be seen to have several sources in 2MASS and WISE. The source dominating at [22] (and presumably IRAS bands) is ‘smearly’ at [3.4]. d1R97 source. Coadella et al. (1995) list it as a candidate to be related to high-mass star forming regions with an ultracompact H II region, though it remained undetected in their survey.
IRAS17582-2619	x	x	The brightest source in the IR has no optical counterpart, and the IR is strongly dominated by the longest wavelengths. The optically brightest source is to the west of the target source, and has faded substantially by [12] and [22] μm . Steep SED to 20 μm , well-defined, with data from multiple surveys in good agreement with each other. Turnover from steep SED happens abruptly at $\sim 20 \mu\text{m}$, shorter wavelengths than most of the other steep SEDs identified here (the other one like this is IRAS19083+0119(PDS562)). d1R97 source. SIMBAD lists this as an OH/IR star. Yoon et al. (2014) and references therein identify it as a post-AGB star (OH4.02-1.68). It appears in Ramos-Larios et al. (2012) and as a heavily obscured post-AGB star or PN candidate, and García-Lario et al. (1997) as a PN candidate. It appears in de la Reza et al. (2015) as an early AGB star.
IRAS17590-2412	x		The brightest source in the IR has no optical counterpart, and is strongly dominated by the longest wavelengths. Diffuse emission can also be seen in the field in various bands. d1R97 source. Messineo et al. (2004) identify a SiO emitter in this region but suggest that it may not be associated with the source from which an optical spectrum had been obtained by d1R97. They note that this IRAS source is the only mid-infrared source within their 86 GHz beam.

Table 4—Continued

name	src conf? ^a	steep SED? ^b	notes
IRAS18334-0631(PDS524)	x (m?)	...	There is no optical source at the target position; the target’s IRAS flux likely has contributions from several sources in this vicinity, including a source resolved as an arc in WISE [3.4] & [4.6] precisely at the target position. The brightest POSS source is to the northwest of the target, and the brightest source by K_s is to the southwest. The brightest source by [22] is to the northeast. SED assembled from closest source by position and thus likely represents fluxes from different sources. dIR97 source.
IRAS18397-0400	x		The brightest source in the IR has no optical counterpart, and is dominated by the longest wavelengths. The brightest POSS source is to the northeast, though it is no longer the brightest source by 2MASS. The source responsible for most of the IR flux is slightly to the west of the target position, and is visible in 2MASS. MSX measurements have very large errors but are consistent with the rest of the SED. dIR97 source.
IRAS18559+0140	x (m?)	...	There is no optical source at the target position; a bright POSS source is to the southwest and is not bright at all in the IR. The target’s IRAS flux has contributions from several sources, including a small clump to the east; the photocenter is pulled to the west, off of the bright clump of sources, and this offset of the IRAS position is the farthest off from the WISE source in the entire dataset. The assembled SED corresponds to the closest source by position and as such does not represent the brightest IR source here, and likely represents more than one source. dIR97 source.
IRAS19083+0119(PDS562)	x	x	The brightest source in the IR has no optical counterpart, and is strongly dominated by the longest wavelengths. There is a faint source at the target position by K_s and it rises quickly through the WISE bands. Steep SED, with data from several surveys in good agreement with each other. Turnover from steep SED happens near $\sim 20 \mu\text{m}$, shorter wavelengths than most of the other steep SEDs identified here (the other one like this is IRAS17582-2619). dIR97 source. SIMBAD lists it as a possible planetary nebula. Yoon et al. (2014) and references therein identify it as a post-AGB star.
IRAS19210+1715	x	x	There is no optical source at the target position; though there is a bright POSS source to the east, which can be seen in the IR. However, the target position matches a very red source, marginally visible in the 2MASS images, and rising quickly through the WISE bands, which most likely dominates the IRAS flux. There may be a contribution at [22] from a nearby source bright at [12]. Steep SED. dIR97 source.

^aThis column is populated if the object is likely subject to source confusion of either of the sorts described in the text. “x (m?)” indicates that there may be multiple sources represented in the SED, e.g., the object shown in the SED at $2 \mu\text{m}$ may not be the same object as that shown at $22 \mu\text{m}$.

^bThis column is populated if the object’s SED rises steadily from 2 to at least $20 \mu\text{m}$, as described in the text.

Table 5. Sources with IR excesses^a

name	[3.4]−[22]	$\chi_{[3.4],[22]}$	Sample	data codes ^b	drop? ^c	lit? ^d	start ^e
IRAS00483-7347	4.71	(large)	Castilho et al. 1998	W M A I S	D?	...	<2
NGC 362 V2	1.13	9.7	Smith et al. 1999	W S	5
HD19745	2.32	(large)	dIR97, Kumar et al. 2011	W A I	...	IRx	10
IRAS03520-3857	8.80	(large)	dIR97	W A I	2?
IRASF04376-3238	3.83	(large)	Torres et al. 2000	W A I	3?
IRAS07227-1320(PDS132)	6.64	(large)	dIR97	W M A I	5?
IRAS07456-4722(PDS135)	5.40	(large)	dIR97	W A I	3?
HD65750	dIR97, Castilho et al. (2000)	(W) A I	...	IRx	2?
IRAS07577-2806(PDS260)	8.75	(large)	dIR97	W M A I	3?
HD233517	5.53	(large)	dIR97, Kumar et al. 2011	W A I	...	IRx	10
IRASF08359-1644	6.00	(large)	Torres et al. 2000	W A I	3?
G0928+73.2600	0.63	6.4	C12	W	22
HD96195	Castilho et al. 2000	(W) M A I	D?	IRx	10
Tyc0276-00327-1	0.36	3.4	C12	W A	22
IRAS12327-6523(PDS355)	3.56	(large)	dIR97	W M A I	2
HD111830	0.63	3.7	dIR97	W A I S	22
PDS365(IRAS13313-5838)	7.37	(large)	dIR97, Kumar et al. 2011	W M A I	...	IRx	2?
PDS68(IRAS13539-4153)	6.04	(large)	dIR97, Kumar et al. 2011	W A I	...	IRx	10
IRAS16086-5255(PDS410)	9.75	(large)	dIR97	W M A I	3?
HD146834	1.07	2.6	dIR97	W A S	...	IRx	20?
IRAS17578-1700	dIR97	(W) M A I	D	...	<2
IRAS17596-3952(PDS485)	5.15	(large)	dIR97, Kumar et al. 2011	W A I	...	IRx	3?
V385 Sct	Castilho et al. 2000	(W) M A I	D	...	3?
IRAS19012-0747	1.39	7.2	dIR97	W M A I	10?
IRAS19038-0026	1.45	4.9	Castilho et al. 2000	W A I	D?	...	10?
PDS100	5.86	(large)	dIR97, Kumar et al. 2011	W A I	...	IRx	4?
Tyc9112-00430-1	0.86	3.1	Ruchti et al. 2011	W	22
HD219025	3.74	9.6	dIR97, Kumar et al. 2011	W A I	...	IRx	3

^aNote that up to two more stars with IR excess could be identified from the relatively sparse SEDs in Sec. 4.2; these are For 90067 and SDSS J0632+2604, with SDSS J0632+2604 being more compelling.

^bW=WISE data in SED, with ‘(W)’ meaning some bands are missing; M=MSX data in SED; A=AKARI data in SED; I=IRAS data in SED; S=Spitzer data in SED.

^cThis column is populated if there is a reasonable likelihood that the star isn’t a first ascent K giant, e.g., of the sort appropriate for this study. ‘D’ means we are fairly confident it should be dropped, and ‘D?’ means there is some doubt as to whether it should be dropped; see text.

^dThis column is populated if recent literature has already identified this source as having an IR excess.

^eThis column contains the approximate wavelength, in microns, of the start of the IR excess.

5. Sources With IR Excesses By $\sim 25 \mu\text{m}$

5.1. Overview of Approach

Having omitted the objects for which we have substantial difficulty making matches across catalogs above, we have now a subset of objects for which we have established reliable multi-wavelength matches across catalogs. All of these objects have no or little ambiguity in the images to which we have access, e.g., they appear as clean point sources. We can now inspect the resultant assembled SEDs for evidence of an infrared excess.

In assessing whether or not a star has an IR excess, one needs to compare a measure of brightness at relatively short wavelengths (expected to be dominated by the stellar photosphere) with that at relatively long wavelengths, where dust emission is likely to be present. We take a two-pronged approach to identifying excesses. There are some objects for which an IR excess is immediately apparent upon inspection of the SED; no detailed analysis is required. These objects are summarized in Sec. 5.2 and detailed in Sec. 5.3. There are other objects for which the IR excess is more subtle. For these latter objects, we employ an approach developed in the context of finding small IR excesses around young stars, which is described in Sec. 5.4. Details of objects found to have these more subtle IR excesses can be found in Sec. 5.5. Table 5 summarizes the stars we identify as having either a large or small IR excess. .

5.2. Overview: Sources with Very Large Excesses

There are 19 stars whose SEDs immediately reveal significant IR excesses at wavelengths $< 20 \mu\text{m}$, and maintain large excesses out to at least $25 \mu\text{m}$. These sources often have detections in more surveys than just WISE; they often have data from MSX, AKARI, IRAS, and even Spitzer. Over the entire sample, including these sources with large excesses, the data from these various surveys are in reasonably good agreement, though some objects have more scatter than others. (The scatter could be due to complex backgrounds and variable beamsize across the surveys, or even intrinsic variability in the source.) If there is disagreement, however, it is typically IRAS that overestimates the flux density from the object, which makes sense since IRAS is the lowest spatial resolution of all the surveys used here.

The SEDs for these objects with unambiguous, large excesses appear in Figures 11 and 12. For stars without circumstellar dust (at least those warm enough to have the peak of their photospheric SED be at $< 1 \mu\text{m}$), measurements in the infrared ($\geq 2 \mu\text{m}$) should fall on a line consistent with a Rayleigh-Jeans (R-J) slope. To guide the eye, in Figs. 11 and 12, we have added an R-J line extended from $2 \mu\text{m}$. All of the sources with very large excesses can be seen to deviate from this line.

Out of these 19 stars with large IR excesses, 14 (73%) are from the dIR97 sample, five are from the literature sample, and none are from C12. However, four of the 19 may not be K giants – one of the dIR97 stars, IRAS17578-1700, is a carbon star, one of the stars from the literature sample, V385 Sct, is a very cool S-type star, and the other two may be too cool to be first ascent K giants. Some of these stars have detections indicating that the SEDs are rising beyond $90 \mu\text{m}$, suggesting that sub-mm observations are needed to constrain the outer extent of the IR excess. Some of these objects have been identified in recent literature (e.g., Kumar et al. 2015) as having an IR excess, but for others, this is the first confirmation that the objects have an IR excess using data more recently obtained than IRAS.

5.3. Notes on Sources with Very Large Excesses

IRAS00483-7347 This is an extremely well-populated SED, with data from WISE, MSX, AKARI, IRAS, and even Spitzer. However, the SED is wide compared to other SEDs in this study. The SED suggests that K_s is not on the R-J side of the SED, perhaps because the star is significantly cooler than a K giant. A R-J line extended from $2 \mu\text{m}$ as shown, or even a R-J line extended from $\sim 5 \mu\text{m}$, suggests a substantial IR excess around this star. Data from multiple sources are in good agreement with each other, and AKARI suggests that there is a significant long-wavelength component to the IR excess, with the SED rising again at the longest wavelengths. This source is identified in Castilho et al. (1998) as a Li-rich K giant, though no T_{eff} estimates are available in the literature. This star may be too cool to be a K giant, though it clearly has a large IR excess. Additional spectroscopy of this source would be helpful for a better understanding of the T_{eff} and where the excess starts.

HD19745 The IR excess for this source starts to appear past $10 \mu\text{m}$; WISE and AKARI are in good agreement. IRAS overestimated the IR flux density from this star, but it still has a clear excess. This source is known to be a Li-rich K giant (Reddy & Lambert 2005), and is incorrectly identified in SIMBAD as a T Tauri. Reddy & Lambert (2005) identify it as a red clump star. This star was identified in Kumar et al. (2015) as having an IR excess.

IRAS03520-3857 This object is a dIR97 source, and it had to be offset from the nominal IRAS position by $11''$ to pick up the counterparts, which is very large in the context of the other positional shifts needed in the rest of our sample. However, the field is relatively clean (consisting of one bright source) and is not suggestive of source confusion. There is good agreement between WISE, AKARI, and IRAS for $10\text{-}20 \mu\text{m}$. There is about an order of magnitude more energy density emerging at $10\text{-}20 \mu\text{m}$ than at $3\text{-}4 \mu\text{m}$. However, compared to other sources here, there are few detections blueward of $\sim 2 \mu\text{m}$, and it would be nice to see the SED turn over to define the Wien side of the SED. This object is identified in two papers as a possible galaxy based on IRAS colors (Saunders et al. 2000, Wang & Rowan-Robinson 2009) but is not identified as a confirmed galaxy in either paper. SIMBAD identifies it as a “peculiar star.” This source has no T_{eff} in the literature.

IRASF04376-3238 This object’s IR excess starts at least by $5 \mu\text{m}$, if not actually at $3 \mu\text{m}$. WISE, AKARI, and IRAS are in good agreement. However, compared to other sources here, there are few detections blueward of $\sim 2 \mu\text{m}$, and it would be nice to see the SED turn over to define the Wien side of the SED. This object is identified as a K giant in Torres et al. (2000), but as a candidate T Tauri in Magnani et al. (1995). It does have an SED consistent with SEDs found in young stars (see, e.g., Rebull et al. 2011). SIMBAD lists it as a “peculiar star.” Spectroscopy would be useful to distinguish a young star with low gravity from an old star with low gravity, and assess its Li abundance. (An uncertain equivalent width for Li is given for it in Torres et al. 2000, but no abundance.) This source has no T_{eff} in the literature.

IRAS07227-1320(PDS132) This star has a substantial IR excess that evidently starts abruptly between 4.6 and $7.8 \mu\text{m}$. AKARI, MSX, WISE, and IRAS are consistent with each other. This object is part of the dIR97 sample, and Torres et al. (2000) list it as a confirmed giant. However, Torres et al. (1995) lists this as “other” and “probably not young” in their paper on young stars; it is implied to be a normal MS star. García-Lario et al. (1997) identify it as a possible PN (planetary nebula) based on its IR excess. It is identified as a post-AGB star and an M 1 I giant in Suárez et al. (2006). Szczerba et al. (2007) identify it as ‘not a post-AGB (asymptotic giant branch) star’, but Yoon et al. (2014) identify it as a post-AGB star of type M3 IV. This source has no T_{eff} in the literature. Additional data are needed to clarify the status of this object.

IRAS07456-4722(PDS135) This star’s IR excess is small at 3.4 and 4.6 μm , but becomes substantial by $\sim 10 \mu\text{m}$. There is scatter but generalized agreement among IRAS, AKARI, and WISE. This object is part of the dIR97 sample. Torres et al. (2000) list it as a confirmed giant, though Torres et al. (1995) categorize it as a “Probable post-FU Ori star.” SIMBAD lists it as a T Tauri, apparently on the basis of Torres et al. (1995). As with other sources here, it has an SED consistent with SEDs found in young stars (see, e.g., Rebull et al. 2011), and spectroscopy would be useful to distinguish a young star with low gravity from an old star with low gravity. This source has no T_{eff} in the literature.

IRAS07577-2806(PDS260) There is good agreement between WISE, AKARI, MSX, and IRAS here, and there is more energy density near 20 μm (from dust) than near 1 μm (from the photosphere). AKARI provides detections out past 100 μm . The IR excess may start at 3.4 μm . This source is from the dIR97 set, and Torres et al. (2000) list it as a confirmed giant. SIMBAD identifies it as a post-AGB star, and reference García-Lario et al. (1997), but this object does not appear in the paper. Szczerba et al. (2007) retain it as a candidate AGB star. It does not have a T_{eff} in the literature.

HD233517 This star’s SED suggests an excess that starts past 5 μm . This is an original dIR97 source, and this star was identified in Kumar et al. (2015) as having an IR excess, as well as in Fekel & Watson (1998), Jasniewicz et al. (1999), and Drake et al. (2002), among others.

IRASF08359-1644 This SED suggests an IR excess that most likely starts at $\sim 10 \mu\text{m}$. WISE and IRAS (and the single AKARI point) are in good agreement with each other. Torres et al. (2000) identify this source as a Li-rich K giant. No other information about this source is apparently available (including T_{eff}); additional data would be useful.

HD96195 This SED is more complicated than ones above. Reliable WISE points at the shortest two bands do not exist; MSX provides a link between K_s and [12]. MSX, AKARI, WISE, and IRAS are all in rough agreement between 10 and 20 μm , though there is some scatter (and large error bars in one case). Assuming that K_s is on the photosphere (and on the R-J side of the SED, that is, assuming that this source is hot enough), there is a significant IR excess by 10 μm : $K_s - [12] = 1.14 \text{ mag}$. We have placed this object in this section with the other large excesses; we might have included it in the set of objects with more subtle excesses (following the method laid out in Sec. 5.4 below, $\chi_{K,[22]} = 6.8$), but close inspection of the SED shows that points $> 10 \mu\text{m}$ are probably above the photosphere. Moreover, the AKARI points, if detecting flux density truly associated with this source, identify a substantial IR excess at the bands $> 50 \mu\text{m}$. This source appears in Castilho et al. (2000) and Pereyra et al. (2006) as a Li-rich giant, but it may be too cool to be a K giant. Its reported T_{eff} in the literature (Castilho et al. 2000) is $\sim 3400\text{-}3600 \text{ K}$. It is also identified in McDonald et al. (2012) as having an IR excess (their $E_{IR} = 1.932$) and having $T_{\text{eff}} = 3400$.

IRAS12327-6523(PDS355) The IR excess for this source appears by 3.4 μm , and increases from there. WISE, MSX, AKARI, and IRAS are all in good agreement with each other (despite large errors on the MSX points). This is part of the dIR97 sample. Torres et al. (2000) list it as a confirmed giant, but also mention that there is some reddening here that likely comes from the Coalsack, and the star may be only 200 pc away, so the IR may be contaminated. Reddy & Lambert (2005) confirm the evolved nature of the star. de la Reza et al. (2015) categorizes this source as an early AGB star.

PDS365(IRAS13313-5838) This star’s IR excess likely starts between 2 and 3 μm ; there is more energy density near 20 μm (from dust) than near 1 μm (from the photosphere). There is good agreement among WISE, MSX, AKARI, and IRAS. This star is part of the dIR97 sample and was identified in Kumar et al. (2015) as having an IR excess. While it is a confirmed Li-rich K giant (e.g., Kumar et al. 2011, Drake et al. 2002, among others), SIMBAD lists it as a ‘Post-AGB Star (proto-PN).’

PDS68(IRAS13539-4153) The IR excess here starts abruptly between 5 and 8 μm ; 3.4 and 4.6 μm are on the photosphere if K_s is as well. WISE, AKARI, and IRAS are in good agreement. If the longest wavelength AKARI bands are detecting flux attributable solely to this source, it suggests that the SED is rising again at the longest bands. This star was identified in Kumar et al. (2015) as having an IR excess. While it is listed as a confirmed Li-rich K giant in several studies (e.g., Kumar et al. 2011, Kumar & Reddy 2009, among others), it also appears in Valenti et al. (2003) as a T Tauri candidate, though no useable spectra are reported of this object in that paper. SIMBAD has adopted the ‘T Tauri’ categorization. The $^{12}\text{C}/^{13}\text{C}$ ratio is only a limit (>20 ; Reddy & Lambert 2005), and cannot conclusively determine whether early RGB first dredge-up mixing (which lowers $^{12}\text{C}/^{13}\text{C}$ from the main sequence value) has occurred.

IRAS16086-5255(PDS410) This star’s IR excess likely starts between 2 and 3 μm ; there is more energy density near 20 μm (from dust) than near 1 μm (from the photosphere). There is good agreement among WISE, MSX, AKARI, and IRAS. This star is part of the dIR97 sample, and is listed in Torres et al. (2000) as a confirmed giant. However, SIMBAD categorizes it as ‘post-AGB, proto-PN,’ and Szczerba et al. (2007) retain it as a candidate AGB. No T_{eff} is available.

IRAS17578-1700 This star has a substantial IR excess that may start at K_s ; it may also be too cool for K_s to be on the R-J side of the SED. There is good agreement between MSX, AKARI, WISE, and IRAS, though there are no viable WISE points at the shortest two bands. This object is part of the dIR97 sample. Chen, Yang, & Zhang (2007), and references therein including Lloyd Evans (1991) identify it as a J-type carbon star based on optical spectra and IR excesses, and that categorization is inherited by SIMBAD. This star is likely too cool to be a K giant, and moreover is likely to be a carbon star.

IRAS17596-3952(PDS485) This object is part of the dIR97 sample, and its position had to be slightly adjusted from the nominal IRAS position to pick up the counterparts, but the field is relatively clean and is not suggestive of source confusion. This star’s IR excess likely starts between 2 and 3 μm ; there is a larger excess by ~ 10 μm , and WISE, AKARI, and IRAS are in good agreement where the points exist. This star was identified in Kumar et al. (2015) as having an IR excess. It is a confirmed Li-rich K giant (e.g., Kumar et al. 2011, Reddy & Lambert 2005).

V385 Sct This is a very bright star, and the K_s mag may not be on the R-J side of the SED; it may be too cool to be a K giant. There are no WISE data for the shortest two bands, and MSX fills the gap between 2 and 10 μm . There is scatter among the MSX, WISE, AKARI, and IRAS data, likely because it is so bright. It does seem to have an obvious IR excess, however. It appears in Castilho et al. (2000) and Pereyra et al. (2005) as a Li-rich K giant. However, it appears as GCSS 557 in Stephenson (1976) and is identified as star of type S in there and subsequent literature (such as Stephenson 1984, where it is CSS 1043). Stars of type S have ZrO bands as well as TiO bands, and other abundance anomalies; they are thermally pulsing AGBs that experience substantial dredge-up. It seems unlikely to be a first-ascent Li rich K giant. The T_{eff} value for it from the literature (Castilho et al. 2000) is ~ 3300 K, so it is also too cool to be a first-ascent K giant.

PDS100 There may be a small excess at 3.4 and 4.6 μm , but there is a clear excess by ~ 10 μm , as seen by WISE, AKARI, and IRAS. This star is part of the dIR97 set, and is also known as V859 Aql. SIMBAD indicates it as a T Tauri, but the literature is clear that it is instead a Li-rich K giant (Reddy et al. 2002, among others). This star was identified in Kumar et al. (2015) as having an IR excess.

HD219025 This star is also known as BI Ind, and its IR excess starts between 2 and 3 μm . There is a viable WISE detection at 3.4 μm , but not at 4.6 μm ; there is good agreement past ~ 10 μm among WISE, AKARI, and IRAS. It has a substantial IR excess. This star is part of the dIR97 set, and is identified in

many places in the literature as a Li-rich K giant (e.g, Kumar et al. 2011). SIMBAD has this as an RS CVn, but it is unlikely to be such an object. This star was also identified in Kumar et al. (2015) as having an IR excess. Jasniewicz et al. (1999) and Whitelock et al. (1991) have previously found a NIR excess for this star. They verify using Hipparcos parallax that this is a red giant and not a young star. It is also a rapid rotator.

5.4. Overview: Sources with Small Excesses

Identifying smaller excesses around the remaining stars requires more analysis than simple SED inspection. We can quantitatively compare the brightness at 2-3 μm (which should be dominated by the stellar photosphere in these cases where there is not much circumstellar dust to create an IR excess) with that at relatively long wavelengths, where dust emission may be present. In considering significant IR excesses, the IR excess is larger than any uncertainties in calibration. However, for small excesses, well-defined errors are important, uncertainties in calibration should be taken into account, and it becomes more important to use data that are uniformly obtained, calibrated, and processed so as to minimize systematics. Additionally, data obtained not over decades but obtained close in time minimize influence from intrinsic stellar variation.

WISE data meet these criteria, as the data are uniformly obtained (at nearly the same time), reduced, and calibrated. Therefore, $[3.4] - [22]$ is essentially an ideal metric with which to identify IR excesses.

There have been several approaches in the literature used to determine with confidence whether or not a star has an IR excess. For example, Mizusawa et al. (2012) tested several methods of finding IR excesses in F stars. To identify sources with small IR excesses, we adopt here the following approach (as in Mizusawa et al. 2012, or Trilling et al. 2008). We calculate χ :

$$\chi_{[3.4],[22]} = \frac{([3.4] - [22])_{\text{observed}} - ([3.4] - [22])_{\text{predicted}}}{\sigma_{([3.4]-[22])}} \quad (1)$$

and take as a significant excess those stars for which $\chi > 3$. For K giants, $[3.4] - [22]_{\text{predicted}}$ is 0, but for cooler objects (such as M giants), the predicted value is not 0 (see, e.g., Gautier et al. 2007). Mizusawa et al. (2012) were able to combine χ calculations for two independent measures of IR excess for most of the targets in their sample, using $K_s - [24]$ and $[3.4] - [22]$. We do not have such uniform independent measures of IR excess, so for the most part, we use $\chi_{[3.4],[22]}$. In order for the χ calculation to be successful, however, one needs good estimates of the star’s brightness at the relevant bands, as well as good estimates of the error on that measurement. Many of our targets are very bright, and saturated in K_s and $[3.4]$, which limits our ability to correctly estimate brightnesses (and errors) and therefore χ . However, we can use the existing measurements and reported errors to identify objects that are likely to have a small IR excess.

Table 5 includes $[3.4] - [22]$ and $\chi_{[3.4],[22]}$ for the sources with IR excesses. (Note that the χ values as calculated for the objects with large and obvious IR excesses above in Sec. 5.2 are often >100 , despite there being, in some cases, an IR excess even at 3.4 μm .)

There are nine stars we identify as having small but significant excesses. Two of the stars with small IR excesses are from the C12 sample, three are from the dIR97 sample, and the remaining four come from the literature sample of Li-rich giants. One may be too cool to be a K giant. Two have been recently identified in the literature as having an IR excess. Comments on each of these excess objects follow in the next section.

5.5. Notes on Sources with Small Excesses

NGC 362 V2 There are Spitzer data for this source, and Spitzer agrees well with WISE. There is a small IR excess here. By inspection of the SED, the excess probably starts relatively early in the SED, $\sim 5 \mu\text{m}$, for a small excess. (The specific values are $[3.4]-[22]=1.13 \text{ mag}$, $\chi_{[3.4],[22]}=9.7$). The star is identified as a Li-rich K giant in Smith et al. (1999).

HD65750 This star is very bright, and as such is missing 3.4 and 4.6 μm data (and the K_s data come from NOMAD). There are, however, WISE, AKARI, and IRAS, all of which are in good agreement with each other. This source can be seen in the SED to have an excess; it has no [3.4], but $\chi_{K,[22]}=11$. It is highly nebulous at POSS, though not at longer bands, so the measured IR flux is not likely contaminated by extended emission. This source comes from the dIR97 sample; it appears in Castilho et al. (2000) as a Li-rich giant. SIMBAD says this is V341 Car, a pulsating variable star of type M0III. It has a T_{eff} of 3600, so it is most likely a borderline case for being a first ascent K giant. McDonald et al. (2012) identified it as having an IR excess in their study of IR excesses around Hipparcos stars, calling it out (HIP 38834) in their Table 3 of luminous giant stars with detected circumstellar emission (their $E_{IR}=5.88$).

G0928+73.2600 This star does not have a very well-populated SED, or an immediately obvious IR excess based on the SED, but the χ calculation supports there being a small but significant IR excess here ($[3.4]-[22]=0.63 \text{ mag}$, $\chi_{[3.4],[22]}=6.4$). This star is identified as a particularly interesting source in C12 and Carlberg et al. (2010) because it has particularly high Li ($A(\text{Li})_{\text{NLTE}}=3.30 \text{ dex}$), relatively rapid rotation (8.4 km s^{-1}), and high $^{12}\text{C}/^{13}\text{C}$ (28). We have more discussion of this source in Sec. 6.4 below.

Tyc0276-00327-1 This source does not have an immediately obvious IR excess from the SED (which is also not terribly well populated), but the χ calculation supports there being a very small but significant IR excess here ($[3.4]-[22]=0.36 \text{ mag}$, $\chi_{[3.4],[22]}=3.4$). In the images, it appears within the extended halo of emission associated with an extended source (possibly a galaxy) that is bright at [12] and [22]. It is possible that this may affect the IR excess, though the AllWISE catalog does profile fitting photometry that should take into account this higher background. Additional data to secure the association of the IR excess with this object would be helpful. This object is from the C12 sample, but is unremarkable in that study, showing low Li, slow rotation, and average $^{12}\text{C}/^{13}\text{C}$.

HD111830 On first glance at the SED, this object seems to have good agreement with photospheric measurements from K_s to 25 μm , with WISE, AKARI, IRAS, and even Spitzer/MIPS falling on the R-J line to 25 μm . However, IRAS and AKARI, if detecting flux density truly associated with this source, identify a substantial IR excess at bands longer than 50 μm . There turns out to be a small but significant excess at 22 μm ($[3.4]-[22]=0.63 \text{ mag}$, $\chi_{[3.4],[22]}=3.7$). $K_s - [24]=0.4 \text{ mag}$, consistent with a small excess. This star is part of the dIR97 sample; it appears in Jasniewicz et al. (1999) as Li-rich but is listed in their table with an upper limit on the Li abundance.

HD146834 This source is also HR 6076. In POSS, there is nebulosity (and SIMBAD categorizes it as “star in nebula”). It is very bright in 2MASS and WISE, with no strong nebular emission, though there is some faint extended emission in the background at 12 and 22 μm . It has WISE, Spitzer (IRAC and MIPS), and AKARI data, all of which are in fairly good agreement. However, near 20 μm , it is confusing. AKARI measures 860 (± 15) mJy at 18 μm , WISE measures 797 (± 12) mJy at 22 μm , and MIPS measures significantly less, 528 mJy, at 24 μm . The original error at 24 μm reported in the SEIP is $\pm 16 \text{ mJy}$, and is likely underestimated, so we have added a 4% error floor, as described above; the net error is 21 mJy, still not enough to bring the measures into alignment within 1σ . The K_s mag is bright, and its error is also likely

underestimated. Following the measurements and errors as reported, however, $[3.4]-[22]=1.07$, $\chi_{[3.4],[22]}=2.6$, and $K_s - [24] = 1.19$, $\chi_{K,[24]}=3.2$. The errors on $[3.4]$ and K_s are both large, which lowers the χ values. It is difficult to decide if the excess here is real and significant. We have opted to call the excess significant because there are three measures of the brightness near $20 \mu\text{m}$, and it does seem to be significantly brighter near $20 \mu\text{m}$ than the photospheric expectations based on the brightness near $2-3 \mu\text{m}$. It also has some long-wavelength AKARI detections; if AKARI is measuring flux associated solely with this star, then it has a significant long-wavelength excess. It appears in McDonald et al. (2012) as having a small IR excess in their study of IR excesses around Hipparcos stars (their $E_{IR}=1.532$). It is from the dIR97 sample.

IRAS19012-0747 There are two sources here in close proximity in POSS, but the target position matches one of the two optically bright sources. Both sources can be seen in J through $[12]$, though the target source is clearly dominating, and overwhelms any flux from the apparent companion by $[22]$ (and presumably in IRAS). While source confusion is possible, it’s reasonably likely that a spectrum was obtained of the source of most of the IR flux. This source has WISE, AKARI, and MSX data, all of which are in good agreement with each other. IRAS and AKARI, if detecting flux density truly associated with this source, identify a substantial IR excess at bands longer than $25 \mu\text{m}$. At $\sim 20 \mu\text{m}$, it has a weaker excess $- [3.4]-[22]=1.39$, $\chi_{[3.4],[22]}=7.2$. This star is part of the dIR97 sample (though its name was incorrectly IRAS19012-0742 in the published table). It appears in Pereyra et al. (2005) as a Li-rich K giant.

IRAS19038-0026 K_s for this object may not be on the R-J side of the SED; it may be too cool to be a K giant. There does not seem to be significant IR excess at 3.4 or $4.6 \mu\text{m}$, but the MSX, AKARI, WISE, and IRAS points suggest an excess may be present starting at $\sim 10 \mu\text{m}$. By $>20 \mu\text{m}$, assuming that the IRAS and AKARI points are detecting flux density truly associated with this source, there is a substantial IR excess. At $\sim 20 \mu\text{m}$, it has a more subtle excess $- 3.4-[22]=1.45$, $\chi_{[3.4],[22]}=4.9$. This object appears in Castilho et al. (2000) and Pereyra et al. (2005) as a Li rich giant, but it may be too cool to be a K giant. The T_{eff} that appears in the literature for it is ~ 3600 K.

Tyc9112-00430-1 This source does not have an immediately obvious IR excess from the SED, but the χ calculation supports there being a small but significant IR excess here: $[3.4]-[22]=0.86$, $\chi_{[3.4],[22]}=3.1$. It is identified as a Li-rich K giant in Ruchti et al. (2011).

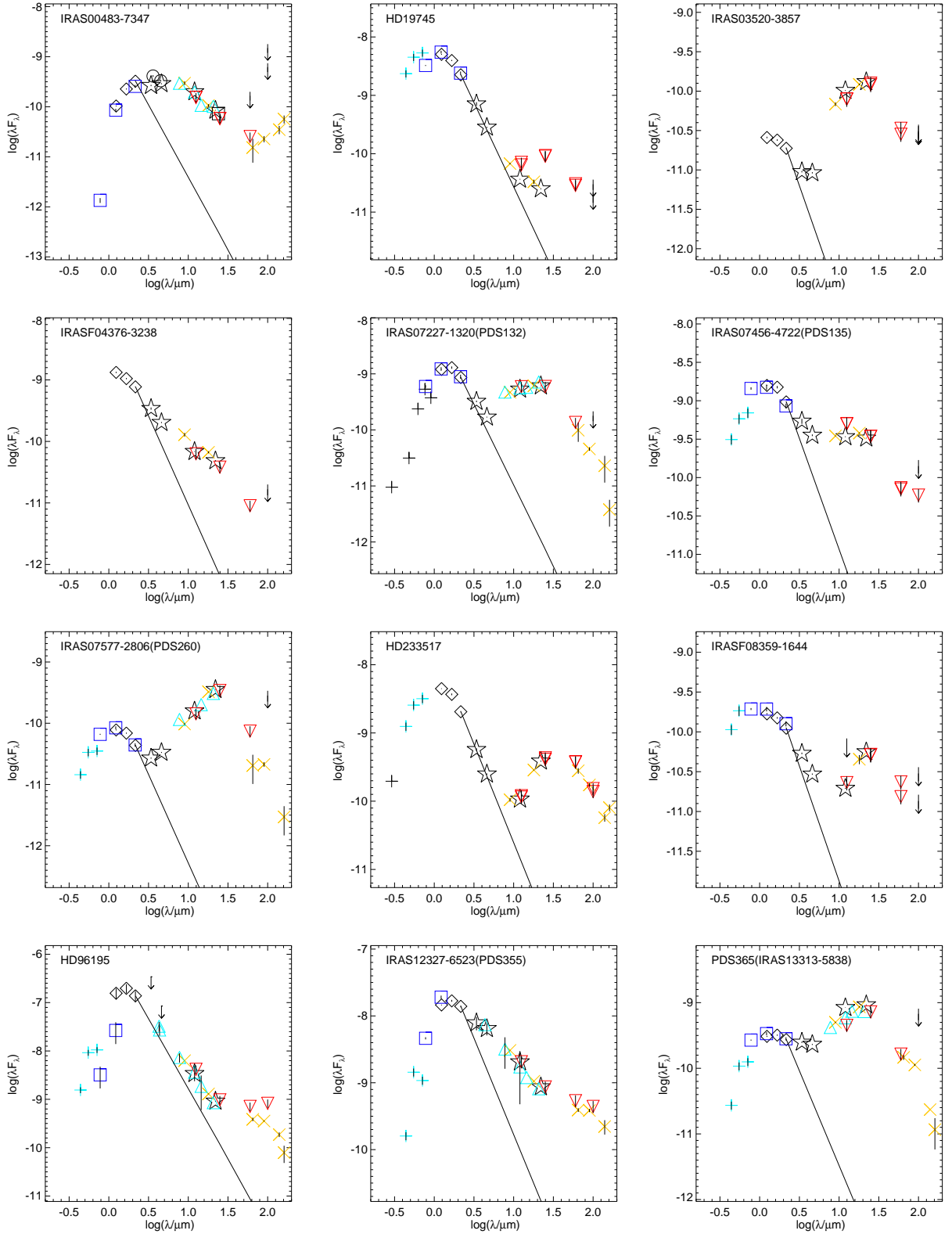


Fig. 11.— SEDs for sources with large IR excesses, part 1; notation is as described in Fig. 8, with an additional line with a Rayleigh-Jeans slope extended from K_s (e.g., if K_s is on the photosphere, the photosphere longward of K_s should fall on this line). All of these objects have a significant excess above this line. See text and table for discussion of individual objects.

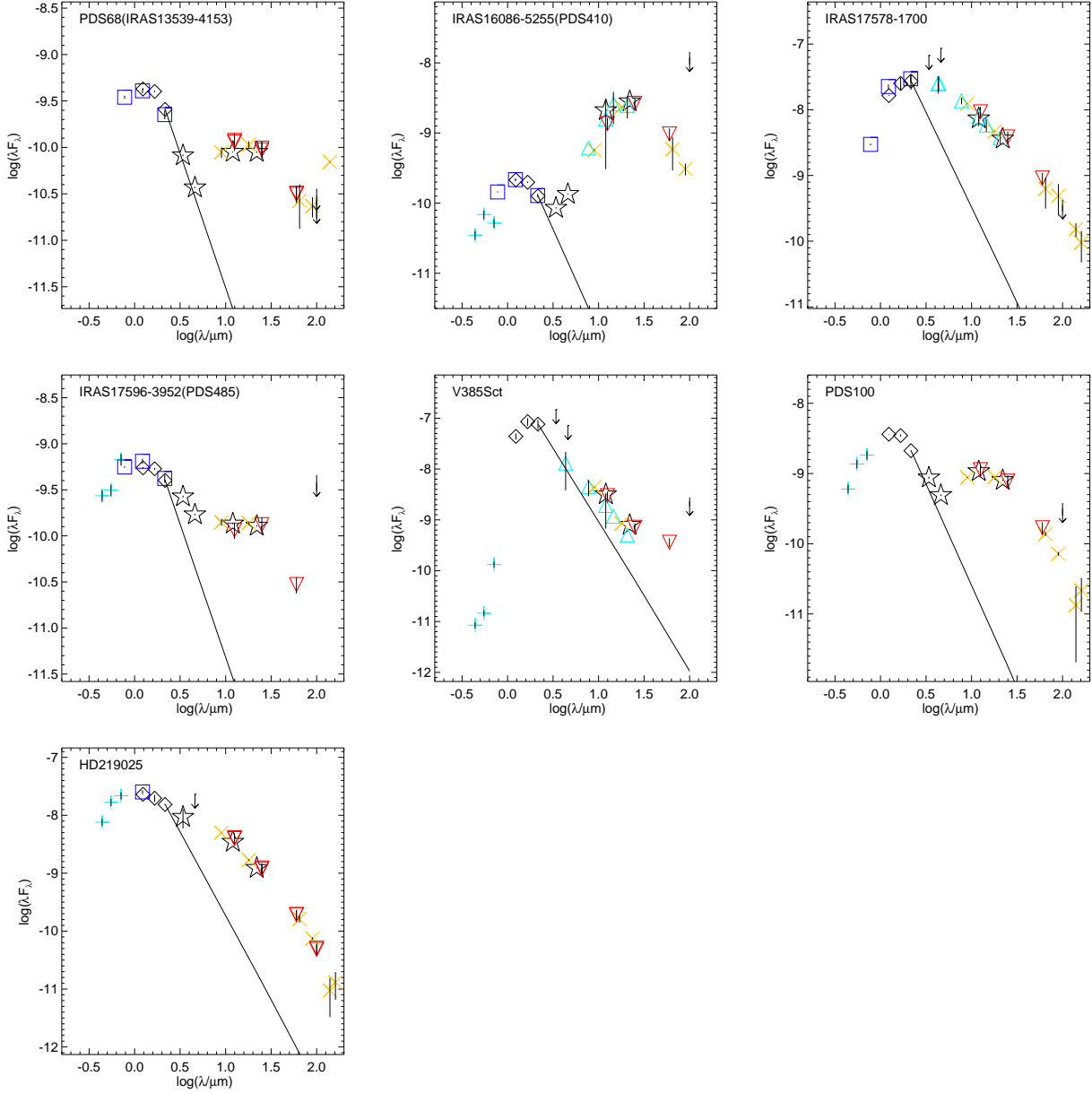


Fig. 12.— SEDs for sources with large IR excesses, part 2; notation is as in Fig. 11. See text and table for discussion of individual objects.

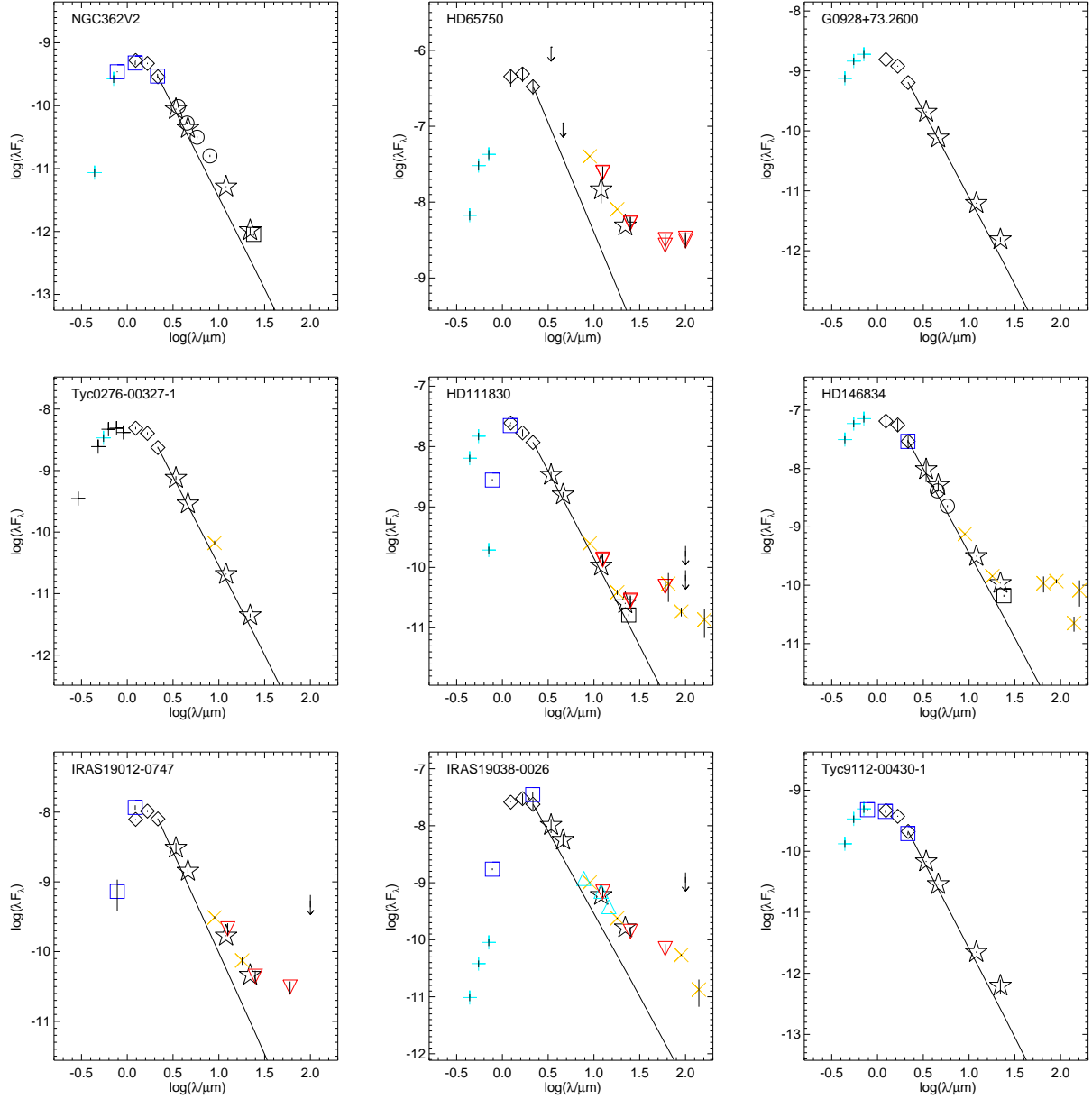


Fig. 13.— SEDs for sources with smaller IR excesses; notation is as in Fig. 11. See text and table for discussion of individual objects.

6. Discussion: Characteristics of the Entire IR Excess Sample

We started with 316 sources. Out of those, 10 have too sparsely populated SEDs for us to sensibly place any strong restrictions on whether or not there is an excess. There are 36 sources that have relatively sparse SEDs, and are often missing at least the [22] band. For these, we can put some constraints on whether or not there is an IR excess, and 2 out of those 36 sources could plausibly have an IR excess. There are 24 sources that we suspect are subject to source confusion, and we drop them from the sample. There are 218 sources with well-populated SEDs and no evidence for IR excesses out to $\sim 20 \mu\text{m}$. There are 28 sources that have well-populated SEDs that do, in fact, have evidence for an IR excess. Out of those 28, 5 are probably giants but may not be K giants. We conclude that IR excesses are rare among our sample of K giants, at best $\sim 10\%$. Given the biases in our sample (described in detail below), this fraction is probably less in Li-rich RGs and substantially less in Li-poor RGs.

We now examine our ensemble population in several different ways.

6.1. Comparison of IR Excesses to Literature

Not all of our IR excess sources are newly identified as having an IR excess; after all, dIR97 and others in the literature identified these sources based on their infrared properties. However, one important goal of our paper was to reassess the IR excesses in these sources given the higher spatial resolution data now available. Other recent papers have identified IR excesses in some of our targets using similar or the same data; McDonald et al. (2012) and Kumar et al. (2015) both identify sources with IR excesses. Kumar et al. (2015) has similar goals to our paper, and many targets overlap. We recover all 7 of their IR excess K giants.

McDonald et al. (2012) did an analysis of more than 107,000 Hipparcos stars, incorporating data from IRAS, SDSS, DENIS, 2MASS, MSX, AKARI, and WISE, in order to identify stars with an IR excess. Out of our targets, 118 are included in the catalog presented in McDonald et al. (2012). Only some of the IR excess objects are explicitly discussed in McDonald et al. (2012), so only one of our objects (HD65750) is mentioned there as having an IR excess; we agree that it has an IR excess. Following the prescription laid out in their paper (in their Fig. 7 and associated discussion), however, 5 more objects (out of the 118 we have in common) can be identified as having at least potentially significant IR excesses: HD6665, HD96195, Tyc3917-01107-1, HD203136, and HD219025. Two of those (HD96195, HD219025) are ones we have already identified above as having IR excesses. The remaining three (HD6665, Tyc3917-01107-1, and HD203136) do not appear to us to have excesses (Figure 14); we investigated why the McDonald et al. calculations might have identified them as excess objects. HD6665 has the IRAS $12 \mu\text{m}$ point slightly above the photosphere, but all other detections are on the photosphere ($[3.4] - [22] = 0.09$); the value of E_{IR} calculated by McDonald et al. is 2.16, likely a result of the IRAS point being slightly high. Tyc3917-01107-1 is in a nearly identical situation, though in this case, the IRAS $12 \mu\text{m}$ point is closer to the photosphere; the McDonald et al. E_{IR} is 1.73, and $[3.4] - [22] = 0.07$, so again, not likely to have a real excess. HD203136 has some irregularities in its SED, where there is a lot of scatter among the the MSX, AKARI, and IRAS points near $8\text{--}12 \mu\text{m}$; they are inconsistent with each other and the rest of the SED, and all of them are too high compared to the WISE [12] and [22] points. The McDonald et al. E_{IR} comes out to be 4.89 most likely because the MSX, AKARI, and IRAS photometric points are high. We take WISE to be the most reliable, because it has the highest spatial resolution; $[3.4] - [22] = -0.21 \pm 0.14$, so there is no detectable IR excess in this object.

Thus, we conclude that we have recovered all of the recent literature-identified IR excess sources. We have identified 18 more objects out of our aggregate data that have IR excesses, though not all of them may

be first ascent K giants.

Many of the sources in our sample had been identified as IR excess sources from IRAS measurements. All 21 of the sources with the largest IRAS IR excesses ($[12]-[25]>0.5$ mag) from detections – not limits – in the PSC are recovered as IR excess sources here. Nearly all, 11 of 14, of the sources with detections and $[12]-[25]>0.5$ in the FSC are recovered.

There are just three sources (HD76066, HD112859, HD203251) for which the FSC detections at $[12]$ and $[25]$ result in $[12]-[25]>0.5$, but the measured WISE flux densities are substantially lower than the IRAS FSC flux densities, such that these stars do not have detectable IR excesses. The $[3.4]-[22]$ for these objects are 0.05, 0.08, 0.08 mag, respectively, so these sources do not have measurable IR excesses to $22\ \mu\text{m}$. This is probably a direct result of the higher spatial resolution of WISE better measuring the flux density of the target.

However, many of the sources with smaller measured IRAS excesses are not recovered as IR excess sources. In the SEDs for these cases, one can often see the IRAS PSC suggesting an IR excess, the IRAS FSC suggesting less of an excess, and WISE (and sometimes AKARI) suggesting a smaller or no excess. (Similarly, and more dramatically, the upper limits are often pushed lower and lower in the SEDs.) In these cases, what is most likely going on is that the increased spatial resolution and the fainter sensitivity reached resolves out extended emission and/or source multiplicity, lowering the overall measured flux density. However, there are also some noticeable calibration offsets between IRAS and 2MASS+WISE; see Sec. 6.5 below.

6.2. SED interpretation

IR excess around stars is commonly interpreted as due to circumstellar dust in a shell or disk or ring. In Table 5, we include an approximate wavelength at which the excess appears. Sources where the IR excess is already present between 2 and $5\ \mu\text{m}$ likely have very large disks or envelopes of dust that reach nearly all the way in to the star. Sources where the IR excess does not start until 10 or $20\ \mu\text{m}$ likely have shells or rings of dust, where there is a gap between the star and the dust. Obtaining total dust masses would require detailed modeling of the star+dust SED (plus assumptions about the composition of the dust) and is beyond the scope of this paper. On the whole, larger excesses likely correspond to larger quantities of dust. For the 7 sources modeled by Kumar et al. (2015), under the array of assumptions they made, they find dust temperatures between 75 and 260 K, but they do not estimate total dust mass.

The circumstellar dust around these stars could plausibly be dust ejected by the K giant, but it could also be residual debris disk dust in the system heated afresh by the first ascent onto the RGB (e.g., Jura 1999). However, debris disks are typically relatively low-mass, producing small IR excesses; (re-)illumination of an old debris disk is not a particularly reasonable explanation for the very large IR excesses.

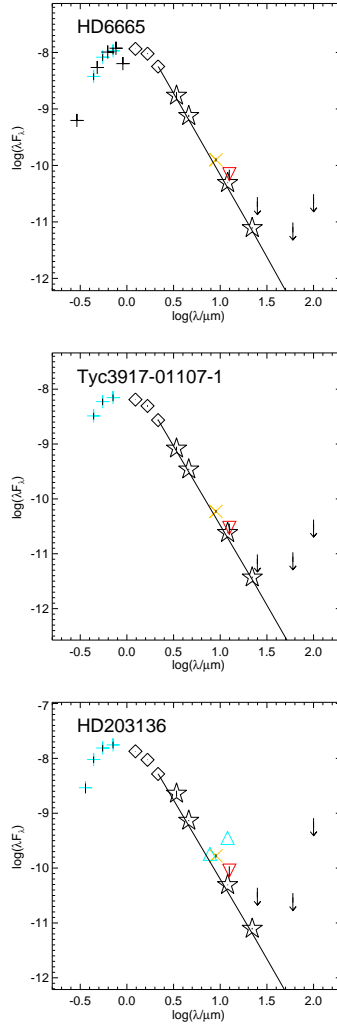


Fig. 14.— SEDs for three sources identified in McDonald et al. (2012) as potentially having IR excesses, but for which we do not identify an IR excess. Notation is as in Fig. 11. See text for discussion of individual objects.

6.3. Color-Magnitude Diagrams

Another view of the IR excesses for the entire sample can be obtained by plotting $[3.4]$ vs. $[3.4]-[22]$, as illustrated in Figure 15. Photospheres (that is, stars without any circumstellar dust) should have $[3.4]-[22]\sim 0$. All of the sources significantly redward of $[3.4]-[22]\sim 0$ are either identified as IR excess sources or are identified as subject to source confusion (§4.3 above). Even though $[3.4]-[22]$ is a nearly ideal metric with which to assess IR excesses, many of our objects are saturated at $[3.4]$. Therefore, it is worthwhile to examine the $K_s-[22]$ plot as well; see Figure 16. More sources are included in this plot, and there are still very large excesses here, even among the objects thought to be K giants. There is more scatter in the $K_s-[22]=0$ photospheric locus, reflecting some of the larger uncertainties in the measurements of the (bright) stars in K_s .

Many of the reddest sources (redward of $[3.4]-[22]\sim 5$ or $K_s-[22]\sim 5$) in either of these Figures are the dropped sources; their location in this diagram is not surprising given some of the SEDs shown in Figs. 8 and 9. Still, many of the large IR excess K giants we identified above are very red in this diagram. For context, young stars in Taurus (which are known to have substantial dusty disks and envelopes) have a typical $[3.4]-[22]\sim 4$, though some extend to $[3.4]-[22]\sim 10$ (Rebull et al. 2011). The range of IR excesses for the objects we believe to be K giants is comparable to the range of IR excesses found in young stars. Some of the IR excesses seen in these K giants are very large indeed, with many well past 4 out to 10. However, these large IR excesses are not distributed uniformly among the subsamples. The dIR97 sample includes the large excesses; the excesses in the literature Li-rich sample are much more moderate. The C12 sample has very few excesses, and those are quite small.

6.4. C12 sample

Recall that the dIR97 sample is biased towards IR-bright sources, and the literature sample is strongly biased towards high $A(\text{Li})$ stars. The C12 sample of red giants (RGs) is unbiased with respect to $A(\text{Li})$ and IR excess, though it does have a larger proportion of fast rotators than a random RG field population. Additionally, it has $A(\text{Li})$, $v \sin i$, and $^{12}\text{C}/^{13}\text{C}$ measured for every star in the sample, in contrast to the rest of the sources, for which only some of these parameters are available. We had hoped that we would detect IR excesses in enough of these sources to look for correlations. However, only two of the C12 sources (G0928+73.2600 and Tyc0276-00327-1) have any excesses, and they are both small, <0.6 mag. Out of the whole 86-star C12 sample, the fraction of stars with an IR excess is 2%. Considering just those with well-populated SEDs to 22 μm , 2/79 ($3_{-0.9}^{+4}$ %) of the stars have an excess by $[22]$ (using the binomial statistics from the appendix in Burgasser et al. 2003 to obtain uncertainties).

The three best candidates for planet accretion listed in C12 are G0928+73.2600, Tyc0647-00254-1, and Tyc3340-01195-1. If the IR excess production process is directly related to planet accretion, one would expect all three of these to have an IR excess, but only one of these has a measurable IR excess. The SEDs for Tyc0647-00254-1 and Tyc3340-01195-1 do not suggest excesses at 22 μm . Admittedly, for Tyc0647-00254-1, the sole non-WISE point beyond 3 μm is an AKARI 9 μm point that is slightly above the photosphere, though the WISE 12 and 22 μm points are not consistent with AKARI and do not suggest an IR excess. (In comparison, Tyc0276-00327-1 has a very similar SED, but in that case, the 22 μm point is enough above the photosphere that a small IR excess is suggested.) Tyc3340-01195-1 has no points other than WISE beyond 3 μm , and neither does G0928+73.2600.

The two stars with a significant IR excess are split in terms of properties. Tyc0276-00327-1 seems

to be a relatively unremarkable star in the C12 data; it has a subsolar Li abundance ($A(\text{Li})_{\text{NLTE}} = -0.24$ dex), is a slow rotator (4.2 km s^{-1}), and has an average $^{12}\text{C}/^{13}\text{C}$ (17). However, G0928+73.2600 is a particularly interesting star (C12, Carlberg et al. 2010) because it has particularly high Li ($A(\text{Li})_{\text{NLTE}} = 3.30$ dex), relatively rapid rotation (8.4 km s^{-1}), and high $^{12}\text{C}/^{13}\text{C}$ (28).

G0928+73.2600 was also included in the ensemble of Li-rich stars in Kumar et al. (2011). Its location on a Hertzsprung-Russell (H-R) diagram is similar to many other Li-rich RGs in that sample. Kumar et al. (2011) noted that many Li-rich RGs have properties consistent with red clump stars, and suggested the possibility that an episode of Li regeneration may occur during the He flash for some red giants. G0928 is noteworthy among that sample of RGs for having the largest $^{12}\text{C}/^{13}\text{C}$. (The importance of $^{12}\text{C}/^{13}\text{C}$ in interpreting Li-rich stars is described in more detail in Sec. 7 below.) Carlberg et al. (2010) and C12 argued in favor of external replenishment as a source of the high Li given its relatively high $^{12}\text{C}/^{13}\text{C}$.

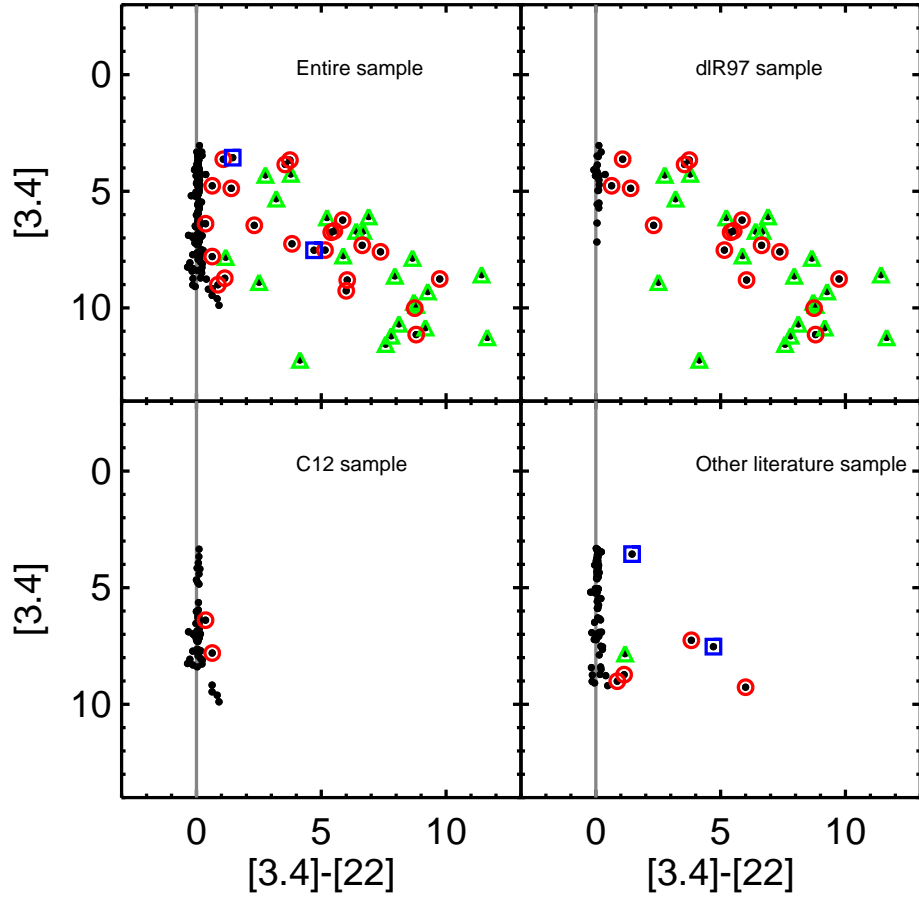


Fig. 15.— $[3.4]$ vs. $[3.4]-[22]$ for the entire sample where $[3.4]$ and $[22]$ are both detected (upper left), the dIR97 sample alone (upper right), the C12 sample alone (lower left), and the remaining literature sample (lower right). All of the sources subject to source confusion (§4.3) have additional green triangles overplotted. The sources we identify as having an IR excess (§5) are circled in red; the sources we called out as having an IR excess but potentially not K giants (§5) are overplotted in blue squares (some of these are not detected at $[3.4]$ and thus do not appear). The vertical line at $[3.4]-[22]=0$ indicates the value expected for photospheres. All of the sources significantly redward of $[3.4]-[22]\sim 0$ are either identified as IR excess sources or are likely to be subject to source confusion.

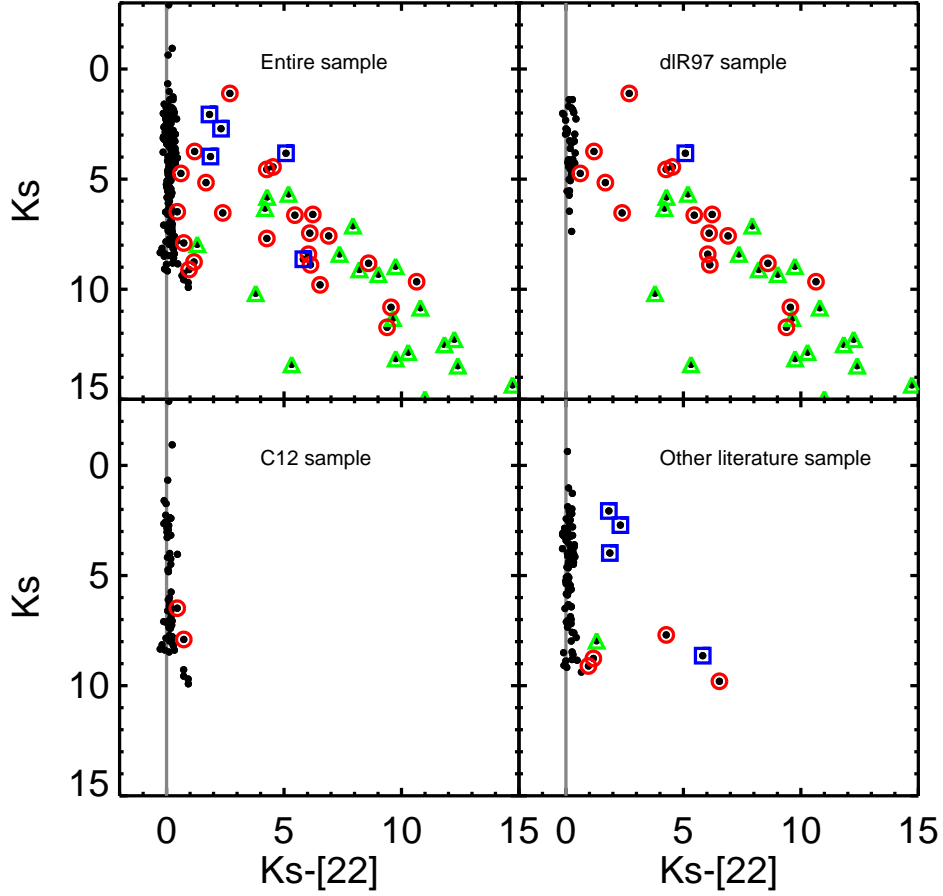


Fig. 16.— K_s vs. $K_s - [22]$ for the entire sample where K_s and $[22]$ are both detected (upper left), the dIR97 sample alone (upper right), the C12 sample alone (lower left), and the remaining literature sample (lower right). Notation is as in Fig 15. There are more sources in this plot than in the prior plot, but the same conclusions apply – all of the sources significantly redward of $K_s - [22] \sim 0$ are either identified as IR excess sources or are subject to source confusion. The scatter in the $K_s - [22] = 0$ locus is larger in this plot, reflecting larger K_s uncertainties.

6.5. The dIR97 Sample and the Original IRAS Color-Color Diagram

The dIR97 sample is strongly biased towards sources that are bright in the infrared, and so it is not surprising that there are many more bright IR sources, and large IR excesses, found in the dIR97 sample than in either the C12 or the ‘other literature’ samples. In de la Reza et al. (1996), dIR97, and Siess & Livio (1999), there is a plot of IRAS colors for their targets, which they use to describe a proposed evolutionary sequence of objects in the diagram. This plot is described as a color-color diagram, where the following is their definition of color:

$$[\lambda_1 - \lambda_2] = \log(\lambda_2 F_1) - \log(\lambda_1 F_2) \quad (2)$$

where λ is wavelength and F is flux density. In more recent papers, driven at least in part by Spitzer and WISE work, the convention for color is instead truly a difference of magnitudes:

$$M_1 - M_2 = 2.5 \times \log\left(\frac{F_2}{F_1}\right) \quad (3)$$

And in the infrared, where the band names are often the wavelength of the bandpass, this difference in magnitudes would be written, e.g., $[\lambda_1] - [\lambda_2]$. In any case, the *shape* (if not the specific *values*) of the distribution of points in the dIR97 color-color plot is recovered by using $[12]-[25]$ and $[25]-[60]$ defined as in equation 3.

In Figure 17, we have made the plot analogous to that from dIR97 and collaborators, namely $[25]-[60]$ against $[12]-[25]$, just for the original dIR97 sample. The first panel uses the values from the IRAS PSC, as in dIR97. The shape of the overall distribution is similar to what they have obtained, in that there is a locus near $[12]-[25] \sim 0$ extending up to a range of $[25]-[60]$ values, and a broad ‘bubble’ of points extending to the right. However, we find that the upper envelope of the distribution (near $[12]-[25]=1$ to 4, and $[25]-[60] \sim 3$ to 4) is defined entirely by objects we suspect should be dropped from the sample because they are subject to source confusion. Removing these points from the plot significantly reduces the range of colors found for K giants. We have also indicated which of these sources are the ones for which we have identified an IR excess. Most of the PSC points that are still thought to be K giants with $[12]-[25] > 0.5$ are also ones we identify as having an IR excess, but there are several that we do not recover. These sources are identified in at least one of $[12]$, $[25]$, or $[60]$ with data quality flag=1, e.g., a limit, not a detection. dIR97 started from the Pico dos Dias Survey (PDS; Gregorio-Hetem et al. 1992), which reports having started from the IRAS PSC, only the high-quality detections. However, several of the points in our version of this diagram (which, again, is just the dIR97 sample) do not have high quality detections at all 3 of the relevant IRAS bands.

The second panel of Figure 17 uses the IRAS FSC instead of the PSC, again, just for the dIR97 sample. (Recall from Sec. 3.2 above that 36 of the dIR97 objects are also detected in the FSC in any band, so not all of the objects from the first panel appear in the second panel.) All of the objects we suspect should be dropped do not have FSC measurements, so they do not appear in the second panel. Again, most of the sources with detections (not limits) in $[12]$, $[25]$, and $[60]$, and large excesses with $[12]-[25] > 0.5$, are also ones we identify as having an IR excess, but there is one that we do not recover. (It is HD76066, discussed above as having significantly lower WISE flux densities than IRAS, and not really having an excess.) Interestingly, in moving between the PSC and FSC plots, the envelope delineating the red excursion of the distribution of points shrinks dramatically in size, and there are fewer points within the ‘bubble’ – more points are on the $[12]-[25] \sim 0$ locus where no IR excess is measured. Whereas $\sim 45\%$ of the K giants in the first panel have $[12]-[25] > 0.5$ mag, by the second panel, just $\sim 30\%$ have $[12]-[25] > 0.5$ mag. However, there are fewer objects overall in the second panel.

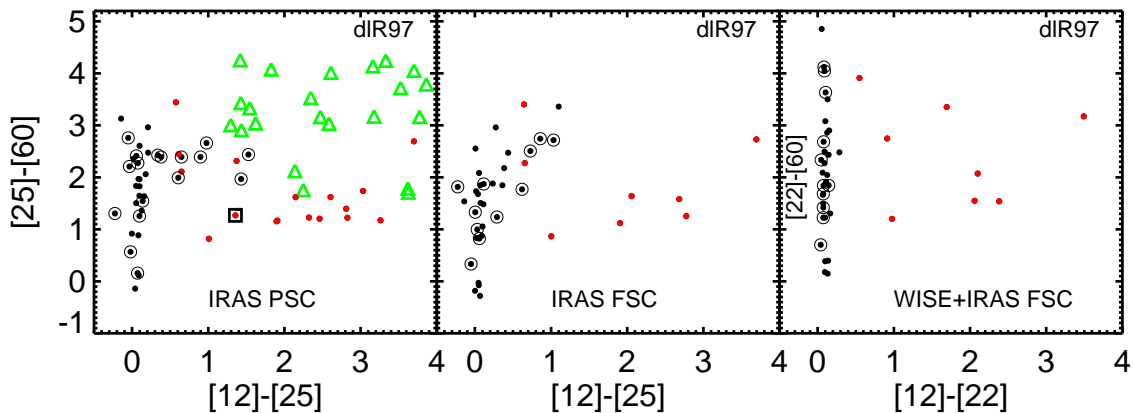


Fig. 17.— Color-color plot of the dIR97 sample in the style of those found in de la Reza et al. (1996), dIR97, and Siess & Livio (1999), where the IRAS [25]–[60] color is plotted against the IRAS [12]–[25] color (see text for clarification of units). The left panel uses IRAS PSC, the middle panel uses IRAS FSC, and the right panel combines WISE [12] and [22] with IRAS FSC [60]. Green triangles (first panel only) are objects we identify as likely subject to source confusion. Red dots are objects we identify as having an IR excess. The square (first panel only) indicates the only object appearing in this plot which we identify as having an IR excess, but that we suspect may not be a K giant. Additional circles around sources are those for which the IRAS PSC (or FSC) data quality flag in at least one of the relevant bands is 1, indicating a limit. Objects may not be the same between the first and second panels; all the objects in the third panel also appear in the second panel. The most important features in these plots are: (1) the bulk of the distribution delineating the reddest IR excesses is composed of objects likely subject to confusion; (2) the envelope of the distribution shrinks when going from the PSC to the FSC, and shrinks further when WISE is used, suggesting that the apparent IR excesses measured in IRAS vanish when higher spatial resolution observations are used. (3) All of the largest excess K giants (those with detections and $[12] - [25] > 0.5$ mag) are recovered as IR excess sources, except for HD76066, discussed in Sec. 6.1.

We can carry this further – both IRAS and WISE had a $12 \mu\text{m}$ channel, and IRAS had a $25 \mu\text{m}$ channel, close to the WISE $22 \mu\text{m}$ channel. Though the filter bandpasses are far from identical, they ought to give similar estimates of the broadband IR excess near their respective wavelengths. In the third panel of Fig. 17, we have used the WISE [12] in place of the IRAS [12], and WISE [22] in place of the IRAS [25]; for $60 \mu\text{m}$, we retain the IRAS FSC values. All of the objects from the middle panel with WISE detections at [12] and [22] appear in the third panel. The distribution continues to shrink towards the $[12] - [22] = 0$ locus, with now only $\sim 20\%$ of the sources having $[12] - [22] > 0.5$ mag. As higher spatial resolution and more sensitive observations are available, the apparent IR excesses shrink.

However, in using WISE in place of the IRAS bands, we are implicitly assuming that the two missions are calibrated in the same fashion, or at least consistently with each other. It is possible that the change in distributions (the shrinking of the ‘bubble’) of points between the panels of Fig. 17 can be accounted for, at least in part, by different calibrations of the instruments. To investigate this, we compared the IRAS PSC to the FSC first, as a check, to make sure that they were internally calibrated consistently with respect to each other. Then, we compared the IRAS FSC to the WISE values. In all cases, we used our entire sample, but only those with data quality flags 3 or 2. The comparison of the 12 and $25 \mu\text{m}$ channels (calculating (PSC-FSC)/PSC with the values in magnitudes) shows that they are indeed well-matched to each other, with

no significant average offset between them. For [12], the center of the best-fit Gaussian to the distribution is 0 mag, with a width of 0.04 mag. For [25], the center is 0.02 mag, and the width is 0.04 mag. However, in comparing the WISE and IRAS FSC 12 μm channels, there is a clear offset of $\sim 30\%$ between WISE and IRAS, in the direction of the FSC being brighter. (At [12], calculating (FSC-WISE)/FSC in mag, the center of the Gaussian is 0.26 mag and the width is 0.05 mag.) For 25 μm , we expected larger differences between WISE and IRAS because of the different bandpasses. There is an offset between IRAS FSC and WISE of $\sim 15\%$. (The center of the Gaussian is 0.14 mag, and the width is 0.06 mag.) It is again in the direction of the FSC being brighter. Once one is made aware of this offset, one can see it systematically in the SEDs of the ensemble where both IRAS and WISE are available. This effect is in the same direction one would expect if the higher spatial resolution of WISE was resolving out background contributions to the IRAS flux, which may still be a part of what is going on. (We note that we only did this comparison for the objects in our sample, not the entire IRAS or WISE catalogs or over a controlled range of backgrounds. Such a comparison is beyond the scope of our study.) Nonetheless, the net effect in the last panel of Fig. 17 is to move the envelope of points left and up. Firstly, on the x -axis in this panel, [12] and [22] now both come from WISE, and are internally well-calibrated, so stars without excesses are closely clumped near 0 in [12]–[22]. They are more tightly clumped than they were for IRAS, which collapses part of the distribution. Stars with excesses have slightly smaller [12]–[22] (from WISE) on average than [12]–[25] (from IRAS), because the systematic calibration offset for [12] is slightly larger than for [25] ([22]). Secondly, on the y -axis, [60] is still from IRAS, presumably well-calibrated internally to the other IRAS bands. Since both [12] and [25] are slightly systematically brighter compared to WISE, if we assume [60] is also slightly brighter as a result of calibration systematics, this will push the distribution of points slightly up in the diagram – which can be seen in the Figure.

So, we conclude that some (but not all) of the reduction in the range of points in Fig. 17 can be accounted for in the different calibrations of IRAS and WISE. The average calibration effect for the ensemble is on the order of a few tenths of a magnitude. However, the movement of individual objects between plots is primarily a reflection of more accurate measurements of the IR flux from the stars.

Kumar et al. (2015) also made plots like our Fig. 17, though in the same units as dIR97 (using equation 2). Their plots have similar distributions of points as ours do.

7. Abundances and Rotation Rates

One of our original goals of this paper was to seek a correlation between lithium abundance (and rotation rate and the $^{12}\text{C}/^{13}\text{C}$ ratio) and IR excess in K giants, but with only $\sim 10\%$ of our sample likely to have IR excesses, our ability to test correlations with IR excess is somewhat limited. However, we can still infer some things about the relationship among these parameters. In order to better understand these relationships, however, we need to make sure that our already biased sample is as clean and internally consistent as possible.

We now discuss how we limit the sample to identify Li-rich stars, and likely first ascent K giants, and look at the relationship between IR excess, Li abundance, rotation rate, and $^{12}\text{C}/^{13}\text{C}$.

7.1. Definition of Li-Rich

A substantial number of objects were added to our sample on the basis of a paper in the literature asserting that the K giant was Li-rich. However, everyone does not use the same definition of Li-rich. For example, dIR97 did not report Li abundances, but identified certain stars as Li-rich based on equivalent widths. C12 included Li abundances, and determined them under both LTE and NLTE assumptions. Other literature sources sometimes report only equivalent widths, or only LTE abundances. If we were to rely solely on literature reporting, 183/316 sources are Li-rich.

However, we wished to be a bit more restrictive, or at least internally consistent. For those sources for which we have NLTE Li abundances, we took those with $A(\text{Li})_{\text{NLTE}} \geq 1.5$ dex as Li-rich. If there was no NLTE abundance available, we took those with $A(\text{Li})_{\text{LTE}} \geq 1.5$ dex as Li-rich. If there was no abundance in the literature (e.g., just equivalent widths), we did not identify it as Li-rich. If we thought (based on the analysis above) that it was not a K giant, we did not identify it as Li-rich (that includes the 24 dropped sources, the carbon star, and the S-type star). A total of 62 sources are missing $A(\text{Li})$, including the dropped sources. Using this approach, 139 stars in our sample are Li-rich. Unfortunately, 10 of these sources are the ones with very sparse SEDs, and 29 more have relatively sparse SEDs (though both of the sources identified as having an IR excess from these SEDs are Li-rich). Just 9 of the remaining 100 sources have well-populated SEDs and an IR excess. There are 115 that are Li-poor, 7 of which have sparse SEDs, and 6 of which have an IR excess.

7.2. Restrictions on $\log g$ and T_{eff}

This study is aimed at understanding the Li-IR connection for K giants (first ascent RGB stars and red clump stars); however, we have already noted above that some of our sample are suspected to be more evolved AGB stars or other non K-giant contaminants. We can try to limit the contamination by requiring that there be an estimate of $\log g$ and T_{eff} , and that these values fall within a certain range.

We identify stars with $\log g > 3.5$ as not likely giants. This selection should weed out subgiant and dwarf stars for which high Li may not be unusual. Out of the entire set of 316(-24 confused sources), 46 have no $\log g$ estimate available to our knowledge. Of the remaining sources, 16 have $\log g > 3.5$ (with 2 more having exactly 3.5 being left in the sample).

We can put both upper and lower constraints on T_{eff} . Temperatures < 3700 K are likely to be AGB stars, not first ascent K giants, because the AGB reaches cooler temperatures. On the upper end, temperatures > 5200 K are likely to be dwarf stars or subgiants that have not yet completed first dredge-up (the deepening of the convection zone that reduces the surface Li abundances during the post-MS phase). Out of the entire set of 316(-24 confused sources), 20 have no T_{eff} estimate at all. Of the ones with T_{eff} , 6 are cooler than 3700 K, several of which we identified above as ‘likely too cool’ for our sample. There are 3 stars with $T_{\text{eff}}=5200$ K (left in our sample), and there are 19 hotter than 5200 K.

The net loss of objects out of our sample by requiring that there be an $A(\text{Li})$ and that T_{eff} and $\log g$ are in the correct range is 97 objects (some objects counted in more than one omission category above), leaving 219 in the sample. That sample includes the 10 very sparse SEDs, and 33 of the relatively sparse SEDs. Of the 219, 119 ($54 \pm 6\%$)⁶ are Li-rich as per our definition above (with 10+26 of those being the very

⁶The errors presented here are assumed to be the larger of either Poisson errors or the binomial approximation found in the

sparse/relatively sparse SEDs). Just 13/219 ($6\pm 2\%$) of this sample have an IR excess. Bringing Li into it, 11/119 ($9\pm 3\%$) of the Li-rich stars have an IR excess, and 2/100 ($2_{-0.6}^{+3}\%$) of the Li-poor stars have an IR excess (with 7 sparse SEDs included).

The sparse SEDs included in the above calculation likely miss more subtle IR excesses, so we can repeat the analysis on the subset of 176 stars with well-populated SEDS. There are 83 stars in this sub-sample that are Li-rich, 93 that are Li-poor, and 11 that have an IR excess. Of the Li-rich stars, 9/83 ($11_{-3}^{+4}\%$) have an IR excess; of the Li-poor stars, 2/93 ($2_{-1}^{+3}\%$) have an IR excess. Although we are well into the regime of small-number statistics, IR excesses appear to be at least 2–3 times as common among Li-rich stars compared to Li-poor stars. Kumar et al. (2015) came to a similar conclusion, that IR excesses are rare in the general K giant population. They found that only $\sim 1\%$ of RGs (their sample is dominated by Li-poor stars) have an IR excess. Of the 40 Li-rich stars in their sample, they find 7 ($18_{-4}^{+8}\%$) with an IR excess.

7.3. Relationships Among $A(\text{Li})$, $v \sin i$, $^{12}\text{C}/^{13}\text{C}$, and IR excess

For the rest of this section, we will only use the cleanest possible sample of 176 RGs with T_{eff} and $\log g$ consistent with K giant stars, and with well-populated SEDs, from the prior section.

Figure 18 shows $A(\text{Li})_{\text{NLTE}}$ vs. $[3.4]-[22]$ for the 176 stars in the cleanest possible sample. This plot suggests that if a star has a large IR excess, it probably has a large $A(\text{Li})$, but having a large $A(\text{Li})$ does not mean that it necessarily has a large IR excess. Smaller excesses can be found at all abundance levels. Very similar results are obtained if LTE rather than NLTE lithium abundances are used, or if $K_s - [22]$ is used instead of $[3.4]-[22]$. Within the sample of Li-rich objects with IR excesses, there does not seem to be a trend that, say, the largest Li abundances are always found with the largest IR excesses.

Figure 19 shows $A(\text{Li})_{\text{NLTE}}$ vs. $v \sin i$. Fast-rotating stars also often (but not exclusively) have large $A(\text{Li})$, which has been previously noted (e.g., Drake et al. 2002). What is further revealed by this plot is that many of the fast rotating, Li-rich stars are also those with IR excesses. Half of the Li-rich stars that also show fast rotation have an IR excess, whereas only one Li-rich star among the more populated slow rotators has an IR excess. Additionally, only one RG with an IR excess shows neither high rotation nor enriched Li. Thus, having both high Li and fast rotation is a stronger predictor for an IR excess than high Li alone. This suggests that relatively enhanced angular momentum is necessary for the ejection of circumstellar shells in Li-enriched stars. We note that there are several IR excess sources unable to be plotted in this diagram because no $v \sin i$ is available, and that a fundamental uncertainty in the use of projected rotational velocities is that inclination effects can mask rapid rotation.

As seen in Figure 20, no correlations can be found between IR excess and the carbon isotope ratio, $^{12}\text{C}/^{13}\text{C}$. Very low $^{12}\text{C}/^{13}\text{C}$ is thought to indicate substantial extra mixing. IR excess sources (extreme and moderate) are found with both low and high $^{12}\text{C}/^{13}\text{C}$, where we have taken 15 as the division between low and high values. The largest IR excesses do not have unusual carbon ratios. However, we note that relatively few of our stars have a measure of $^{12}\text{C}/^{13}\text{C}$, so this may introduce some additional biases.

In Figure 21, we plot the $A(\text{Li})$ versus $^{12}\text{C}/^{13}\text{C}$, a plot that should give some insight into the Li enrichment mechanism. In the presence of extra mixing, the surface values of both $^{12}\text{C}/^{13}\text{C}$ and $A(\text{Li})$ will be reduced if the mixing proceeds slowly (e.g., Denissenkov & Vandenberg 2003). However, when the mixing

proceeds rapidly, newly synthesized Li can be brought into the convection zone, where it is long-lived, such that the surface Li is enhanced while $^{12}\text{C}/^{13}\text{C}$ decreases (e.g., Denissenkov & Herwig 2004). Once the source of the Li (^3He) is considerably depleted, a net destruction of Li begins and $A(\text{Li})$ will again be reduced. The physical mechanism behind this very fast mixing is still under investigation. Denissenkov & Herwig (2004) argued that rotation-induced mixing was required, and since RGs are slow rotators, an outside source of angular momentum such as binary interactions or planet engulfment was required. However, Palacios et al. (2006) argued that the shear turbulence caused by differential rotation was not sufficiently fast to increase Li at the surface. Magnetic buoyancy is another possible model (e.g., Guandalini et al. 2009).

Planet engulfment that does *not* trigger fast mixing could be identified with higher than expected Li, but with a relatively high $^{12}\text{C}/^{13}\text{C}$. In Figure 21, the C12 sample shows the most homogeneously measured $^{12}\text{C}/^{13}\text{C}$ and the only sample unbiased towards Li. The stars generally show the expected linear trend of lower $^{12}\text{C}/^{13}\text{C}$ and lower $A(\text{Li})$ for stars that experience different degrees of mixing. Other panels of the plot show the addition of the large sample of all the literature Li-rich stars, which span a large range of $^{12}\text{C}/^{13}\text{C}$. Red circles again indicate IR excess. Stars with the clearest sign of substantial internal mixing (very low $^{12}\text{C}/^{13}\text{C}$ and high Li) show no evidence of an IR excess. However, this is not entirely unexpected. As pointed out by Denissenkov & Herwig (2004), the timescale over which a shell is ejected and dissipates (e.g., the timescale for the IR excess to appear/disappear) is of order 10^4 - 10^5 years, compared to the timescale of Li regeneration, which is of order 10^5 - 10^6 yrs. Very low values of $^{12}\text{C}/^{13}\text{C}$ are only reached at the latest stages of Li regeneration, well after the IR excess has disappeared. Figure 21 does, however, exhibit a tantalizing correlation between the Li and $^{12}\text{C}/^{13}\text{C}$ of many of the IR excess stars in this plot. We offer no explanation for this trend but suggest that it may be informative on the conditions of the star when the shell is ejected. Adding additional objects to this plot (via determinations of $^{12}\text{C}/^{13}\text{C}$) will likely further illuminate any relationship.

Given the relative shortness of the IR phase compared to the Li synthesis phase, one would expect little change in $A(\text{Li})$ for any particular star as it traverses the IR color-color diagram (Figure 17). This expectation is confirmed by the fact that we do not see a correlation between level of Li-richness and the strength of the IR-excess (Figure 18). Furthermore, since IR excess is seen around a wide range of $A(\text{Li})$, we can speculate that the Li regeneration reaches different maximum $A(\text{Li})$ values in each star.

7.4. Biases and Future Work

An additional concern in interpreting Figs. 18-20 is that our sample has many substantial biases within it. One very significant bias is that many of the sources were discovered based on their IRAS colors, e.g., they are biased towards IR-bright sources. The subsamples are separated out in Figs. 18-20 specifically because of this bias – a substantial fraction of the dLR97 sample and a smaller fraction of the literature sample is based on IRAS colors. In Fig. 18, it can be seen that all of the large IR excesses are from the dLR97 sample. (Some of the large excesses seen in, e.g., the literature sample in Fig. 15 do not appear in this plot because they do not have $\log g$ or T_{eff} in the correct range, etc.) Those largest excesses draw the eye and dominate the relationships found in the plots. The relationships are not as obvious in just the C12 sample, which is the least biased with respect to IR properties.

To first order, we hoped we could try to constrain the influence of this bias by omitting K giants known primarily by their IRAS names. Only 5 of the sources making it into our ‘cleanest possible’ sample have IRAS names, but 4 of them are among the largest IR excesses ($[3.4]-[22]>2$).

We also have biases in the sample due to the incomplete information for stars in the sample. A number of the IR excess sources have no T_{eff} and/or $\log g$ and were removed from our detailed analysis of IR excess among K giants. Furthermore, half of the Li-rich sample has no measure of $^{12}\text{C}/^{13}\text{C}$ and/or $v \sin i$. This makes comparisons between, e.g., Figures 19 and 20, difficult because the IR excess stars appearing in each plot are not all the same stars. Follow-up high resolution optical spectra to measure these missing stellar parameters would be extremely valuable.

It is also worth considering if the objects with the largest excesses are not really old dusty giants ascending the giant branch, but young dusty giants, still contracting along their Hayashi track. This could explain both the very large excesses as well as the high lithium abundances, since young stars are known to often have high $A(\text{Li})$. Young, actively accreting stars with substantial disks would have strong and variable $\text{H}\alpha$ profiles, and have significant variability at essentially all wavelengths, both of which are different than expectations for old giant stars. Detailed isotopic ratios (such as $^{12}\text{C}/^{13}\text{C}$) that trace mixing and chemical evolution would also be of help. Additional detailed spectroscopic data and modeling is required to distinguish old dusty stars from young dusty stars.

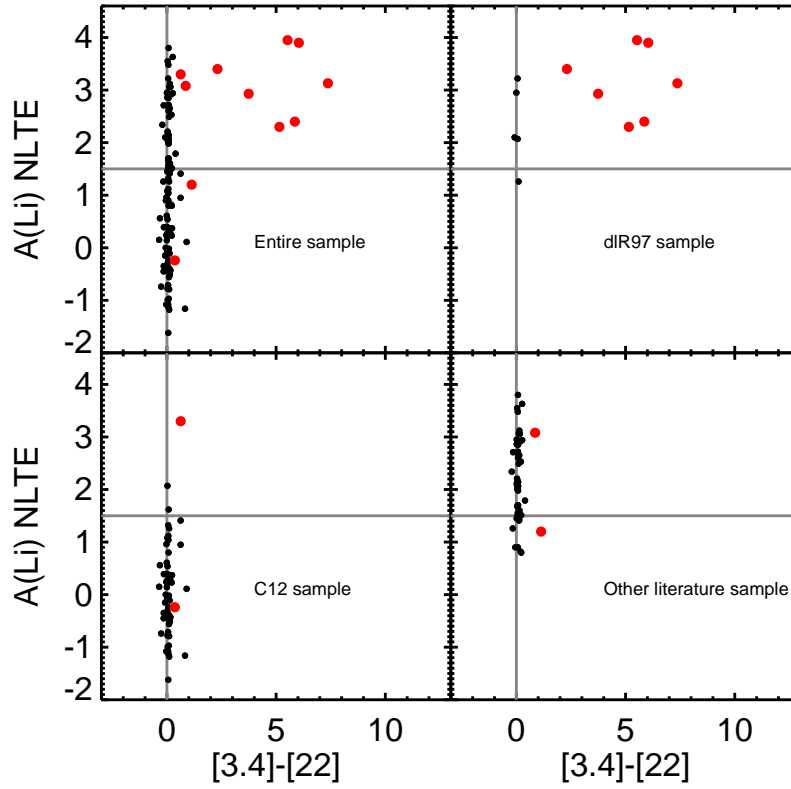


Fig. 18.— $A(\text{Li})_{\text{NLTE}}$ vs. $[3.4]-[22]$ for the 176 stars in the cleanest possible sample. The vertical line at $[3.4]-[22]=0$ indicates the photospheric locus, and the red points are the IR excess stars. The horizontal line at $A(\text{Li})=1.5$ dex indicates our adopted division between Li-rich and not Li-rich. The entire (available) sample is plotted in the upper left, and the component samples (dIR97, C12, and the other literature) are shown in separate panels. A very similar plot is obtained if $A(\text{Li})_{\text{LTE}}$ is used instead of $A(\text{Li})_{\text{NLTE}}$, or $K_s - [22]$ rather than $[3.4]-[22]$. If a star has a large IR excess, it probably has a large $A(\text{Li})$, but having a large $A(\text{Li})$ does not necessarily indicate it has a large IR excess.

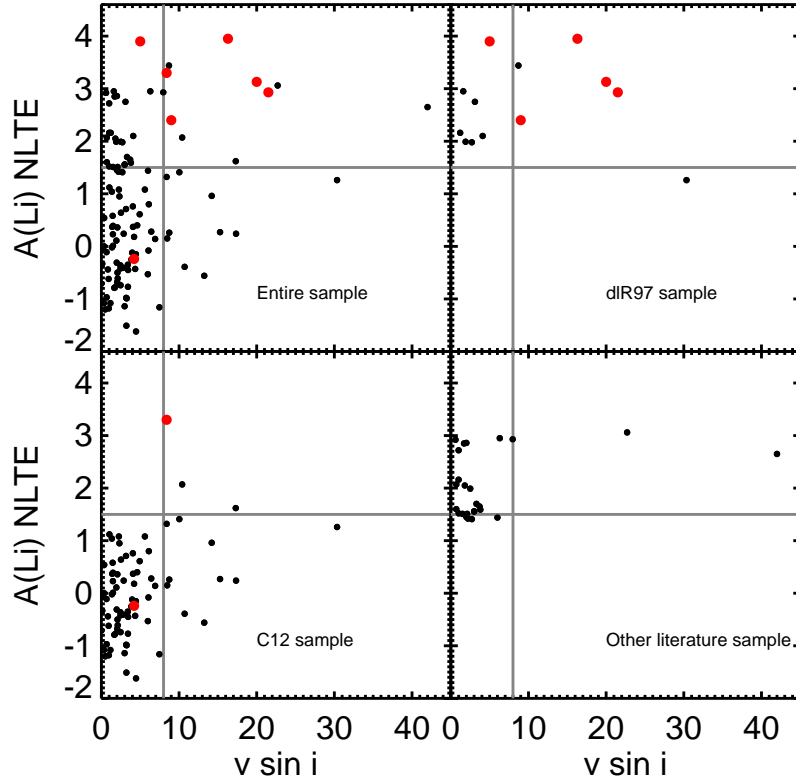


Fig. 19.— $A(\text{Li})_{\text{NLTE}}$ vs. $v \sin i$ in km s^{-1} for the cleanest possible sample. The vertical line at 8 km s^{-1} divides the fast from the slow rotators. The red points are the IR excess stars. The horizontal line at $A(\text{Li})=1.5$ dex is the division between Li-rich and not Li-rich. The entire (available) sample is plotted in the upper left, and the component samples (dR97, C12, and the other literature) are shown in separate panels. A very similar plot is obtained if $A(\text{Li})_{\text{LTE}}$ is used instead of $A(\text{Li})_{\text{NLTE}}$. Fast-rotating stars also often (but not exclusively) have large $A(\text{Li})$, and often also have an IR excess.

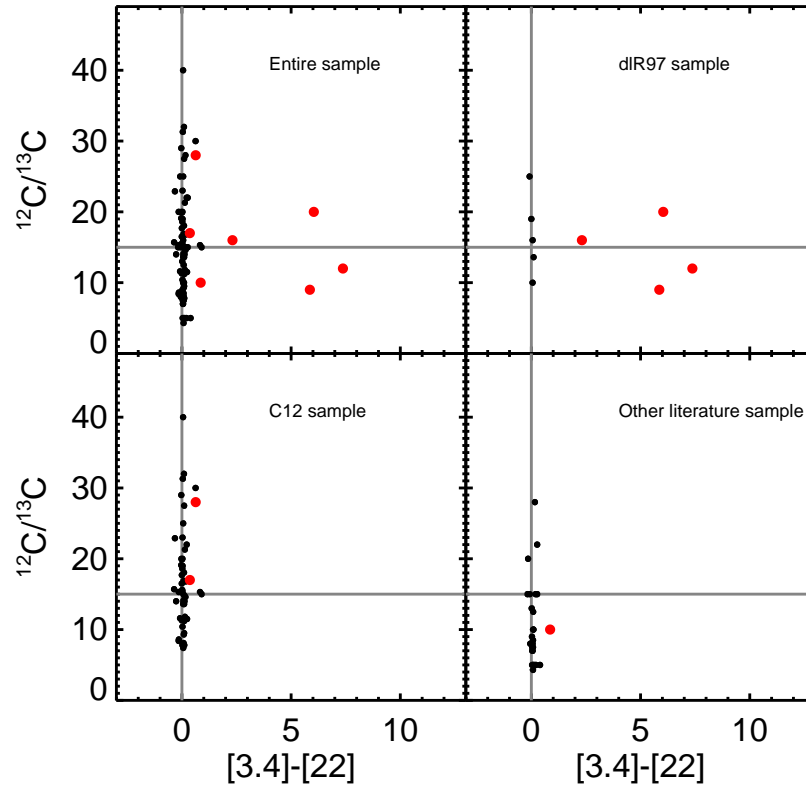


Fig. 20.— $^{12}\text{C}/^{13}\text{C}$ vs. $[3.4]-[22]$ for the cleanest possible sample. The vertical line at $[3.4]-[22]=0$ indicates the photospheric locus, and the red points are the IR excess stars. The horizontal line at $^{12}\text{C}/^{13}\text{C}=15$ is the division between a high and low ratio. The entire (available) sample is plotted in the upper left, and the component samples (dIR97, C12, and the other literature) are shown in separate panels. A very similar plot is obtained if $A(\text{Li})_{\text{LTE}}$ is used instead of $A(\text{Li})_{\text{NLTE}}$. There is no discernible correlation of IR excess with $^{12}\text{C}/^{13}\text{C}$.

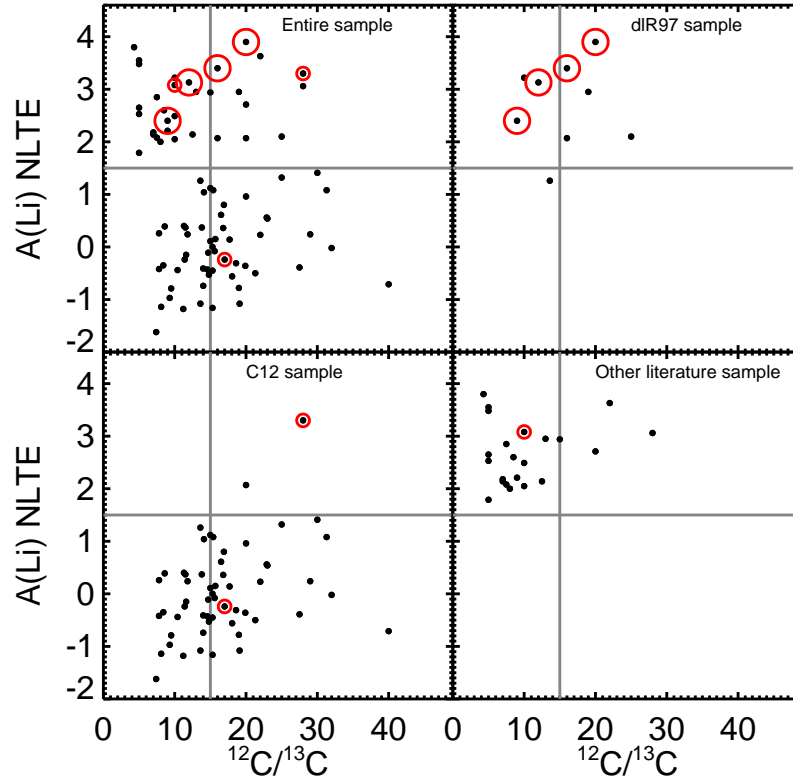


Fig. 21.— $A(\text{Li})$ vs. $^{12}\text{C}/^{13}\text{C}$ for the cleanest possible sample. The vertical line at $^{12}\text{C}/^{13}\text{C}=15$ is the division between a high and low ratio; the horizontal line at $A(\text{Li})=1.5$ is the division between Li-rich and Li-poor. The red points highlight the IR excess stars; smaller circles are the smaller excesses, and larger circles are larger excesses ($[3.4]-[22]>1$). The entire (available) sample is plotted in the upper left, and the component samples (dIR97, C12, and the other literature) are shown in separate panels.

8. Conclusions

In the past, dIR97 and others have suggested a connection between enhanced lithium and IR excesses in K giants. However, others (e.g., Fekel & Watson 1998, Jasniewicz et al. 1999; Lebzelter et al. 2012; Kumar et al. 2015) have questioned the association between Li and IR abundances. We have assembled a set of 316 targets thought to be K giants, two-thirds of which are thought to be Li-rich, in order to test the association between IR excesses and lithium abundances. The targets come from the dIR97 study (biased towards IR-bright sources), the C12 study (assembled with limited biases to test correlations of various stellar parameters), and a wide variety of literature identifying Li-rich K giants. For these targets, we assembled a multiwavelength catalog spanning optical through 100 μm data, using SDSS, NOMAD, 2MASS, DENIS, WISE, IRAS, AKARI, MSX, and Spitzer data.

We inspected each source in as many different images as possible. In 24 cases, all identified first as IR-bright sources with IRAS, we believe that source confusion is playing a role, in that either (a) the source that is bright in the optical (and most likely the source of which a spectrum was obtained to assess lithium) is not responsible for the IR flux, or (b) there is more than one source responsible for the IR flux as measured in IRAS.

We looked for IR excesses by $\sim 20 \mu\text{m}$ using two different approaches : (a) simple SED construction and assessment, and (b) an approach drawn from studies of young stars used to identify small but significant IR excesses. We identify 19 stars with large IR excesses, and 9 more stars that have small but significant IR excesses. However, 5 of these 28 may not be first ascent K giants. (There are 2 more K giants that may have IR excesses by $\sim 10 \mu\text{m}$, identified from relatively sparse SEDs.) Ten of the 28 clear IR excess K giants were already recently identified in the literature as having IR excesses, but this is the first recent confirmation of IR excess for 18 of these targets. Some of these giants have IR excesses that start at or before $5 \mu\text{m}$, but others have excesses that start near $20 \mu\text{m}$.

IR excesses by $20 \mu\text{m}$, though rare, are about twice as common among Li-rich K giants ($11^{+4}_{-3}\%$) as in Li-poor K giants ($2^{+3}_{-1}\%$). Despite identifying very few IR excesses (by number or fraction of sample), we find that if a RG has a large IR excess, it probably has a large $A(\text{Li})$ and is a fast rotator, but having a large $A(\text{Li})$ (or being a fast rotator) does not mean that it necessarily has a large IR excess. Smaller excesses can be found at all abundance levels. This is consistent with the idea that the IR excess lifetime of a single ejected shell is very short-lived compared to the timescale of Li enrichment. It could also suggest that not all Li-rich stars eject shells, and some other parameter (such as fast rotation, or even rotation history) dictates whether shell ejection occurs. Stars with the clearest sign of substantial internal mixing (very low $^{12}\text{C}/^{13}\text{C}$ and high Li) show no evidence of an IR excess. This could be also explained by a shorter timescale for the IR excess than the Li regeneration, since the lowest $^{12}\text{C}/^{13}\text{C}$ are realized near the end of the Li-enrichment stage. An external Li regeneration mechanism identified in the literature is planet injection. However, we identify only one of the three best candidates for planet accretion listed in C12 as having a measurable IR excess, and it is a small excess. The largest IR excesses are all found in the dIR97 sample, which is strongly biased towards IR-bright objects. There remains a possibility that at least some of these largest excess objects may not be old dusty stars, but instead young dusty stars.

Support provided for this work by the NASA/IPAC Teacher Archive Research Program (NITARP; <http://nitarp.ipac.caltech.edu>), which partners small groups of high school educators with a mentor astronomer for an authentic research project. It receives funding from the NASA ADP program and the IPAC archives. We acknowledge the following students who helped out at various phases of this project: Rosie

Buhrley, Julie Herring, Kendall Jacoby, and Elena Mitchell, from Walden School of Liberal Arts.

JKC was supported by an appointment to the NASA Postdoctoral Program at the Goddard Space Flight Center, administered by Oak Ridge Associated Universities through a contract with NASA.

This research has made extensive use of the NASA/ IPAC Infrared Science Archive, which is operated by the Jet Propulsion Laboratory, California Institute of Technology, under contract with the National Aeronautics and Space Administration.

The Digitized Sky Survey was produced at the Space Telescope Science Institute under U.S. Government grant NAG W-2166. The images of these surveys are based on photographic data obtained using the Oschin Schmidt Telescope on Palomar Mountain and the UK Schmidt Telescope. The plates were processed into the present compressed digital form with the permission of these institutions.”

Funding for SDSS-III has been provided by the Alfred P. Sloan Foundation, the Participating Institutions, the National Science Foundation, and the U.S. Department of Energy Office of Science. The SDSS-III web site is <http://www.sdss3.org/>. SDSS-III is managed by the Astrophysical Research Consortium for the Participating Institutions of the SDSS-III Collaboration including the University of Arizona, the Brazilian Participation Group, Brookhaven National Laboratory, University of Cambridge, Carnegie Mellon University, University of Florida, the French Participation Group, the German Participation Group, Harvard University, the Instituto de Astrofísica de Canarias, the Michigan State/Notre Dame/JINA Participation Group, Johns Hopkins University, Lawrence Berkeley National Laboratory, Max Planck Institute for Astrophysics, Max Planck Institute for Extraterrestrial Physics, New Mexico State University, New York University, Ohio State University, Pennsylvania State University, University of Portsmouth, Princeton University, the Spanish Participation Group, University of Tokyo, University of Utah, Vanderbilt University, University of Virginia, University of Washington, and Yale University.

This publication makes use of data products from the Two Micron All Sky Survey, which is a joint project of the University of Massachusetts and the Infrared Processing and Analysis Center/California Institute of Technology, funded by the National Aeronautics and Space Administration and the National Science Foundation.

This publication makes use of data products from the Wide-field Infrared Survey Explorer, which is a joint project of the University of California, Los Angeles, and the Jet Propulsion Laboratory/California Institute of Technology, funded by the National Aeronautics and Space Administration.

This research is based on observations with AKARI, a JAXA project with the participation of ESA.

This work is based in part on observations made with the Spitzer Space Telescope, which is operated by the Jet Propulsion Laboratory, California Institute of Technology under a contract with NASA.

This research made use of data products from the Midcourse Space Experiment. Processing of the data was funded by the Ballistic Missile Defense Organization with additional support from NASA Office of Space Science. This research has also made use of the NASA/ IPAC Infrared Science Archive, which is operated by the Jet Propulsion Laboratory, California Institute of Technology, under contract with the National Aeronautics and Space Administration.

This research has made use of NASA’s Astrophysics Data System (ADS) Abstract Service, and of the SIMBAD database, operated at CDS, Strasbourg, France.

REFERENCES

- Adamów, M., Niedzielski, A., Villaver, E., Wolszczan, A., Nowak, G., 2014, *A&A*, 569, 55
- Ahn, C., Alexandroff, R., Allende Prieto, C., et al. 2014, *ApJS*, 211, 17
- Alcaino, G., 1977, *A&AS*, 29, 9
- Anthony-Twarog, B., Deliyaniis, C., Rich, E., Twarog, B., 2013, *ApJ*, 767, 19
- Beichman, C., et al., *Infrared Astronomical Satellite (IRAS) Catalogs and Atlases*, vol. 1, Explanatory Supplement, 1988, NASA RP-1190 (Washington, DC: GPO) (<http://irsa.ipac.caltech.edu/IRASdocs/exp.sup/>)
- Burgasser, A. J., Kirkpatrick, J. D., Reid, I. N., Brown, M. E., Miskey, C. L., & Gizis, J. E. 2003, *ApJ*, 586, 512
- Carlberg, J., Smith, V., Cunha, K., Majewski, S., Rood, R., 2010, *ApJ*, 723, 103
- Carlberg, J., Cunha, K., Smith, V., Majewski, S., 2012, *ApJ*, 757, 109 (C12)
- Carney, B., Fry, A., Gonzalez, G., 1998, *AJ*, 116, 2984
- Castilho, B., Gregorio-Hetem, J., Spite, F., Spite, M., Barbuy, B., 1998, *A&AS*, 127, 139
- Castilho, B., Gregorio-Hetem, J., Spite, F., Barbuy, B., Spite, M., 2000, *A&A*, 364, 674
- Chen, P.-S., Yang, X.-H., & Zhang, P., 2007, *AJ*, 134, 214
- Coadella, C., Palumbo, G., Pareschi, G., et al., 1995, *MNRAS*, 276, 57
- Cutri, R., Wright, E., Conrow, T., et al., 2014, Explanatory Supplement to the AllWISE Data Release Products, <http://wise2.ipac.caltech.edu/docs/release/allwise/expsup/>
- de la Reza, R., Drake, N., da Silva, L., 1996, *ApJ*, 456, 115
- de la Reza, R., Drake, N., da Silva, L., Torres, C., Martin, E., 1997, *ApJ*, 482, 77 (dlR97)
- de la Reza, R., Drake, N., Oliveira, I., Rengaswamy, S., 2015, in press, arXiv:1504.05983
- Denissenkov, P. A., & Vandenberg, D. A., 2003, *ApJ*, 593 509
- Denissenkov, P. A., & Herwig, F., 2014, *ApJ*, 612, 1081
- Drake, N., de la Reza, R., da Silva, L., Lambert, D., 2002, *AJ*, 123, 2703
- Egan et al. 2003, Air Force Research Laboratory Technical Report AFRL-VS-TR-2003-1589
- Fazio, G., et al., 2004, *ApJS*, 154, 10
- Fekel, F., & Watson, L., 1998, *AJ*, 116, 2466
- García-Lario, P., Manchado, A., Pych, W., Pottasch, S., 1997, *A&AS*, 126, 479
- Gautier, T., Rieke, G., Stansberry, J., et al., 2007, *ApJ*, 667, 527
- Gillett, F., 1986, in *Light on Dark Matter*, ed., F. P. Israel (Dordrecht: Reidel), 61

- Gregorio-Hetem, J., Lépine, J., Quast, G., Torres, C., de la Reza, R., 1992, *AJ*, 103, 549
- Guandalini, R., Palmerini, S., Busso, M., Uttenthaler, S., 2009, *PASA*, 26, 168
- Hill, V., & Pasquini, L., 1999, *A&A*, 348, 21
- Jasniewicz, G., Parthasarathy, M., de Laverny, P., & Thévenin, F., 1999, *A&A*, 342, 831
- Jura, M., 1999, *ApJ*, 515, 706
- Kirby, E., Fu, X., Guhathakurta, P., Deng, L., 2012, *ApJ*, 752, 16
- Kraft, R., Peterson, R., Guhathakurta, P., Sneden, C., Fulbright, J., Langer, G., 1999, *ApJ*, 518, 53
- Kumar, Y., and Reddy, B., 2009, *ApJ*, 703, 46
- Kumar, Y., Reddy, B., Lambert, D., 2011, *ApJ*, 730, 12
- Kumar, Y., Reddy, B., Muthumariappan, C., Zhao, G., 2015, *A&A*, in press (arXiv: 1503.01548)
- Liu, Y., Tan, K., Wang, L., Zhao, G., Sato, B., Takeda, Y., Li, H., 2014, *ApJ*, 785, 94
- Lloyd Evans, T., 1991, *MNRAS*, 249, 409
- Luck, R. E., & Heiter, U. 2007, *AJ*, 133, 2464
- Magnani, L., Caillault, J.-P., Buchalter, A., & Beichman, C. A., 1995, *ApJS*, 96, 159
- Martell, S., Shetrone, M., 2013, *MNRAS*, 430, 611
- McDonald, I., Zijlstra, A., Boyer, M., 2012, *MNRAS*, 427, 343
- Messineo, M., Habing, H., Menten, K., Omont, A., Sjouweman, L., 2004, *A&A*, 418, 103
- Mizusawa, T., Rebull, L., Stauffer, J., Bryden, G., Meyer, M., & Song, I. 2012, *AJ*, 144, 135
- Monaco, L., Boffin, H., Bonifacio, P., et al., 2014, *A&A*, 546, 6
- Moshir, M. et al. 1992, Explanatory Supplement to the IRAS Faint Source Survey, version 2, JPL D-10015 8/92 (Pasadena: JPL). (<http://irsa.ipac.caltech.edu/IRASdocs/surveys/D-10015.pdf>)
- Murakami, H., et al. 2007, *PASJ*, 59, 369
- Neugebauer, G., Habing, H., van Duinen, et al. 1984, *ApJ*, 278, 1
- Palacios, A., Charbonnel, C., Talon, S., Siess, L., 2006, *A&A*, 453, 261
- Paresce, F., & Burrows, C., 1987, *ApJ*, 319, 23
- Pereyra, A., Castilho, B., & Magalhães, A., 2006, *A&A*, 449, 211
- Pilachowski, C., Sneden, C., Freeland, E., Casperson, J., 2003, *AJ*, 125, 794
- Ramos-Larios, G., Guerrero, M., Suárez, O, Miranda, L., Gómez, J., 2012, *A&A*, 545, 20
- Rebull, L., Koenig, X., Padgett, D., et al., 2011, *ApJS*, 196, 4

- Reddy, B., Lambert, D., Hrivnak, B., Bakker, E., 2002, *AJ*, 123, 1993
- Reddy, B., & Lambert, D., 2005, *AJ*, 129, 2831
- Rieke, G., et al. 2004, *ApJS*, 154, 25
- Ruchti, G., Fulbright, J., Wyse, R., et al., 2011, *ApJ*, 743, 107
- Saunders, W., et al., 2000, *MNRAS*, 317, 55
- Siess, L., and Livio, M., 1999, *MNRAS*, 308, 1133
- Silva Aguirre, V., Ruchti, G., Hekker, S., et al., 2014, *ApJ*, 748, 16
- Skrutskie, M., Cutri, R. M., Stiening, R., et al., 2006, *AJ*, 131, 1163
- Smith, V., Shetrone, M., Keane, M., 1999, *ApJ*, 516, 73
- Stephenson, C., 1976, *PW&SO*, 2, 21
- Stephenson, C., 1984, *PW&SO*, 3, 1
- Suárez, O., et al., 2006, *A&A*, 458, 173
- Szczerba, R., Siódmiak, N., Stasinska, G., Borkowski, J. 2007, *A&A*, 469, 799
- Torres, C., Quast, G., de la Reza, R., Gregorio-Hetem, J., Lépine, J., 1995, *AJ*, 109, 2146
- Torres, C., Quast, G., de la Reza, R., da Silva, L., 2000, *IAUS*, 198, 320
- Tosi, M., Pulone, L., Marconi, G., Bragaglia, A., 1998, *MNRAS*, 299, 834
- Trilling, D., Bryden, G., Beichman, C., et al. 2008, *ApJ*, 674, 1086
- Valenti, J., Fallon, A. & Johns-Krull, C., 2003, *ApJS*, 147, 305
- Wang, L., Rowan-Robinson, M., 2009, *MNRAS*, 398, 109
- Werner, M., et al., 2004, *ApJS*, 154, 1
- Whitelock, P., Menzies, J., Catchpole, R., Feast, M., Roberts, G., Marang, F., 1991, *MNRAS*, 250, 638
- Wright, E., Eisenhardt, P. R. M., Mainzer, A. K., et al., 2010, *AJ*, 140, 1868
- Yoon, D.-H., Chos, S.-H., Kim, J., Yun, Y., Park, Y.-S., 2014, *ApJS*, 211, 15
- Zacharias N., Monet D.G., Levine S.E., Urban S.E., Gaume R., Wycoff G.L., *BAAS*, 205, 48.15 (San Diego AAS Meeting, January 2005) <http://adsabs.harvard.edu/abs/2005yCat.1297....0Z>

Appendix: Notes on individual sources

This Appendix contains human-readable notes on the entire set of sources; position, photometric, and abundance data are in the machine-readable table in Table 1. Detailed notes on the sources we suspect are subject to source confusion appear in Table 4. Much more detailed notes on the sources we believe have IR excesses are in Section 5.

Table 6. Special Notes on Targets

name	dIR97	C12	Other lit	status	notes	$A(\text{Li}), \log g, T_{\text{eff}}?$
HD787	dIR97	(no excess)
Tyc3663-01966-1	Adamow et al. (2014)	(no excess)	...	Not Li rich.
HD4893	Castilho et al. (2000)	(no excess)	May be too cool to be a K giant.	Not Li rich.
IRAS00483-7347	Castilho et al. (1998)	IR excess (but maybe not K giant)	May be too cool to be a K giant.	No $A(\text{Li})$. No T_{eff} . No $\log g$.
Scl 1004838	Kirby et al. (2012)	sparse SED but probably no IR excess
Scl 1004861	Kirby et al. (2012)	sparse SED but probably no IR excess
NGC 362 V2	Smith et al. (1999)	IR excess (small)	...	Not Li rich.
HD6665	Kumar et al. (2011)	(no excess)	Identified in McDonald et al. (2012) as having an IR excess, but IR excess is not real.	...
HD7087	Liu et al. (2014)	(no excess)
HD8676	Kumar et al. (2011)	(no excess)
HD9746	dIR97	(no excess)
HD10437	Kumar et al. (2011)	(no excess)
HD12203	Kumar et al. (2011)	(no excess)
CPD-55395	dIR97	(no excess)	...	Not Li rich. No T_{eff} . No $\log g$.
HD13189	...	C12	...	(no excess)	...	Not Li rich.
HD15866	Liu et al. (2014), Luck & Heiter (2007)	(no excess)	...	T_{eff} too warm to be RG. $\log g$ too large to be RG.
For 55609	Kirby et al. (2012)	sparse SED but probably no IR excess
For 60521	Kirby et al. (2012)	sparse SED but probably no IR excess
Tyc3300-00133-1	Adamow et al. (2014)	(no excess)
For 90067	Kirby et al. (2012)	sparse SED but possible IR excess
For 100650	Kirby et al. (2012)	sparse SED but probably no IR excess
Tyc3304-00090-1	Adamow et al. (2014)	(no excess)
Tyc1780-00654-1	...	C12	...	(no excess)	...	Not Li rich.
HD17144	Drake et al. (2002)	(no excess)	...	Not Li rich. No $\log g$.
SDSS J0245+7102	Martell et al. (2013)	(no excess)
Tyc0647-00254-1	...	C12	...	(no excess)
SDSS J0301+7159	Martell et al. (2013)	(no excess)
G0300+00.29	...	C12	...	sparse SED but probably no IR excess	...	Not Li rich.
Tyc3318-01333-1	Adamow et al. (2014)	(no excess)
SDSS J0304+3823	Martell et al. (2013)	sparse SED but probably no IR excess
Tyc5868-00337-1	...	C12	...	(no excess)	...	Not Li rich.
HD19745	dIR97	IR excess	Also identified in Kumar et al. (2015) as an IR excess star.	...
Tyc3314-01371-1	Adamow et al. (2014)	(no excess)	...	Not Li rich.
HD21078	Fekel & Watson (1998)	(no excess)	...	Not Li rich. No $\log g$.
G0319+56.5830	...	C12	...	(no excess)	...	Not Li rich.
HD21018	Kumar et al. (2011)	(no excess)
G0319+56.6888	...	C12	...	(no excess)	...	Not Li rich.
Tyc5881-01156-1	...	C12	...	(no excess)	A	Not Li rich.
IRAS03520-3857	dIR97	IR excess	Given position is offset $\sim 11''$ from object taken as match (which is large in the context of the rest of this data set), but relatively isolated source and relatively clean field (e.g., unlikely to be confused).	No $A(\text{Li})$. No T_{eff} . No $\log g$.
HD26162	...	C12	...	(no excess)	...	Not Li rich.
Tyc3340-01195-1	...	C12	...	(no excess)	...	Not Li rich.
HD27497	Jasniewicz et al. (1999)	(no excess)	...	Not Li rich.

Table 6—Continued

name	dIR97	C12	Other lit	status	notes	$A(\text{Li})$, $\log g$, $T_{\text{eff}}?$
RAVEJ043154.1-063210	Ruchti et al. (2011)	sparse SED but probably no IR excess	...	T_{eff} too warm to be RG.
IRASF04376-3238	Torres et al. (2000)	IR excess	Also CD-32 1919.	No $A(\text{Li})$. No T_{eff} . No $\log g$.
HD30238	dIR97	(no excess)	...	Not Li rich.
HD30197	Liu et al. (2014), Luck & Heiter (2007)	(no excess)
Tyc0684-00553-1	Adamow et al. (2014)	(no excess)
HD30834	dIR97	(no excess)
Tyc5904-00513-1	...	C12	...	(no excess)	...	Not Li rich.
G0453+00.90	...	C12	...	sparse SED but probably no IR excess	...	Not Li rich.
HD31993	dIR97	C12	...	(no excess)	Only target in common between dIR97 and C12	Not Li rich.
HD34198	...	C12	...	(no excess)	Also UU Lep	Not Li rich.
HD33798	Drake et al. (2002)	(no excess)	...	$\log g$ too large to be RG.
HD33363	...	C12	...	(no excess)	...	Not Li rich.
HD35984	Liu et al. (2014), Luck & Heiter (2007)	(no excess)	...	T_{eff} too warm to be RG. $\log g$ too large to be RG.
SDSS J0535+0514	Martell et al. (2013)	sparse SED but probably no IR excess
HD37719	Kumar et al. (2011)	(no excess)
Be 21 T50	Hill & Pasquini (1999)	sparse SED but probably no IR excess	Hill & Pasquini call this T33 but it is not; based on photometry from Tosi et al. (1998), it is T50.	...
HD39853	dIR97	(no excess)
HD40359	Fekel & Watson (1998)	(no excess)	...	Not Li rich. No $\log g$.
HD40168	Kumar et al. (2011)	(no excess)
HD40827	Kumar et al. (2011)	(no excess)
HD43827	Jasniewicz et al. (1999)	(no excess)	...	Not Li rich. No $\log g$.
Tyc1890-01314-1	...	C12	...	(no excess)	...	Not Li rich.
HD44889	Castilho et al. (2000)	(no excess)	...	Not Li rich.
SDSS J0632+2604	Martell et al. (2013)	sparse SED but probably IR excess
Tr5 3416	Monaco et al. (2014)	sparse SED but probably no IR excess
HD47536	...	C12	...	(no excess)	WISE measurements from AllWISE reject catalog	Not Li rich.
IRAS06365+0223	dIR97	drop due to source confusion	2MASS measurements from Extended Source Catalog; WISE has 2 similar sources at this location in catalog, but not in image, so taking slightly closer. Extended source is origin of most of IR emission.	No $A(\text{Li})$. No T_{eff} . No $\log g$.
G0639+56.6179	...	C12	...	(no excess)	...	Not Li rich.
SDSS J0652+4052	Martell et al. (2013)	(no excess)
Tyc3402-00280-1	...	C12	...	(no excess)	...	Not Li rich.
SDSS J0654+4200	Martell et al. (2013)	sparse SED but probably no IR excess
HD51367	Kumar et al. (2011)	(no excess)
G0653+16.552	...	C12	...	sparse SED but probably no IR excess	...	Not Li rich.
G0654+16.235	...	C12	...	sparse SED but probably no IR excess	...	Not Li rich.
HIP35253	...	C12	...	(no excess)	...	Not Li rich.
SDSS J0720+3036	Martell et al. (2013)	sparse SED but probably no IR excess	...	T_{eff} too warm to be RG.
HD57669	Jasniewicz et al. (1999)	(no excess)	...	No $\log g$.
IRAS07227-1320(PDS132)	dIR97	IR excess	Also GSC 05408-03215.	No $A(\text{Li})$. No T_{eff} . No $\log g$.
HD59686	...	C12	...	(no excess)	...	Not Li rich.
HIP36896	...	C12	...	(no excess)	...	Not Li rich.
NGC 2423 3	Carlberg in prep	(no excess)
IRAS07419-2514	Torres et al. (2000)	drop due to source confusion	Target position is photocenter of small group of objects. Torres et al. (2000) notes IRAS flux may come from CO cloud WB 1046.	No $A(\text{Li})$. No T_{eff} . No $\log g$.

Table 6—Continued

name	dIR97	C12	Other lit	status	notes	$A(\text{Li}), \log g, T_{\text{eff}}?$
HD62509(Pollux)	...	C12	...	(no excess)	...	Not Li rich.
IRAS07456-4722(PDS135)	dIR97	IR excess	...	No $A(\text{Li})$. No T_{eff} . No $\log g$.
Tyc5981-00414-1	...	C12	...	(no excess)	...	Not Li rich.
HD63798	Kumar et al. (2011)	(no excess)
HD65750	dIR97	IR excess (small)	POSS images have strong nebulosity. Also V341 Car – a pulsating variable star. Identified in McDonald et al. (2012) as having an IR excess.	Not Li rich. T_{eff} too cool to be RG.
HD65228	Liu et al. (2014)	(no excess)	...	T_{eff} too warm to be RG.
Tyc1938-00311-1	...	C12	...	(no excess)	...	Not Li rich.
IRAS07577-2806(PDS260)	dIR97	IR excess	...	No $A(\text{Li})$. No T_{eff} . No $\log g$.
G0804+39.4755	...	C12	...	(no excess)	...	Not Li rich.
SDSS J0808_0815	Martell et al. (2013)	sparse SED but probably no IR excess
Tyc0195-02087-1	...	C12	...	(no excess)	...	Not Li rich.
HD70522	Liu et al. (2014), Luck & Heiter (2007)	(no excess)	...	T_{eff} too warm to be RG. $\log g$ too large to be RG.
HD233517	dIR97	IR excess	Also identified in Kumar et al. (2015) as an IR excess star, among many other references.	...
Tyc0205-01287-1	...	C12	...	(no excess)	...	Not Li rich.
G0827-16.3424	...	C12	...	(no excess)	...	Not Li rich. $\log g$ too large to be RG.
SDSS J0831+5402	Martell et al. (2013)	sparse SED but probably no IR excess
IRASF08359-1644	Torres et al. (2000)	IR excess	...	No $A(\text{Li})$. No T_{eff} . No $\log g$.
HD73108	...	C12	...	(no excess)	...	Not Li rich.
G0840+56.9122	...	C12	...	(no excess)	...	Not Li rich.
G0840+56.5839	...	C12	...	(no excess)	...	Not Li rich.
HD76066	dIR97	(no excess)	IRAS FSC [12]-[25] > 0.5 but WISE says no excess.	No $A(\text{Li})$. No T_{eff} . No $\log g$.
HD77361	Kumar et al. (2011)	(no excess)
HD78668	Liu et al. (2014)	(no excess)
G0909-05.211	...	C12	...	(no excess)	...	Not Li rich.
Tyc3809-01017-1	...	C12	...	(no excess)	...	Not Li rich.
G0912-05.11	...	C12	...	(no excess)	...	Not Li rich.
G0928+73.2600	...	C12	...	IR excess (small)
HD82227	dIR97	(no excess)	...	No $A(\text{Li})$. No $\log g$.
HD82421	dIR97	(no excess)	...	No $A(\text{Li})$. No $\log g$.
HD82734	Liu et al. (2014)	(no excess)
SDSS J0936+2935	Martell et al. (2013)	sparse SED but probably no IR excess
G0935-05.152	...	C12	...	sparse SED but probably no IR excess	...	Not Li rich.
G0946+00.48	...	C12	...	sparse SED but probably no IR excess	...	Not Li rich.
HD85444	Liu et al. (2014)	(no excess)
IRAS09553-5621	dIR97	drop due to source confusion	Target position is in between two sources	No $A(\text{Li})$. No T_{eff} . No $\log g$.
LeoI 71032	Kirby et al. (2012)	sparse SED but probably no IR excess
LeoI 60727	Kirby et al. (2012)	sparse SED but probably no IR excess
LeoI 32266	Kirby et al. (2012)	sparse SED but probably no IR excess
LeoI 21617	Kirby et al. (2012)	sparse SED but probably no IR excess
C1012254-203007	Ruchti et al. (2011)	sparse SED but probably no IR excess
HD88476	Kumar et al. (2011)	(no excess)
Tyc3441-00140-1	...	C12	...	(no excess)	...	Not Li rich.

Table 6—Continued

name	dIR97	C12	Other lit	status	notes	$A(\text{Li}), \log g, T_{\text{eff}}?$
BD+202457	Carlberg in prep	(no excess)	...	Not Li rich.
Tyc5496-00376-1=BD-12d3141	Ruchti et al. (2011)	(no excess)
HD90082	Castilho et al. (2000)	(no excess)	WISE measurements from AllWISE reject catalog	Not Li rich. T_{eff} too cool to be RG.
Tyc3005-00827-1	...	C12	...	(no excess)	...	Not Li rich.
HD90633	Kumar et al. (2011)	(no excess)
HD92253	dIR97	(no excess)	...	No $A(\text{Li})$. No $\log g$.
G1053+00.15	...	C12	...	(no excess)	...	Not Li rich.
Tyc2521-01716-1	...	C12	...	(no excess)	...	Not Li rich.
HD95799	dIR97	(no excess)
HD96195	Castilho et al. (2000)	IR excess (but maybe not K giant)	May be too cool to be a K giant. Identified in McDonald et al. (2012) as having an IR excess.	Not Li rich. T_{eff} too cool to be RG.
SDSS J1105+2850	Martell et al. (2013)	sparse SED but probably no IR excess	...	T_{eff} too warm to be RG. $\log g$ too large to be RG.
IRAS11044-6127	dIR97	drop due to source confusion	Optical counterpart hard to locate, steep SED.	No $A(\text{Li})$. No T_{eff} . No $\log g$.
HD96996	dIR97	(no excess)	...	No $A(\text{Li})$. No T_{eff} . No $\log g$.
HD97472	dIR97	(no excess)	...	No $A(\text{Li})$. No $\log g$.
LeoII C-7-174	Kirby et al. (2012)	sparse SED but probably no IR excess
LeoII C-3-146	Kirby et al. (2012)	sparse SED but probably no IR excess
G1124-05.61	...	C12	...	(no excess)
Tyc3013-01489-1	...	C12	...	(no excess)	...	Not Li rich.
G1127-11.60	...	C12	...	sparse SED but probably no IR excess	...	Not Li rich.
G1130+39.9414	...	C12	...	(no excess)	G1130+37.9414 in C12 is a misprint for G1130+39.9414. It is also Tyc3013-01163-1.	Not Li rich.
HD102845	Liu et al. (2014)	(no excess)
Tyc5523-00830-1	...	C12	...	(no excess)	...	Not Li rich.
Tyc0276-00327-1	...	C12	...	IR excess (small)	Also HD103915. In halo of bright galaxy(?) that appears by 12, 22 μm . Likely high background, but probably ok.	Not Li rich.
G1200+67.3882	...	C12	...	(no excess)	...	Not Li rich.
Tyc6094-01204-1	...	C12	...	(no excess)	...	Not Li rich.
HD104985	...	C12	...	(no excess)	...	Not Li rich.
Tyc2527-01442-1	...	C12	...	(no excess)	...	Not Li rich.
G1213+33.15558	...	C12	...	(no excess)	...	Not Li rich.
HD107484	Kumar et al. (2011)	(no excess)
NGC 4349 127	Carlberg in prep	(no excess)	...	Not Li rich.
HD108225	...	C12	...	(no excess)	...	Not Li rich.
IRAS12236-6302(PDS354)	dIR97	drop due to source confusion	Cluster of possible sources. Steep SED. Torres et al. (2000) mention that optical spectrum of source taken as counterpart has strong H α emission and could be an H II region.	No $A(\text{Li})$. No T_{eff} . No $\log g$.
HD108471	dIR97	(no excess)
IRAS12327-6523(PDS355)	dIR97	IR excess	...	No $A(\text{Li})$.
HD109742	...	C12	...	(no excess)	...	Not Li rich.
M68-A96=C1* NGC 4590 HAR 1257	Ruchti et al. (2011)	sparse SED but probably no IR excess	The coordinates in the paper are incorrect; used finding chart, Fig 2, in Alcaino (1977) to ID by eye.	...
G1240+56.8464	...	C12	...	(no excess)	...	Not Li rich.
HD112127	dIR97	(no excess)
HD111830	dIR97	IR excess (small)	...	No $A(\text{Li})$. No $\log g$.
HD112859	...	C12	...	(no excess)	IRAS FSC [12]-[25] > 0.5 but WISE says no excess.	...

Table 6—Continued

name	dIR97	C12	Other lit	status	notes	$A(\text{Li}), \log g, T_{\text{eff}}?$
SDSS J1310_0012	Martell et al. (2013)	sparse SED but probably no IR excess
HD115478	...	C12	...	(no excess)	WISE measurements from AllWISE reject catalog	Not Li rich.
HD115659	Liu et al. (2014)	(no excess)
HD116010	...	C12	...	(no excess)	...	Not Li rich.
HD116292	Liu et al. (2014), Kumar et al. (2011)	(no excess)
CVnI 195_195	Kirby et al. (2012)	sparse SED but probably no IR excess
CVnI 196_129	Kirby et al. (2012)	sparse SED but probably no IR excess
G1331+00.13	...	C12	...	(no excess)	...	Not Li rich.
PDS365(IRAS13313-5838)	dIR97	IR excess
HD118319	Kumar et al. (2011)	(no excess)
HD118344	dIR97	(no excess)	...	No $A(\text{Li})$. No $\log g$.
HD118839	...	C12	...	(no excess)	...	Not Li rich.
M3-IV101=C1* NGC 5272 SK 557	Kraft et al. (1999), P-lachowski et al. (2003), Ruchti et al. (2011)	sparse SED but probably no IR excess
HD119853	dIR97	(no excess)	...	No $A(\text{Li})$. No $\log g$.
HD120048	Liu et al. (2014)	(no excess)
HD120602	dIR97	(no excess)
HD121710(9Boo)	dIR97	(no excess)	...	Not Li rich. No $\log g$.
PDS68(IRAS13539-4153)	dIR97	IR excess	Also GSC 07798-00578.	...
Tyc3027-01042-1	...	C12	...	(no excess)	...	Not Li rich.
HD122430	...	C12	...	(no excess)	...	Not Li rich.
Tyc0319-00231-1	...	C12	...	(no excess)	...	Not Li rich.
HD124897(Arcturus)	...	C12	...	(no excess)	high enough proper motions that automatic merging not possible; matches done via SIMBAD and by hand	Not Li rich.
HD125618	dIR97	(no excess)	...	No $A(\text{Li})$. No T_{eff} . No $\log g$.
Tyc1469-01108-1	...	C12	...	(no excess)	...	Not Li rich.
IRAS14198-6115	dIR97	drop due to source confusion	Cluster of possible sources.	No $A(\text{Li})$. No T_{eff} . No $\log g$.
G1421+28.4625	...	C12	...	(no excess)	...	Not Li rich.
RAVEJ142546.2-154629	Ruchti et al. (2011)	(no excess)
HD126868	Jasniewicz et al. (1999)	(no excess)	...	T_{eff} too warm to be RG.
IRAS14257-6023	dIR97	drop due to source confusion	Cluster of possible sources.	No $\log g$. No $A(\text{Li})$. No T_{eff} . No $\log g$.
SDSS J1432+0814	Martell et al. (2013)	sparse SED but probably no IR excess
HD127740	Liu et al. (2014), Luck & Heiter (2007)	(no excess)	...	T_{eff} too warm to be RG. $\log g$ too large to be RG.
Tyc0913-01248-1	...	C12	...	(no excess)	...	Not Li rich.
Tyc0914-00571-1	...	C12	...	(no excess)	...	Not Li rich.
HD128309	dIR97	(no excess)	...	No $A(\text{Li})$. No T_{eff} . No $\log g$.
HD129955	dIR97	(no excess)	...	No $A(\text{Li})$. No T_{eff} . No $\log g$.
HD131530	dIR97	(no excess)	...	No $A(\text{Li})$. No $\log g$.
HD133086	Kumar et al. (2011)	(no excess)
Tyc0347-00762-1	...	C12	...	(no excess)	...	Not Li rich.
M5 V42	Carney et al. (1998)	(no excess)
SDSS J1522+0655	Martell et al. (2013)	sparse SED but probably no IR excess
HD137759	...	C12	...	(no excess)	...	Not Li rich.

Table 6—Continued

name	dIR97	C12	Other lit	status	notes	$A(\text{Li})$, $\log g$, $T_{\text{eff}}?$
HD138525	Liu et al. (2014), Luck & Heiter (2007)	(no excess)	...	T_{eff} too warm to be RG. $\log g$ too large to be RG.
HD138688	Jasniewicz et al. (1999)	(no excess)	...	Not Li rich.
G1551+22.9456	...	C12	...	(no excess)	...	Not Li rich.
SDSS J1607+0447	Martell et al. (2013)	sparse SED but probably no IR excess
HD145206	Jasniewicz et al. (1999)	(no excess)	...	Not Li rich.
HD145457	Kumar et al. (2011)	(no excess)
IRAS16086-5255(PDS410)	dIR97	IR excess	...	No $A(\text{Li})$. No T_{eff} . No $\log g$.
IRAS16128-5109	dIR97	drop due to source confusion	Appears in SIMBAD as an H II region; the morphology of the image suggests a dense clump of sources from which emanate long streamers of extended emission.	No $A(\text{Li})$. No T_{eff} . No $\log g$.
HD146850	dIR97	(no excess)
HD146834	dIR97	IR excess (small)	Also HR 6076. Also identified in McDonald et al. (2012) as having an IR excess.	No $A(\text{Li})$. No $\log g$.
HD148293	dIR97	(no excess)
Tyc2043-00747-1	...	C12	...	(no excess)	...	Not Li rich.
IRAS16227-4839	dIR97	drop due to source confusion	Match forced to be IR-bright source (not found automatically given this position).	No $A(\text{Li})$. No T_{eff} . No $\log g$.
HD148317	Liu et al. (2014), Luck & Heiter (2007)	(no excess)	...	T_{eff} too warm to be RG. $\log g$ too large to be RG.
IRAS16252-5440	dIR97	drop due to source confusion	Also PDS 146. Cluster of IR-bright sources.	No $A(\text{Li})$. No T_{eff} . No $\log g$.
HD150902	Kumar et al. (2011)	(no excess)
HIP81437	...	C12	...	(no excess)	...	Not Li rich.
G1640+56.6327	...	C12	...	(no excess)	...	Not Li rich.
IRAS16514-4625(PDS432)	dIR97	drop due to source confusion	Torres et al. (2000) list it as a confirmed giant but the source that was measured may not be responsible for the IR flux. Cluster of sources, steep SED.	No $A(\text{Li})$. No T_{eff} . No $\log g$.
HD153135	dIR97	(no excess)	...	No $A(\text{Li})$. No $\log g$.
HD152786	Jasniewicz et al. (1999)	(no excess)	...	Not Li rich.
HD153687	Jasniewicz et al. (1999)	(no excess)	...	Not Li rich.
HD155646	Liu et al. (2014), Luck & Heiter (2007)	(no excess)	...	T_{eff} too warm to be RG. $\log g$ too large to be RG.
IRAS17102-3813	dIR97	drop due to source confusion	Cluster of sources.	No $A(\text{Li})$. No T_{eff} . No $\log g$.
IRAS17120-4106	dIR97	drop due to source confusion	Two possible sources.	No $A(\text{Li})$. No T_{eff} . No $\log g$.
HD156115	dIR97	(no excess)	...	No $A(\text{Li})$. T_{eff} too cool to be RG. No $\log g$.
HD156061	dIR97	(no excess)	...	No $A(\text{Li})$. No $\log g$.
IRAS17211-3458	dIR97	drop due to source confusion	Two possible sources.	No $A(\text{Li})$. No T_{eff} . No $\log g$.
HD157457	Jasniewicz et al. (1999)	(no excess)
HD157919	Liu et al. (2014), Luck & Heiter (2007)	(no excess)	...	T_{eff} too warm to be RG. $\log g$ too large to be RG.
IRAS17442-2441	dIR97	drop due to source confusion	Cluster of possible sources.	No $A(\text{Li})$. No T_{eff} . No $\log g$.

Table 6—Continued

name	dIR97	C12	Other lit	status	notes	$A(\text{Li}), \log g, T_{\text{eff}}?$
PDS97(IRAS17554-3822)	de la Reza, Drake, & da Silva (1996)	drop due to source confusion	Target position in between two sources of comparable brightness.	No $A(\text{Li})$. No T_{eff} . No $\log g$.
IRAS17576-1845	dIR97	drop due to source confusion	The multi-wavelength images suggest extinction in this field. Coadella et al. (1995) list it as a candidate to be related to high-mass star forming regions with an ultracompact H II region, though it remained undetected in their survey.	No $A(\text{Li})$. No T_{eff} . No $\log g$.
IRAS17578-1700	dIR97	IR excess (but maybe not K giant)	Also C* 2514, CGCS 3922 - likely carbon star.	No $A(\text{Li})$. No T_{eff} . No $\log g$.
HD162298	dIR97	(no excess)	...	No $A(\text{Li})$. No $\log g$.
G1800+61.12976	...	C12	...	(no excess)	...	Not Li rich.
IRAS17582-2619	dIR97	drop due to source confusion	Brightest source in IR has no optical counterpart. SIMBAD lists this as an OH/IR star. Yoon et al. (2014) and references therein identify it as a post-AGB star (OH4.02-1.68).	No $A(\text{Li})$. No T_{eff} . No $\log g$.
IRAS17590-2412	dIR97	drop due to source confusion	Position shifted slightly to pick up WISE source. Diffuse emission can also be seen in the field in various bands. Messineo et al. (2004) identify a SiO emitter in this region but suggest that it may not be associated with the source from which an optical spectrum had been obtained by dIR97. They note that this IRAS source is the only mid-infrared source within their 86 GHz beam.	No $A(\text{Li})$. No T_{eff} . No $\log g$.
IRAS17596-3952(PDS485)	dIR97	IR excess	Position shifted slightly to pick up WISE source. Also identified in Kumar et al. (2015) as IR excess star.	...
Tyc0435-03332-1	Adamow et al. (2014)	(no excess)
HD164712	dIR97	(no excess)	...	No $A(\text{Li})$. No T_{eff} . No $\log g$.
HD167304	Kumar et al. (2011)	(no excess)
HD170527	Kumar et al. (2011)	(no excess)
HD169689	Jasniewicz et al. (1999)	(no excess)	...	Not Li rich.
V385 Sct	Castilho et al. (2000)	IR excess (but maybe not K giant)	Too cool to be a K giant. S-type star.	Not Li rich. T_{eff} too cool to be RG.
IRAS18334-0631(PDS524)	dIR97	drop due to source confusion	No optical source at the target position, and cluster of IR sources.	No $A(\text{Li})$. No T_{eff} . No $\log g$.
Tyc3105-00152-1	Adamow et al. (2014)	(no excess)
Tyc3917-01107-1	Adamow et al. (2014)	(no excess)	Identified in McDonald et al. (2012) as having an IR excess, but IR excess is not real.	...
IRAS18397-0400	dIR97	drop due to source confusion	Brightest source in the IR has no optical counterpart.	No $A(\text{Li})$. No T_{eff} . No $\log g$.
Tyc3930-00681-1	Adamow et al. (2014)	(no excess)	...	Not Li rich.
HD175492	Jasniewicz et al. (1999)	(no excess)	...	Not Li rich. T_{eff} too warm to be RG.
IRAS18559+0140	dIR97	drop due to source confusion	No optical source at the target position, and cluster of IR sources.	No $A(\text{Li})$. No T_{eff} . No $\log g$.
HD176588	dIR97	(no excess)
SDSS J1901+3808	Martell et al. (2013)	sparse SED but probably no IR excess
HD176884	Jasniewicz et al. (1999)	(no excess)	...	Not Li rich.
IRAS19012-0747	dIR97	IR excess (small)	Name as appearing in dIR97 had a typo; this is the correct name.	No $A(\text{Li})$.
HD177830	...	C12	...	(no excess)	...	Not Li rich.

Table 6—Continued

name	dIR97	C12	Other lit	status	notes	$A(\text{Li}), \log g, T_{\text{eff}}?$
IRAS19038-0026	Castilho et al. (2000)	IR excess (small but maybe not K giant)	May be too cool to be a K giant.	Not Li rich. T_{eff} too cool to be RG.
HD177366	dIR97	(no excess)	...	No $A(\text{Li})$. No $\log g$.
HD178168	Castilho et al. (2000)	(no excess)	...	Not Li rich.
SDSS J1909+3837	Martell et al. (2013)	sparse SED but probably no IR excess
IRAS19083+0119(PDS562)	dIR97	drop due to source confusion	Brightest source in the IR has no optical counterpart. Steep SED.	No $A(\text{Li})$. No T_{eff} . No $\log g$.
KIC 5000307	Silva Aguirre et al. (2014)	(no excess)
HD181154	dIR97	(no excess)	...	No $A(\text{Li})$. No $\log g$.
IRAS19210+1715	dIR97	drop due to source confusion	Brightest source in the IR has no optical counterpart. Steep SED.	No $A(\text{Li})$. No T_{eff} . No $\log g$.
HD182900	Liu et al. (2014), Luck & Heiter (2007)	(no excess)	...	T_{eff} too warm to be RG. $\log g$ too large to be RG.
HD182901	Liu et al. (2014), Luck & Heiter (2007)	(no excess)	...	T_{eff} too warm to be RG. $\log g$ too large to be RG.
HD183492	Kumar et al. (2011)	(no excess)
HD183202	dIR97	(no excess)	...	No $A(\text{Li})$. No T_{eff} . No $\log g$.
PDS100	dIR97	IR excess	Also V859 Aql and IRAS 19285+0517. Also identified in Kumar et al. (2015) as IR excess star.	...
G1936+61.14369	...	C12	...	(no excess)	...	Not Li ¹ rich.
HD185194	Liu et al. (2014)	(no excess)
KIC 4937011	Anthony-Twarog et al. (2013)	sparse SED but probably no IR excess
HD187114	dIR97	(no excess)	...	No $A(\text{Li})$. No $\log g$.
RAVEJ195244.9-600813	Ruchti et al. (2011)	(no excess)
Tyc1058-02865-1	Adamow et al. (2014)	(no excess)	...	Not Li rich.
HD188376	Liu et al. (2014), Luck & Heiter (2007)	(no excess)	...	T_{eff} too warm to be RG. $\log g$ too large to be RG.
HD188993	Liu et al. (2014), Luck & Heiter (2007)	(no excess)	...	T_{eff} too warm to be RG. $\log g$ too large to be RG.
HD190299	dIR97	(no excess)	...	No $A(\text{Li})$. No T_{eff} . No $\log g$.
HD191277	...	C12	...	(no excess)	...	Not Li rich.
SDSS J2019+6012	Martell et al. (2013)	sparse SED but probably no IR excess
HD194317(39Cyg)	dIR97	(no excess)	...	Not Li rich. No $\log g$.
HD194937	Liu et al. (2014), Luck & Heiter (2007), Kumar et al. (2011)	(no excess)
Tyc9112-00430-1	Ruchti et al. (2011)	IR excess (small)
Tyc2185-00133-1	...	C12	...	(no excess)	...	Not Li rich.
HD202261	Liu et al. (2014)	(no excess)
HD203136	Kumar et al. (2011)	(no excess)	Identified in McDonald et al. (2012) as having an IR excess, but IR excess is not real.	...
HD203251	dIR97	(no excess)	IRAS FSC [12]-[25] > 0.5 but WISE says no excess.	Not Li rich. No T_{eff} . No $\log g$.
HD204540	dIR97	(no excess)	...	No $A(\text{Li})$. No $\log g$.
HD205349	Kumar et al. (2011)	(no excess)
HD206445	...	C12	...	(no excess)	...	Not Li rich.
Tyc6953-00510-1	Ruchti et al. (2011)	(no excess)

Table 6—Continued

name	dIIR97	C12	Other lit	status	notes	A(Li), log g , T_{eff} ?
G2200+56.3466	...	C12	...	(no excess)	...	Not Li rich.
SDSS J2200+4559	Martell et al. (2013)	sparse SED but probably no IR excess
SDSS J2206+4531	Martell et al. (2013)	sparse SED but probably no IR excess
HD212271	Liu et al. (2014)	(no excess)
HD212430	Liu et al. (2014)	(no excess)
HD213619	Liu et al. (2014), Luck & Heiter (2007)	(no excess)	...	T_{eff} too warm to be RG. log g too large to be RG.
HD213930	Liu et al. (2014)	(no excess)
HD214995	Liu et al. (2014), Luck & Heiter (2007), Kumar et al. (2011)	(no excess)
HD217352	Kumar et al. (2011)	(no excess)
HD218527	dIIR97	(no excess)	...	No A(Li). No T_{eff} . No log g .
Tyc8448-00121-1	Ruchti et al. (2011)	(no excess)
HD219025	dIIR97	IR excess	Also BI Ind. Also identified in Kumar et al. (2015) as an IR excess star.	...
HD219449	...	C12	...	(no excess)	...	Not Li rich.
HD221776	dIIR97	(no excess)	...	No A(Li). No log g .
HD221862	...	C12	...	(no excess)	...	Not Li rich.
SDSS J2353+5728	Martell et al. (2013)	(no excess)
SDSS J2356+5633	Martell et al. (2013)	(no excess)